

國立交通大學
材料科學與工程學系

博士論文

應用於 **OLED** 封裝之紫外光硬化環氧樹脂膠材
之性質與改善研究



**A Study and Property Modification of UV-curable
Epoxide Resins Applied to OLED Packaging**

學生姓名：江姿萱 (Tzu-Hsuan Chiang)

指導教授：謝宗雍 博士 (Dr. Tsung-Eong Hsieh)

中華民國九十五年七月

應用於 OLED 封裝之紫外光硬化環氧樹脂膠材之性質與改善研究

學生姓名：江姿萱

指導教授：謝宗雍 博士

國立交通大學 材料科學與工程學系

摘 要

本論文研究應用在有機發光二極體元件 (OLEDs) 封裝用之紫外光硬化樹脂的特性和改質方法。OLEDs 需要氣密性優良的封裝結構以防止發光層及高活性的陽極金屬因水氣入侵而劣化，良好的黏著性質為達成此一目標的必要性質之一；本研究因此探討紫外光硬化環氧樹脂之組成對黏著以及各種相關物理性質之影響，進而提出改善黏著等性質的方法。

本論文的主要研究項目包含：(i) 單體種類對於樹脂黏著強度的影響；(ii) 偶合劑對於樹脂黏著強度的影響；(iii) 三級胺對樹脂之紫外光/熱硬化、黏著強度及黃化的影響；(iv) 含 hBN (六方氮化硼) 無機填充材之環氧樹脂做為覆晶 IC 封裝之填充底膠之研究。第一部分研究聚醇類、乙烯酯類和壓克力酸類單體，對於樹脂縮收率、紫外光轉化率及玻璃接著強度的影響，實驗結果顯示聚醇類單體效果最佳，其在進行陽離子光聚合反應時，擁有最小的縮收率 (1.72%)、最慢的光聚合轉化率 (0.09 sec^{-1}) 和最大的黏著強度 (153.35 kg/cm^2)。第二部分研究填加不同種類之偶合劑的樹脂在 ITO 玻璃上之黏著強度的影響，偶合劑種類包含乙烯類、胺類、環氧類，乙基類及壓克力酸類；實驗結果顯示乙烯類偶合劑可以促進自由基聚合，當其添加量在 1.0 wt.% 時，樹脂在 ITO 玻璃及玻璃基板有最大的接著強度，其值分別為 91.42 kg/cm^2 及 153.35 kg/cm^2 。第三部分研究添加不同種類三級胺的紫外光硬化樹脂之特性，其種類包含咪唑、1,2-二甲基咪唑、2,4,6-三(二甲基胺-甲基)酚、1-甲基咪唑和 2-甲基咪唑；實驗結果顯示 2,4,6-三(二甲基胺-甲基)可提高樹脂的玻璃轉化溫度 ($T_g = 72.3^\circ\text{C}$)、降低熱膨脹係數 (CTE

= 70.8 ppm/°C)，在玻璃 (> 199 kg/cm²)、ITO 玻璃 (> 182 kg/cm²)、PET (約 115 kg/cm²) 和不銹鋼 (約 232 kg/cm²) 等基板上亦有最大的黏著強度，此外，2,4,6-三(二甲基胺-甲基)酚亦有最高的紫外光反應性和最佳的黃化改善效果(黃化指數 = 11.27；顏色參數 = 6.48)。

前述之研究成果亦被應用於 IC 之填充底膠製備研究，其利用六方氮化硼 (hBN) 做為無機物填充物，添加量為 9.2 至 25.7 vol.%，並對電氣性質、熱性質、硬化動力學、接著強度及黏度進行探討。與商用含二氧化矽之底膠比較發現，當 hBN 添充量在 15 vol.%以上時，擁有較高的 T_g 與較低的 CTE 值；當 hBN 添充量在 25.7 vol.%時則有最大的熱傳導係數 (= 1.08 W/m²K)；hBN 添加量愈高對於基材的黏著強度愈低，對於不同的基材之黏著強度大小依序為氧化鋁 > 矽晶片 > 錫鉛基板。



A Study and Property Modification of UV-curable Epoxide Resins Applied to OLED Packaging

Student: Tzu-Hsuan Chiang

Advisor: Dr. Tsung-Eong Hsieh

Department of Materials Science and Engineering

National Chiao Tung University

Abstract

This thesis studies the properties and modifications of UV-curable epoxide resins applied to the packaging of organic light-emitting devices (OLEDs). A hermetic packaging structure is essential to OLEDs since the light-emitting layer and highly active cathode electrode inside the devices are rather vulnerable to moisture attack. Since good adhesion is one of the key properties for sealing resins to achieve such a purpose, a thorough study on the UV-curable epoxide resins was hence carried out so that an in-depth understanding on the effects of resin constitution on adhesion and methods of property improvements could be obtained. The main topics included in this work are: (i) the effects of monomer types on adhesion strength of resins; (ii) the effects of organo-functional silanes on adhesion strength of resins; (iii) the effects of tertiary amines on UV/thermal curing, adhesion strength and etiolation of resins; (iv) epoxide resins containing hBN (hexagonal boron nitride) as inorganic filler for underfill of flip-chip interconnection.

In part (i), epoxide resins containing polyol, vinyl ether and acrylate monomers were prepared and their effects on resin shrinkage, conversions and adhesion strength on glass substrate were investigated *via* a pull test. The polyol monomer was found to be the best since it provided the smallest shrinkage (1.72%) for cationic

photopolymerization, the slowest rates of polymerization at 0.09 sec^{-1} and the highest adhesion strength (153.35 kg/cm^2). In part (ii), epoxide resins containing various organo-functional silanes including vinyl, epoxy, amino, methacrylic and acrylic groups were prepared and the adhesion strengths on indium tin oxide (ITO) substrate were studied. The vinyl silane was found to be able to promote the free-radical polymerization and the sample containing 1.0 wt.% of vinyl silane possessed the highest adhesion strength of 91.42 kg/cm^2 on ITO glass and 153.35 kg/cm^2 on glass substrate. In part (iii), various tertiary amines including imidazole, 1,2-dimethylimidazol, 2,4,6-tris(dimethylamino-methyl)phenol, 1-methylimidazole, and 2-methylimidazole were respectively added into the UV-curable epoxide resins. The addition of 2,4,6-tris(dimethylamino-methyl)phenol offered the highest glass transition temperature ($T_g = 72.3^\circ\text{C}$), the lowest coefficient of thermal expansion (CTE = $70.8 \text{ ppm/}^\circ\text{C}$) and the highest adhesion strengths on glass ($> 199 \text{ kg/cm}^2$), ITO ($> 182 \text{ kg/cm}^2$), PET ($\sim 115 \text{ kg/cm}^2$), and stainless steel ($\sim 232 \text{ kg/cm}^2$) substrates. 2,4,6-tris(dimethylamino-methyl)phenol also exhibited the highest UV reactivity and the best efficiency on the etiolation improvement that the values of ΔYI and ΔE^*_{ab} as low as 11.27 and 6.48 were achieved in the UV-curable epoxide resins.

The knowledge acquired from the studies presented above was also applied to the preparation of underfill resin containing hBN filler for flip-chip interconnection. It was found that the hBN-resin possesses better dielectric properties in comparison with conventional underfill resins containing SiO_2 filler. The hBN-resin also exhibited a lower CTE and a higher T_g and, for the resin containing 25.7 vol.% hBN, it possessed the largest thermal conductivity ($1.08 \text{ W/m}^\circ\text{K}$). The adhesion strengths of the composite resins decreased with the increase of hBN content and the adhesion strengths on various substrates was found to be in the order of alumina (Al_2O_3) > Si wafer > eutectic PbSn solder.

誌 謝

首先要感謝我的父母親，因為他們的包容與支持，使我無顧之憂，得以完成這最後一個階段的學業。

其次，我要感謝實驗室的學弟妹們，如羽筠、佳瑩和婉琪，與她們相處很愉快，排解我在實驗時的低潮與苦悶；另外，我要感謝在實驗中協助過的朋友及學長，如小余、明樺、沈明傑、王欽宏及陳建明學長等等；有這朋友及學長的幫忙，才能使我的實驗能順利完成。

最後要感謝我的指導教授謝宗雍博士，平時對我的關心與鼓勵，讓我慢慢從錯誤中成長，讓我學會獨立思考及獨立運作的能力；期望能以過去四年所學，在未來翱翔出自己的一片天空。

最後在此再一次感謝大家，成就現在的我。



Contents

Chinese Abstract	i
Abstract	iii
Acknowledgments	v
Contents	vi
Figure Captions	viii
Table Captions	xi
List of Symbols	xii
Chapter 1 Introduction	1
Chapter 2 Literature Review	5
2.1. Introduction of OLED Packaging	5
2.2. Sealing Technologies of Electronic Devices	7
2.3. Requirements of Sealing Resins for OLED Packaging	9
2.4. Comparisons of UV- and Thermal-curable Resins	10
2.5. Comparison of UV-Curable Epoxy and Acrylic adhesives	11
2.6. Commercial Sealing Resins for OLED Packaging	15
2.7. Formulations of UV-curable Epoxide Resins	16
2.7.1. Reaction Mechanisms of Photoinitiators	16
2.7.2. Reaction Mechanisms of Monomers	18
2.7.3. Effects of Silane Coupling Agents on Adhesion Strengths	26
2.7.4. Effects of Tertiary Amines on Etiolation	27
2.8. Adhesion Strengths of Polymer Resins	29
2.9. Underfill for Flip-chip IC Packaging	31
Chapter 3 Experimental Methods	34
3.1. Experimental Methods of Sealing Resins for the OLED Packaging	34
3.1.1. Materials	34
3.1.2. Experimental flow	37
3.1.3. Characterization Methods	38
3.2. Underfill Resins for Flip-chip Interconnections	44
3.2.1. Materials	44
3.2.2. Sample Preparation	45
3.2.3. Dielectric Properties	46
3.2.4. Curing Kinetics of Resins	46
3.2.5. Coefficient of Thermal Expansion (CTE)	47
3.2.6. Thermal Conductivity	47

3.2.7. Morphology.....	49
3.2.8. Adhesion Strengths	49
3.2.9. Viscosity Measurement	49
Chapter 4 Results and Discussion.....	50
4.1. Effects of Monomer Types on Adhesion Strengths of UV-Curable Resins..	50
4.1.1. Kinetics of Photo-Polymerization of Resins.....	50
4.1.2. Effects of UV Curing Times on Shrinkages of Resins.....	52
4.1.3. Effects of <i>R</i> Values	55
4.1.4. Effects of the Number of Hydroxyl Functional Groups	57
4.1.5. The Effects of BPO and UV Reactivity	59
4.2. Effects of Organo-Functional Silanes on Adhesion Strengths of UV-Curable Resins	62
4.2.1. Chemical Reaction of Silane Containing Alkoxy Groups	62
4.2.3. Effects of Silane Functional Groups on Adhesion Strengths.....	74
4.2.4. Effect of Weight Percentage of Vinyl Group Silane on Adhesion Strengths.....	75
4.3. Effects of Tertiary Amines on UV-Curable Epoxide Resins.....	76
4.3.1. UV Conversions of Tertiary Amines.....	76
4.3.2. Tertiary Amines React with BPO under UV Irradiation	77
4.3.3. Effect of Tertiary Amines on Thermal Conversions	81
4.3.4. Effect of Tertiary Amines on Adhesion Strengths.....	85
4.3.5. Effects of BPO Contents on Amine-free Samples on Etiation	88
4.3.6. Effects of UV Irradiation Times on Etiation.....	89
4.3.7. Effects of Post Curing Temperatures on Etiation.....	91
4.3.8. Effects of Amine Types and Contents on Etiation	91
4.4. Study of Underfill Resins Containing hBN for Flip-chip Interconnection...	94
4.4.1. Dielectric Properties.....	94
4.4.2. Curing Kinetics	97
4.4.3. Effects on Coefficient of Thermal Expansion (CTE)	100
4.4.4. Effects on Thermal Conductivity	101
4.4.5 Effects on Adhesion Strengths	103
4.4.6. Viscosity of hBN-Resin	105
Chapter 5 Conclusions	106
Prospective Researches	111
References.....	116
Curriculum Vitae.....	135

Figure Captions

Figure 2-1. Schematic structure of the OLED device.....	6
Figure 2-2. Encapsulation methods for conventional bottom-emitting OLEDs.....	7
Figure 2-3. Encapsulation methods utilizing transparent, multiple organic and inorganic barrier coatings for FOLEDs.	8
Figure 2-4. Monomer types can be utilized in photoinitiated cationic polymerization.	19
Figure 3-1. Experimental flow.....	37
Figure 3-2. (a) The form and size of the truncated glass substrate and (b) the test scheme of adhesion strength.	43
Figure 3-3. Test assembly of thermal conductivity measurement.....	48
Figure 4-1. Conversion versus the time of UV irradiation for various monomers.	51
Figure 4-2. Conversion rate versus UV irradiation time for acrylate and epoxy groups in HDDA.....	52
Figure 4-3. Shrinkage change versus UV curing time of resin containing TPPG, BVBP and HDDA monomers.....	53
Figure 4-4. Surface morphology of epoxide resins containing (a) TPPG (b) BVBP and (c) HDDA after UV curing.....	54
Figure 4-5. Adhesion strength and scatter range for the various monomers.	55
Figure 4-6. The R-value versus adhesion strength of resins containing polyol monomer.	57
Figure 4-7. Adhesion strength <i>versus</i> numbers of hydroxyl group of polyol monomers.....	58
Figure 4-8. Surface morphology of epoxide resins containing (a) EOM (b) PCAT after UV curing.	59
Figure 4-9. ¹ H-NMR spectra of vinyl silane (a) before UV irradiation and (b) after UV irradiation.	60
Figure 4-10. Conversions of resin samples evaluated by absorbance change of peak corresponding to (a) –SiCH=CH ₂ group located at 975.4 cm ⁻¹ and (b) epoxy group at 910 cm ⁻¹ of FTIR spectra <i>versus</i> the UV irradiation times.....	61
Figure 4-11. FTIR spectra of vinyl group silane and silane blended with photoinitiator after UV curing for 60 min.....	64

Figure 4-12. ^{13}C -NMR spectra of (a) the alkoxy group of vinyl silane and (b) vinyl silane blended with photoinitiator after UV curing. ^1H -NMR spectra of (c) the alkoxy group of vinyl silane and (d) vinyl silane blended with photoinitiator after UV curing.	65
Figure 4-13. ^{13}C -NMR spectra of (a) the epoxy silane and (b) epoxy silane blended with photoinitiator after UV curing. ^1H -NMR spectra of (c) the epoxy silane and (d) epoxy silane blended with photoinitiator after UV curing.	67
Figure 4-14. ^1H -NMR spectra of (a) vinyl silane and (b) vinyl silane blended with photoinitiator after UV curing.	69
Figure 4-15. ^1H -NMR spectra of (a) acrylic silane and (b) acrylic silane blended with photoinitiator after UV curing.	70
Figure 4-16. ^1H -NMR spectra of (a) methacrylic silane and (b) methacrylic silane blended with photoinitiator after UV curing.	71
Figure 4-17. ^1H -NMR spectra for (a) amino silane and (b) amino silane blended with photoinitiator after UV curing.	72
Figure 4-18. OM images of epoxide resins containing: (a) vinyl, (b) epoxy, (c) amino, (d) acrylic, (e) methacrylic silanes and (f) free of silane additive after UV curing.	73
Figure 4-19. Adhesion strength of epoxide resins containing various types of silanes to ITO glass.	75
Figure 4-20. Adhesion strengths of epoxide resins containing different weight percentages of vinyl silane to ITO glass.	76
Figure 4-21. UV conversion versus the irradiation time of resin samples containing various amounts of 3-amine.	77
Figure 4-22. 4-amine mixed with BPO before and after UV irradiation.	79
Figure 4-23. ^1H -NMR spectra of 4-amine mixed with BPO (a) before UV irradiation and (b) after irradiation.	80
Figure 4-24. Structure of radicals generated by reactions of singlet oxygen with (a) 1-amine, (b) 2-amine, (c) 3-amine, (d) 4-amine and (e) 5-amine.	80
Figure 4-25. 1-amine mixed with BPO before and after UV irradiation.	81
Figure 4-26. Thermal conversion of resin samples containing various types of amines subjected to post-curing at 80°C	84
Figure 4-27. (a) Adhesion strengths of resins containing 3-amine and 5-amines cured in air ambient and airtight environment. Adhesion strengths of resins contained	

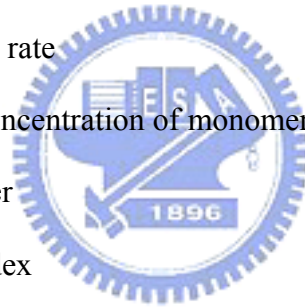
various types of amines on (b) glass and (c) ITO substrates (d) shore D hardness of resins contained 1- to 4-amines. Adhesion strengths of resins contained various types of amines on (e) PET and (f) stainless steel substrates.....	87
Figure 4-28. The transmittance changes <i>versus</i> the BPO contents of resin samples. ...	89
Figure 4-29. (a) ΔE^*_{ab} and (b) ΔYI values of resin samples containing various type of tertiary amines subjected <i>versus</i> the UV irradiation time.	91
Figure 4-30. (a) ΔE^*_{ab} and (b) ΔYI values of resin samples containing various type of tertiary amines subjected <i>versus</i> the post-curing temperatures.....	92
Figure 4-31. Transmittance of resin sample containing various amounts of 3-aimine.	93
Figure 4-32. Dielectric constants of hBN-resins as a function of test frequency.	95
Figure 4-33. Dielectric constants of composite resins as a function of filler content measured at 1 GHz.....	96
Figure 4-34. Tangent loss of composite resins as a function of filler content measured at 1 GHz.	97
Figure 4-35. Isothermal DSC thermograms of hBN-resins obtained at 150°C.	98
Figure 4-36. Conversion of hBN-resins.....	99
Figure 4-37. Isothermal DSC thermograms of hBN and SiO ₂ -resins containing 25.7 vol.% filler.....	100
Figure 4-38. CTE as a function of hBN and SiO ₂ content.....	101
Figure 4-39. Thermal conductivity of an EMC with various volume fractions of filler.	102
Figure 4-40. SEM morphology of (a) hBN-resin and (b) SiO ₂ -resin.	102
Figure 4-41. Adhesion strengths of hBN- and SiO ₂ -resins on various types of substrates.....	104
Figure 4-42. Adhesion strengths as a function of filler content of hBN-resin on various substrates	104

Table Captions

Table 2-1. A comparison of thermal- and UV-curable resins.....	11
Table 2-2. Comparison of free-radical and cationic polymerization resins.....	12
Table 2-3. Commerical Sealing Resins for OLED Packaging.....	15
Table 2-4. A summary of studies related to momomers for cationic polymerization.....	20
Table 2-5. Dielectric properties of inorganic fillers.....	32
Table 3-1. The types and chemical structures of monomers.....	35
Table 3-2. Structures and designated names of organo-functional silanes.....	36
Table 3-3. Chemical structures and designated names of tertiary amines.....	36
Table 4-1. Number of hydroxyl group (–OH) of various poly monomers.....	58
Table 4-2. Curing times of samples containing various silanes.....	74
Table 4-3. CTE and T_g of resin samples containing various types of amines.....	84
Table 4-4. ΔL^* , Δa^* , Δb^* , ΔE^*_{ab} and ΔYI of resin samples with different BPO content.....	89
Table 4-5. ΔL^* , Δa^* , Δb^* , ΔE^*_{ab} and ΔYI of resin samples containing tertiary amines.	93
Table 4-6. T_g of hBN-resins measured by DSC.....	99
Table 4-7. Viscosity of resins at various hBN loadings.....	105

List of Symbols

d_{before}	Density of sample before curing
d_{after}	Density of a resin after curing
ΔH_T	Total enthalpy change
CTE	Coefficient of thermal expansion
T_g	Glass transition temperature
ΔL^*	Degree of lightness
Δa^*	Coordinates designate the positions on red or green
Δb^*	Coordinates designate the positions on yellow or blue
X, Y, Z	Tristimulus values
R_p	Polymerization rate
$[M_o]$	Initial molar concentration of monomer before irradiation.
ΔE^*_{ab}	Color parameter
ΔYI	Yellowness index
ε	Dielectric constants
$\tan \delta$	Tangent loss
κ	Thermal conductivity
ε_c	Dielectric constants of the composite
ε_1	Dielectric constants of filler
ε_2	Dielectric constants of resin matrix
$(\tan \delta)_c$	Tangent loss of the composite
$(\tan \delta)_1$	Tangent loss of the filler
$(\tan \delta)_2$	Tangent loss of the resin matrix
ϕ	Volume fraction of inorganic filler.



Chapter 1

Introduction

Organic light-emitting device (OLED) become one of the promising flat panel displays (FPDs) technologies in the new millennium due to its excellent properties such as low power consumption, high efficiency, wide viewing angle, fast response time and compact and lightweight natures [1]. At present, bottleneck for the realization of OLEDs is the packaging technologies that must offer excellent hermetic sealing in order to prevent the moisture/oxygen attack on light-emitting materials and highly active cathode electrode in the devices. Sealing of electronic devices can be accomplished by three ways: plastic, ceramics and metal. Conventional plastic packaging is impractical to OLEDs since it utilizes thermal molding to achieve the sealing. This is opposite to the fact that the light-emitting materials in OLEDs cannot tolerate high-temperature thermal processes [2], not even mention the high pressures involve during the hardening of sealing resins. Besides, plastic packaging is non-hermetic. Ceramic and metal packagings both provide good hermetic capability; unfortunately, they are not applicable to OLED packaging since their sealing processes often required high temperatures. Localized sealing methods such as welding could avoid overall heating of devices, however, it is unlikely to perform such a process on the ITO substrates of OLEDs due to the existence of anode electrode. In the sealing of conventional bottom-emitting OLEDs, first the UV-curable sealing resin is dispensed on the edge of ITO substrate that already contains sequent layers of light-emitting material and cathode electrode. A metal or glass lid is then pressured on the frame-like resin region and the whole structure is sent to the ovens for UV curing and post thermal baking to complete the sealing. The UV-curable resins

with good physical/chemical properties are thus specifically required for packaging of OLEDs. In addition, as the developing trend switches from bottom-emitting OLEDs to top-emitting OLEDs (TOLEDs) and flexible OLEDs (FOLEDs), encapsulation of devices is accomplished all over the light-emitting area so that transparency of resins becomes a further requirement for sealing resins [3-4].

The key components of UV-curable resins include oligomer, monomer and photoinitiator. According to either monomer type or photoinitiator type, the UV-curable resins can be classified into two main catalogies: free-radical photo-polymerization and cationic photo-polymerization. Most of the UV-curable resins are free-radical polymerization; however, they are not suitable for OLED packaging due to its inferior adhesion, low resistance to oxygen permeation and high etiolation under UV irradiation. As to the UV-curable epoxide resins *via* cation polymerization, their advantages include low shrinkage, good mechanical properties and high adhesion strengths on various substrates. Recently, many researches efforts have been poured on the developments of UV-curable epoxide resins specifically for OLED packaging [5]. The primary purpose of this work is hence to explore the UV-curable epoxide resins so that a collaboration development of sealing resins for OLEDs packaging can be accomplished. We respectively studied at the effects of monomer type, organo-functional silane types and tertiary amine types on the curing process, adhesion and related physical properties of the epoxide resins. The effects of tertiary amine types on the etiolation improvements of resins were also investigated in detail. With the knowledge obtained above, the resins with satisfactory properties were also adopted to prepare the underfill resin containing hBN inorganic filler for filp-chip interconnection.

In the part of study related to monomer types, polyol, vinyl ether and acrylate monomers were chosen and their effects on the cationic polymerization and adhesion

of epoxide resins were investigated. It is found that the resin sample containing polyol monomer possesses the lowest polymerization reaction rate, the smallest shrinkage and the highest adhesion strength on glass substrate. Thus resin containing polyol monomer was also chosen as the base for subsequent studies related to organo-functional silane and tertiary amines.

In the part of study related to organo-functional silanes, vinyl, epoxy, amino, methacrylic and acrylic groups were chosen and the adhesion strengths of resins containing various silanes on ITO and glass substrates were studied. The vinyl silane was found to be able to promote the free-radical polymerization and the sample containing 1.0 wt.% of vinyl silane possessed the highest adhesion strengths of 91.42 kg/cm² on ITO glass and 153.35 kg/cm² on glass substrate.

Etiolation of UV-curable resin was resulted from the residual free radicals generated by photolysis of photoinitiator, polymer or photosensitizer. Though imidazole and other types of tertiary amines have been widely studied in the field related to thermal polymerization [6-9], their effects on the UV-curable epoxide resins and key physical properties are rarely reported. In this part of work, tertiary amines including imidazole, 1,2-dimethylimidazole, 2,4,6-tris(dimethylamino-methyl)phenol, 1-methylimidazole, and 2-methylimidazole were respectively added into the UV-curable epoxide resins and their effects on UV curing process, etiolation and adhesion were examined. The experimental results indicated that the addition of 2,4,6-tris(dimethylamino-methyl)phenol provided the best curing characteristics and physical property improvements of UV-curable epoxide resins. In addition to the best improvements of adhesion strengths on various substrates, such as glass, ITO, PET and stainless steel, appropriate amount (about 1.0 wt.%) of 2,4,6-tris(dimethylamino-methyl)phenol added in the resins also offered the highest UV reactivity, highest T_g (= 72.3°C), the lowest CTE (= 70.8 ppm/°C) and the best etiolation suppression (ΔYI and

ΔE^*_{ab} as low as 11.27 and 6.48, respectively) of the UV-curable epoxide resins.

In the part of study related to underfill resin containing hBN filler, it was found that the addition of hBN is able to improve the dielectric properties of resin. It may also improve the physical properties such as CTE, T_g and thermal conductivity. However, increase in hBN content might deteriorate the adhesion strength of the composite resins and the adhesion strengths of hBN resin on various substrates was found to be in the order of alumina (Al_2O_3) > Si > eutectic PbSn solder.



Chapter 2 Literature Review

2.1. Introduction of OLED Packaging

Figure 2-1 depicts the typical structure of OLEDs consisting of ITO glass substrate with anode electrode, hole-transport layer, hole-injection layer, light-emitting layer, electron transport layer, and cathode electrode [10]. The light-emitting layer inside can be either small-molecule or polymer based. The anode electrode is transparent conducting material with good hole injecting capability. It can be either ITO or a combination of ITO and poly(ethylenedioxy) thiophene (PEDOT). Insertion of hole transport material such as *N,N'*-diphenyl-*N,N'*-(3-methylphenyl)-[1,1' biphenyl]-4,4'-diamine (TPD) is for the enhancement of thermal stability and decrease of energy gap between hole transport layer and anode [11].

Various organic light-emitting materials have been developed for RGB color requirements. Tang and van Slyke adopted tris(8-hydroxyquinoline)aluminum (Alq_3) as light-emitting/electron transport layer, triaryl amine as hole transport layer to prepare the first thin-film type OLED [10]. Alq_3 was subsequently utilized as the singlet host material in the guest-host doped emitter systems, a key concept on the development of OLEDs, and incorporated with various dopants to emit desired lights. For instance, Alq_3 can be doped with various coumarin compounds to emit orange, green and blue lights, respectively [12]. Further, anthracene and its derivatives (ADN) have been widely used as the blue light-emitting materials [13]. The cathode electrode must possess good electron injecting properties and low work function. Presently, the available metals and alloys satisfied such requirements include Ca, Ag, Al, AlLi, Mg, MgAg, *etc.* However, they are highly active and may not be exposed in air ambient

during device operation. Besides, it is known that the light-emitting layers are vulnerable to the attack of moisture/oxygen [14]. A hermetic packaging structure is thus required for OLEDs.

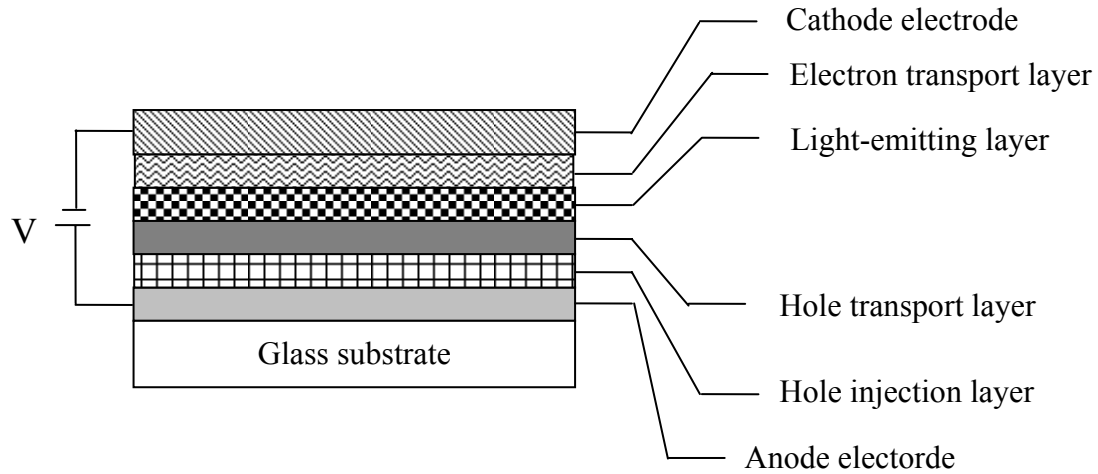


Figure 2-1. Schematic structure of the OLED device [10].

There are many studies relating to the deterioration of OLEDs [15]. Most of them agreed that the dominant degradation mechanism in un-encapsulated OLEDs is the exposure of the organic-cathode interface to ambient moisture and oxygen. This leads to the oxidation and delamination of the active cathode as well as the chemical reactions of the light-emitting layers during device operation [16]. In order to inhibit the degradation, the packaging of OLEDs are commonly accomplished by first dispersing the UV-cured sealing adhesive around the active part of the device. After attaching a metal or glass lid on the frame-like resin region on ITO substrate, the UV curing is then carried to complete the sealing [17]. A schematic packaging structure of conventional bottom-emitting OLED is illustrated in Fig. 2-2. The sealing process must be carried out in an extremely dry ambient (< 1 ppm v/v; dew point = -76°C) [18] or at least in an atmospheres purged with dry nitrogen or argon. Desiccant such as calcium oxide (CaO) or barium oxide (BaO) is often spread on the device side of lid so as to getter the residual moisture/oxygen in the package or the undesired

substances diffusing through the sealing resin afterward [10]. Further, in order to terminate the photo-polymerization, increase the crosslinking density and eliminate residual stress of sealing resin, a post thermal curing at 80°C for 1 hr is usually performed.

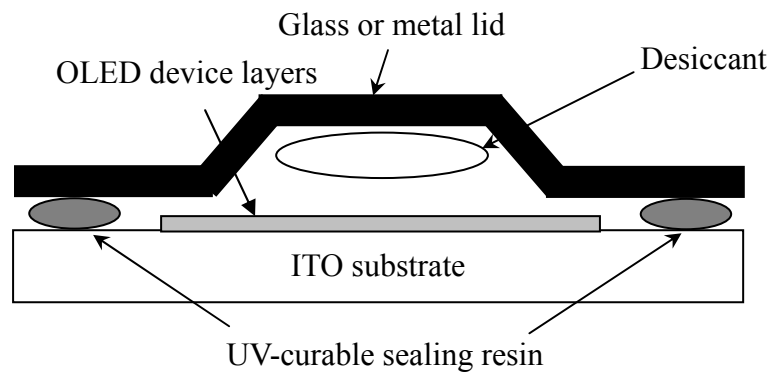


Figure 2-2. Encapsulation methods for conventional bottom-emitting OLEDs.

Conventional lid-attachment packaging methods described above become inapplicable as the developments of OLEDs switching to TOLED and FOLEDs. The metal lid is incompatible with TOLEDs since it is not transparent; it may be replaced by glass lid or the devices may be encapsulated directly by resins with suitable transparency. FOLEDs cannot be capped by metal or glass lid due to its rigidity. As shown in Fig. 2-3, encapsulation methods utilizing transparent, multiple organic and inorganic barrier coatings for FOLEDs has been demonstrated [19-20].

2.2. Sealing Technologies of Electronic Devices

The sealing technologies in electronic packaging can be classified into ceramic packaging, metal packaging and plastic packaging according to packaging structure and material usage. Ceramics/glasses and metals have relatively low moisture and gas permeability and hence ceramic packaging and metal packaging are known as the hermetic packaging. In these two types of packagings, hermetic sealing is achieved by

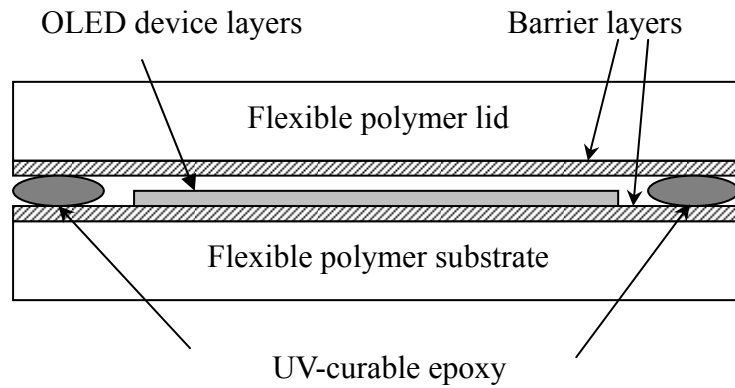


Figure 2-3. Encapsulation methods utilizing transparent, multiple organic and inorganic barrier coatings for FOLEDs [14].

one of the following methods: welding, brazing, soldering or glass frit sealing. However, these sealing methods all demand relatively high processing temperatures (*e.g.*, commercial soldering process reaches as high as 350°C) that would definitely destroy the light-emitting material in OLEDs. Further, welding, brazing and soldering all require certain type of sealed interface metallization that is incompatible with the substrate fabrication of OLEDs. Brazing and soldering may also leave flux to reside in the packaging, which is harmful to the reliability. As a result, it may rule out the applications of ceramic packaging and metal packaging to OLEDs.

It seems plastic packaging is the only choice for OLED packaging. Plastic packaging indeed provides advantages such as thin outline appearance, ease of automation and low cost. However, it does *not* offer the hermetic sealing since the encapsulation resins are polymeric that do not resist well to moisture/gas permeation. Modification of resin structure to suppress its permeability is hence a must if plastic packaging were applied to OLEDs. Further, conventional plastic packaging employs thermal molding, radical spray or stencil printing to achieve the device sealing. They are impractical to OLED packaging since in these processes the polymeric resins are *directly* encapsulated on the device parts. In addition, these processes use

thermosetting resins, *i.e.*, the high temperatures and pressures involved in subsequent thermal curing of resins would definitely damage the light-emitting layer and active cathode electrode of OLEDs. In order to suppress the possible deteriorations caused by thermal effects, OLEDs hence requires UV-curable resins to achieve the sealing. The packaging structure commonly seen in conventional bottom-emitting OLEDs is illustrated in Fig. 2-2.

2.3. Requirements of Sealing Resins for OLED Packaging

For the sealing resins for OLED packaging, appropriate thermal properties compatible with those of substrate materials, high mechanical strengths, low outgassing, low oxygen permeability ($< 10^{-5}$ cc/m²/day) and moisture permeability ($< 10^{-6}$ g/m²/day) are generally require for satisfactory reliability [21]. In application points of view, low curing temperature, fast polymerization rate, high T_g , high adhesion strengths on various substrates and appropriate flow properties are specifically demanded.

In addition to the diffusion through the resin matrix, moisture and oxygen atoms may also permeate into the device *via* the resin/substrate and/or resin/lid interfaces to induce the degradation. Hence, good adhesion properties of resin on substrate and anode electrode are required. Meanwhile, it may enhance the permeation and adhesion strength of resin by the addition of appropriate inorganic fillers [22]. Therefore, the choice of monomer is essential for the synthesis of resins for OLED packaging because the monomer type affects the reaction rate, shrinkage and adhesion strength of resin.

Outgassing of resins may result from the following sources: moisture in resin formulation, silane coupling agent, by-product of resin and cationic photoinitiator [23]. The outgassing phenomenon can be eliminated by: (i) curing at room-temperature and

reducing the curing time so as to avoid the evaporation of low molecular weight elements in coupling agent; (ii) utilizing the resin with solvent-free formula; (iii) utilizing the low volatility, high-purity elements for resin synthesis; (iv) increasing the crosslinking density of resin to suppress the permeation path of moisture and oxygen.

2.4. Comparisons of UV- and Thermal-curable Resins

During the past two decades, the science and materials related to photopolymerization have grown from esoteric researches into various industrial applications and become one of importance topics in polymer science and technologies. Inherency of these studies is the use of a specific photoactivator system that is able to absorb the incident UV and/or visible radiation and convert monomer or prepolymer into polymer or crosslinked network. In recent years, many studies related to the synthesis and photochemical properties of novel photoinitiators with more desirable properties haven been proposed [24-25]. The photoinitiators are virtually 100% “solids” and essentially there is no solvent or moisture entrapped in the adhesive stratum. Compare to traditional solvent-based or water-based thermal-curable resins, the UV-curable resins generally possess less shrinkage [26]. A comparison of thermal- and UV-curable resins is given in Table 2-1.

According to Table 2-1, though the thermal-curable resins exhibit higher T_g , lower CTE and higher adhesion strengths than those of UV-curable resins, they do not fit to OLED applications due to higher curing temperatures, longer curing times and solvent-contained. As a result, how to improve the properties such as T_g , CTE and adhesion strength of UV-curable resins becomes a challenge for their applications to OLED packaging.

Table 2-1. A comparison of thermal- and UV-curable resins.

Properties	Thermal-curable resins	UV curable resins
Propagation	Thermal	UV light
Curing temperature	High	Low (room temperature)
Curing time	Long	Short
Solvent	Yes	No
Shrinkage	Large	Small
T_g	High	Low
CTE	Low	High
Adhesion strength	High	Low

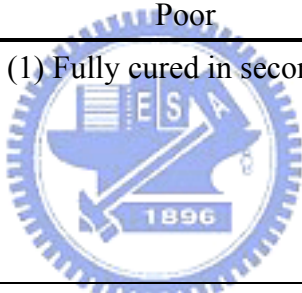
2.5. Comparison of UV-Curable Epoxy and Acrylic adhesives

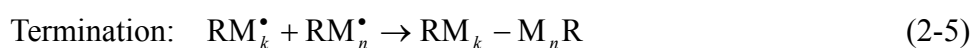
UV-curable resins have been widely used in many applications such as coatings, encapsulation, inks, adhesives, and in the preparation of assembly substrates due to its fast curing and solvent-free features [27]. According to photoinitiator or monomer type in the resins, UV-curable resins can be classified into epoxy and acrylic resin systems that their photo-polymerization are *via* cationic polymerization and free-radical polymerization, respectively. Table 2-2 presents the comparison of chemical/physical properties, advantage and disadvantage of free-radical and cationic polymerization resins.

The mechanisms of free-radical polymerization include radical formation from initiator, initiation, propagation and termination [28]. As shown in Eq. (2-1), free radicals formed when the photoinitiator is irradiated by UV light. The free radicals then couple with monomers to initiate more free radicals as shown in Eq. (2-2). Initiation creates a free radical of polymer and a hydrogen atom with an unpaired electron. Propagation involves a variety of reactions (see Eq. (2-3)) and one of these is the reaction of free radical with an oxygen molecule to form a peroxy radical (Eq. (2-4)). The termination of photodegradation can be achieved by mopping up the free radicals to create inert products (Eq. (2-5)). This occurs naturally by the combination

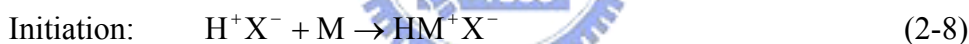
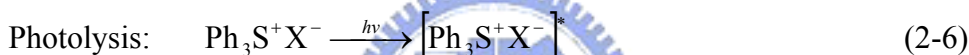
of free radicals or can be assisted by using stabilizers in the polymer.

Table 2-2. Comparison of free-radical and cationic polymerization resins.

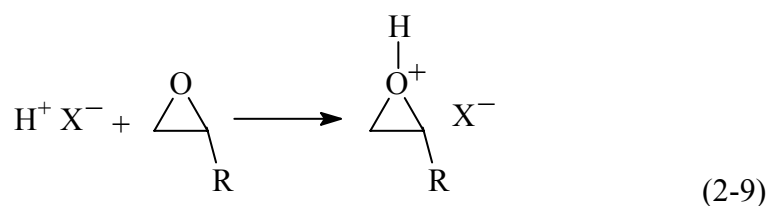
Chemical/physical property	Free-radical polymerization	Cationic polymerization
Main component	Acrylic	Epoxy
Polymerization rate	High	Moderate
Initiation	UV	UV
Propagation	UV	UV and thermal
Post thermal curing	No	Yes
Oxygen resistance	Poor	Good
Moisture resistance	Good	Poor
Shrinkage	Large	Small
Adhesion strength	Moderate	High
Chemical resistance	Moderate	Good
Outgassing	Poor	Good
Advantages	(1) Fully cured in seconds. 	(1) Excellent pot life; (2) Multi-performance after cured (heat resistance/low shrinkage).
Disadvantages	(1) Poor oxygen inhibition; (2) Poor adhesion; (3) High shrinkage; (4) High outgassing.	(1) Poor moisture resistance; (2) Photo-polymerization inhibited by alkali compound; (3) Fully cured in mins.



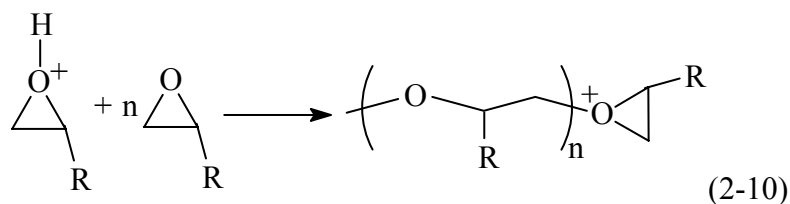
The mechanisms of cationic polymerization include photolysis, initiation, propagation and termination [29]. Photolysis occurs as the UV irradiation generates a number of reactive species (see Eqs. (2-6) and (2-7)) that subsequently react with the monomer to release the Brønsted acid (2-8). In the propagation step, ring-opening polymerization takes place by the attack of Brønsted acid to the epoxy groups and then repeating the addition of molecules of the monomer on to the oxiranium ion of polymer chain end as show in Eq. (2-9). Termination of the growing ionic chain can be caused by hydrogen-donating molecules as shown in Eq. (2-10). In cationic polymerization, termination process is relatively slow and is known to responsible to the dark cure phenomenon.



Propagation:



Termination:



The activation steps are similar in free-radical and cationic polymerization, however, initiation and propagation of free-radical polymerization are faster than those of cationic polymerization.

The UV-curable epoxy resins are specifically applicable to OLED packaging due to their small shrinkage, excellent adhesion strengths and good resistance to chemical/oxygen permeation. Oligomers of UV-curable epoxy resins *via* cationic polymerization include glycidyl ether [30], cycloaliphatic epoxide [31] and oxetanes [32-33]. The cycloaliphatic epoxide containing epoxycyclohexane rings that possess higher polymerization rate in comparison with other known epoxide monomers such as glycidyl ethers, glycidyl esters, and epoxides of α -olefins [34]. The ester and ether groups in glycidyl ethers are considerably less reactive than oxiranium cations in cycloaliphatic epoxide. The presence of ester and ether groups in monomers thus depresses their reactivity [35]. In addition, the ring strain of ethylene oxide (epoxy group) are known to be 114 kJ/mole while that for oxetane is 107 kJ/mol [36]. At the same time, the basicity (pK_a) for above two ethers is 3.7 and 2.02 [37], respectively. Thus, with similar steric factors and ring strains in both cyclic ethers, the basicity of oxetane is considerably larger than that of ethylene oxide. Oxetanes is then more reactive than cycloaliphatic epoxides during the cationic photo-polymerization. The order of polymerization rate is oxetanes > cycloaliphatic epoxide > glycidyl ether, therefore adhesion strength of glycidyl ether will be the lowest when the three cyclic ethers are subjected to the same exposure time span of UV irradiation [34]. Further, adhesion strength of oxetanes is lower than that of cycloaliphatic epoxide due to its small molecular weight and fewer hydroxyl groups [38]. The cycloaliphatic epoxides thus become the most appropriate oligomer type for UV-curable epoxy resins applied to OLED packaging. Cycloaliphatic epoxides were hence adopted as the oligomer for sample preparation in this work

2.6. Commercial Sealing Resins for OLED Packaging

Most of the commercially available UV-curable resins for OLED packaging are of cation polymerization due to the advantages such as less outgassing during UV irradiation. Table 2-3 lists the products and properties of UV-curable resins for OLED packaging currently available in the market [39].

Table 2-3. Commercial Sealing Resins for OLED Packaging [39].

Company	Nagase Chemtex		Kyoritsu Chemicals	Taiyo Ink.	Mitsui Chemicals.
Products	XNR5516HP	XNR5516HV	8723K3	Phermetic Seal PHS-100	Structbond
Main resin	Epoxy	Epoxy	Epoxy	Epoxy	Epoxy
Exteriority	Ivory	Ivory	Undertone-biscuit and opaque	--	Ivory
Viscosity	--	--	10 ~ 100 Pas EHD-type, 2.5 rpm	150 Pas 25°C, E-type, 5 rpm	60 ~ 150 Pas EHD 3° Corn, 2.5 rpm
T_g	131°C (DMA)	134°C (DMA)	155±5°C (TMA)	80°C (TMA)	120±10°C (TMA)
CTE	37 ppm/°C	39 ppm/°C	88 ppm/°C	---	50±10 ppm/°C
Shrinkage	4%	3%	---	---	---
Moisture absorption	1.0 % 25°C, 168 hrs	1.0 % 25°C, 168 hrs	---	---	1.0 % 100°C, 30 min
Adhesion strength	140± 50 kg _f /cm ² Pull test	140± 50 kg _f /cm ² Pull test	---	1 MPa Corning#1737	150±30 kg _f /cm ² Glass cross peel
Mositure permeability	16 g/m ² -day 60°C/90%RH, thickness: 100 μm	16 g/m ² -day 60°C/90%RH, thickness: 100 μm	10.6 g/m ² -day (85°C/85%RH) 4.9 g/m ² -day; (65°C/95% RH)	20 g/m ² -day 65°C/90%RH, thickness: 100 μm 8.5 g/m ² -day 65°C/90%RH, thickness: 100 μm	70±10 g/m ² -day 80°C/95%RH, thickness: 100 μm 9±2 g/m ² -day 40°C/90%RH, thickness: 100 μm
Cure conditions	6 J/cm ² + 80°C/1hr	6 J/cm ² + 80°C/1hr	6 J/cm ² + 100°C/10min or 80°C/30min	2 J/cm ² + 80°C/1hr	8 J/cm ²

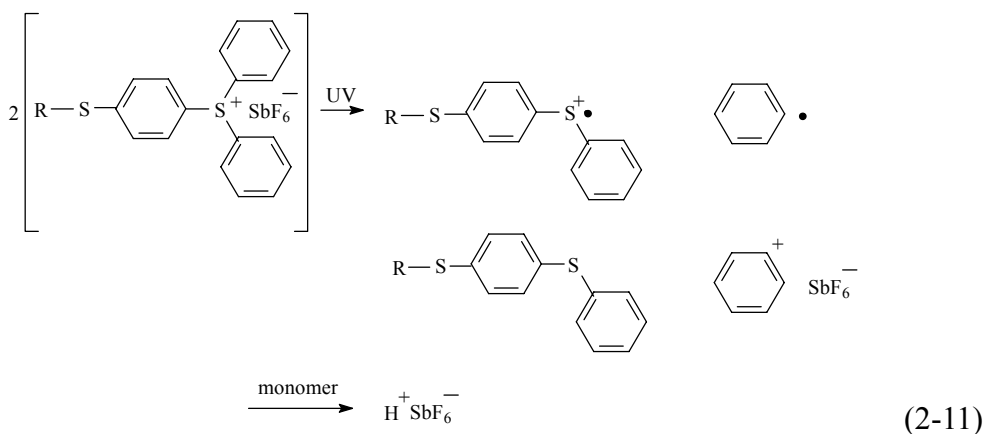
2.7. Formulations of UV-curable Epoxide Resins

There are three essential components of UV-curable epoxide resins: oligomer, photoinitiator and monomer. The maximum amount of oligomer is determined by its molecular weight that, in turn, is determined by the maximum viscosity that could be handled by the end user. In addition, a high molecular weight and low functionality ensure the small shrinkage and thereby the good adhesion strengths. The photoinitiator and monomer determine the reactivity, viscosity, physical properties and reaction mechanism of resin during UV irradiation. Other additives such as silane coupling agent and tertiary amines are for the promotion of adhesion strength, acceleration of thermal crosslinking density, and suppression of etiolation. In below, reaction mechanisms of the photoinitiator, monomer, silane coupling agent and tertiary amines in epoxide resins during UV irradiation are discussed.

2.7.1. Reaction Mechanisms of Photoinitiators

Photoinitiators available for cationic polymerization include aryl diazonium salts, diaryliodonium salts and triarylsulfonium salts, phenacylsulfonium, 4-hydroxyphenylsulfonium salts, sulfoxonium salts and mixed-ligand arene cyclopentadienyl metal salts [40]. The most widely used cationic photoinitiators are the onium salts, in particular the triarylsulfonium and diaryliodonium salts. Onium salts and mixed ligand arene cyclopentadienyl metal salts with complex metal halide anions are the commercially available photoinitiators for crosslinking the epoxy groups *via* cationic polymerization. The onium salts are thermally stable ionic compounds with good solubility properties in both organic solvents and water. The most important property of onium salts is their ability to decompose and efficiently generate acid upon UV irradiation. The rates of polymerization depend on the acids derived from anion and the order of reactivity for common anions is: $\text{BF}_4^- < \text{PF}_6^- <$

$\text{AsF}_6^- < \text{SbF}_6^-$. In addition, the nucleophilicity of the counterions decreases as $\text{BF}_4^- > \text{PF}_6^- > \text{AsF}_6^- > \text{SbF}_6^-$. The tendency of the propagating chains was related to F^- abstraction and hence the highest termination of cationic chain ends by SbF_6^- [41]. This study adopted triphenylsulfonium salts as the photoinitiator since they contain the anion with the faster polymerization rate, SbF_6^- . The photolysis of triphenylsulfonium salts was first reported by Knapzyck and McEwen [42-43] and the reaction mechanism was studied by Crivello *et al.* in 1978 [44]. In particular, diaryliodonium salts and triarylsulfonium salts are also investigated as photoinitiator and thermal initiators of cationic polymerization [45]. Triarylsulfonium salts possess high thermal stability; they undergo rapid photolysis when irradiated by UV light of wavelengths ranging from 200 to 300 nm. Both homolytic and heterolytic cleavage mechanisms are involved in the photolysis of the triarylsulfonium salts photoinitiator. In the homolytic process, the excited state first cleaves to release diphenylsulfinyl radical cation, phenyl radical and anion. Equation (2-11) depicts the reactive species including aryl radicals, aryl cationic radicals, aryl cations and the Brønsted acid (H^+SbF_6^-) generated by the photolysis of the photoinitiator [44-46].



2.7.2. Reaction Mechanisms of Monomers

In UV-curable epoxide resins, monomers determine the properties of reacting systems and final cured products according to their chemical structures. As described previously, free-radical and cationic polymerizations can also be classified according to monomer types. The components containing electron-rich centers, such as the double bonds in vinyl ethers and the oxirane groups in epoxy resins, are suitable for cationic polymerization. On the contrary, electron-deficient double bonds such as those in acrylates and maleate systems may be readily polymerized in the presence of free radicals induced by appropriate photoinitiators [47].

Cationic photopolymerization was first studied by Crivello, *et al.* [41] who adopted diaryliodonium salts to react with various monomers such as cyclic ethers, cyclic formals and acetals, lactones, vinyl monomers, sulfur containing monomers, organosilicone monomers and monomers containing the epoxide group. They also discussed the cationic polymerization of multifunctional vinyl ether monomers [48] and the reactivity of cycloaliphatic epoxide [31]. Furthermore, a series of cationic photopolymerizable epoxide monomers containing benzyl, allyl, propargyl acetal and ether groups that can stabilize free radicals were synthesized [41]. These monomers may enhance the reactivity of cationic photopolymerization in the presence of onium salt photoinitiators [49].

Figure 2-4 lists the monomer types reported by Crivello [50] that can be utilized in cationic photo-polymerization and their nucleophilicities determine the rate of the attack by a cationogen and by the subsequent attack of additional monomer molecules on the growing cationic center. Among these, the most popular monomer is the epoxy group. Oxetanes monomer was also studied by Crivello *et al.* and it is the monomer type with the fastest polymerization rate [32,33,51]. In addition to epoxy monomer, vinyl ether, polyol, glycidyl ether and epoxy-functional siloxane monomer are also

investigated in details and the related studies are summarized in Table 2-4.

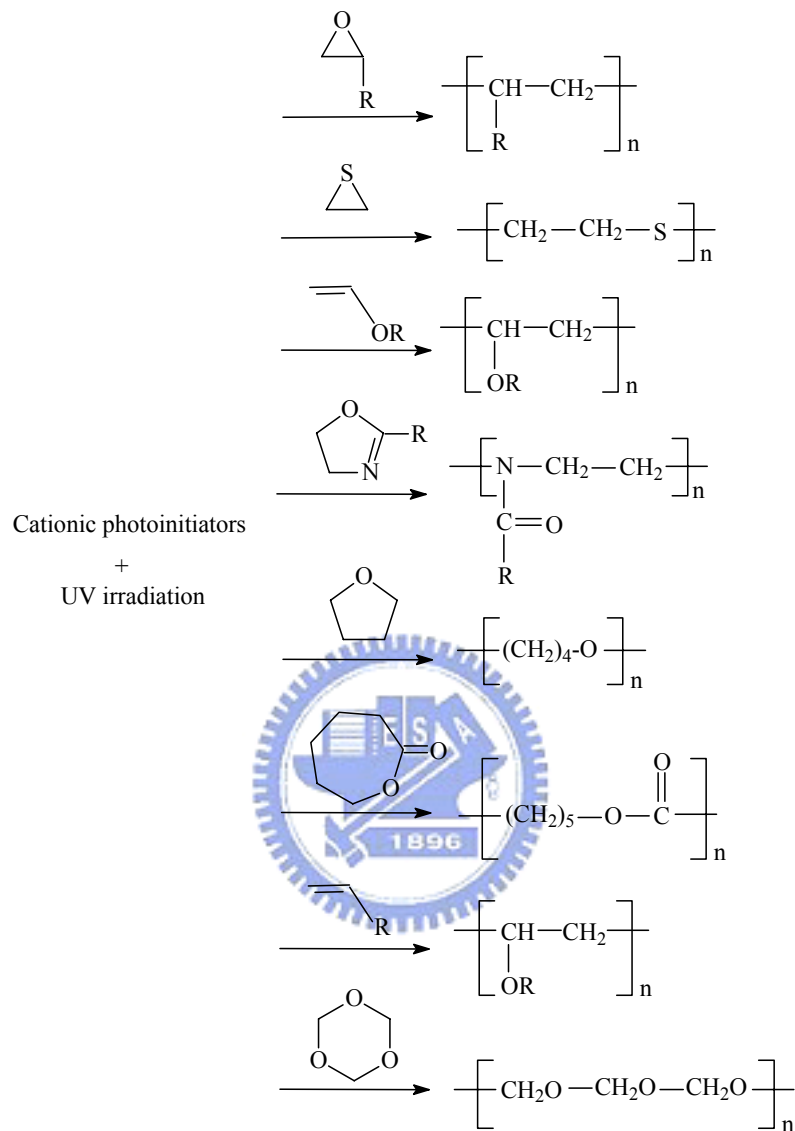


Figure 2-4. Monomer types can be utilized in photoinitiated cationic polymerization.

Table 2-4. A summary of studies related to monomers for cationic polymerization.

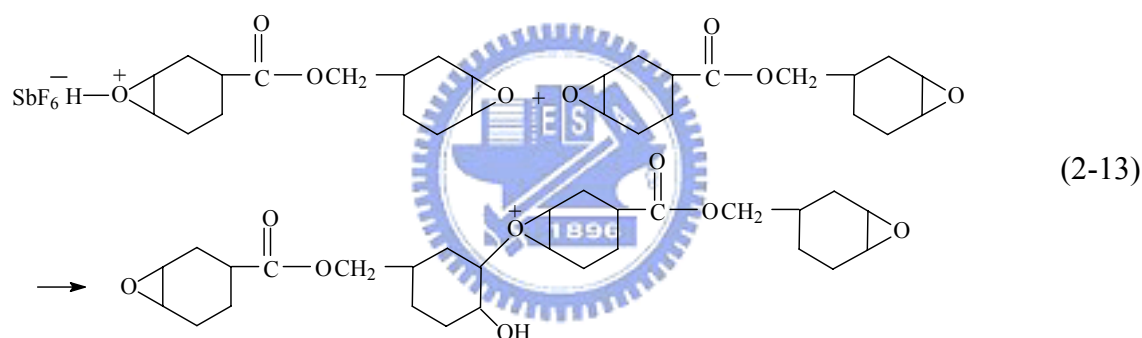
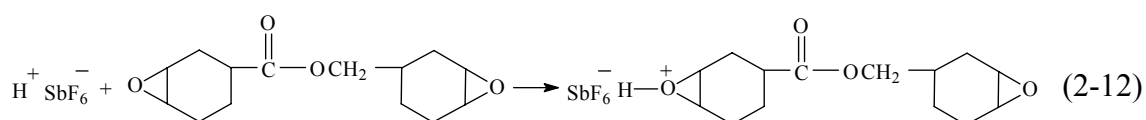
Monomer	References
Triethyleneglycol divinyl ether	Decker <i>et al.</i> (1996) [52]
Synthesis of Silicon-containing vinyl ether	Itoh <i>et al.</i> (1997) [53]
Caprolactone polyols	Wu <i>et al.</i> (1999) [54]
Poly(ϵ -caprolactone) polyols	Yagci and Schnabel (1999) [55]
Synthesis 1-butenyl and 1-pentenyl ethers	Kaur <i>et al.</i> (1999) [56]
Poly(tetrahydrofuran), poly(caprolactone triol) and ethylene glycol	Tilbrook <i>et al.</i> (2000) [57]
Diethyleneglycol divinylether and isobutylvinylether	Toba, Y. (2000) [58]
Aliphatic urethane divinylether, isophthalate divinylether Aliphatic ester divinylether	Decker <i>et al.</i> (2001) [5]
Cycloaliphatic epoxide resin, DGEBA and SU8	Boey <i>et al.</i> (2001) and (2002) [59,60]
Ethyleneglycol divinyl ether, di(ethyleneglycol) divinyl ether, tri(ethyleneglycol) divinyl ether, butanediol vinyl ether, cyclohexanedimethanol divinyl ether and glycidyl vinyl ether	Chappelow <i>et al.</i> (2002) [61]
Butyl vinyl ether and methyl methacrylate mixtures	Braun <i>et al.</i> (2002) [62]
Cyclic acetals (1,3-dioxolane, 1,3-dioxane and 1,3,6-trioxocane)	Pantiru <i>et al.</i> (2002) [63]
1-propenyl-vinyl ether	Sangermano, <i>et al.</i> (2002) [64]
Siloxane functionalized polyols, cycloaliphatic epoxide resin and ϵ -caprolactone derived polyols	Chen and Soucek (2003) [65-66]
5,5-dimethyl-1,3-dioxane-2-thione	Yonet (2003) [67]
Epoxy-functional siloxane monomers and oligomers	Jang and Crivello (2003) [68]
Oxetane Monomers, fluorinated oxetane monomer and silicon-containing oxetane monomers	Sangermano <i>et al.</i> (2004) [69,70]
Oxiranes and oxetanes	Falk, <i>et al.</i> (2005) [51]

In this work, curing behaviors of resins containing various monomers such as polyol, vinyl ether and acrylate *via* cationic polymerization were investigated. The mechanisms involved during UV exposure for each type of monomers are briefly

described as follows:

(1) Reaction Mechanisms for Epoxide Resin:

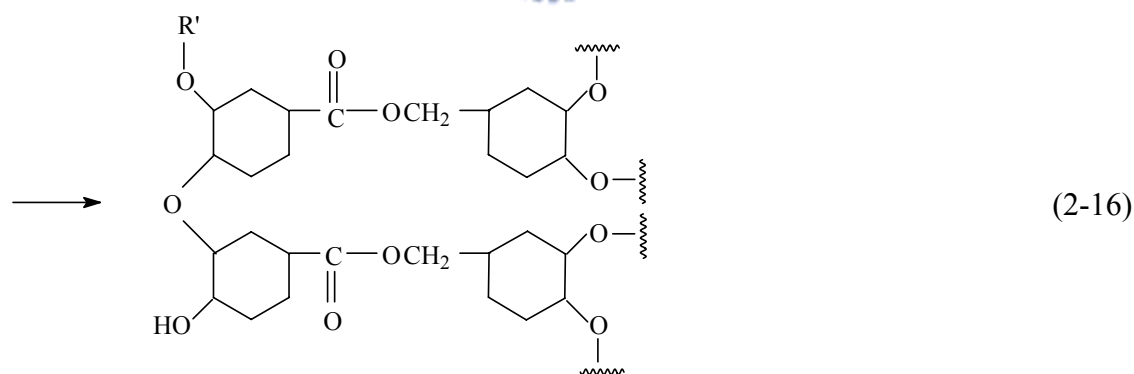
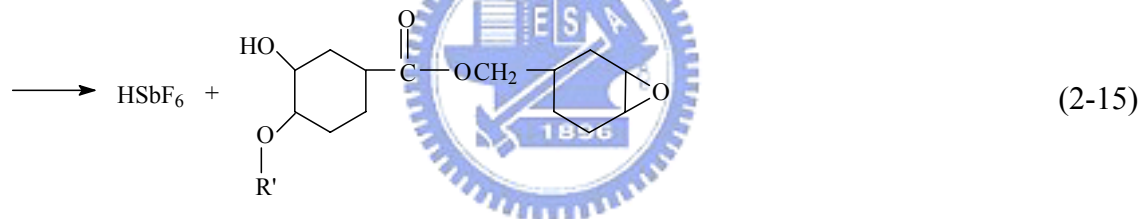
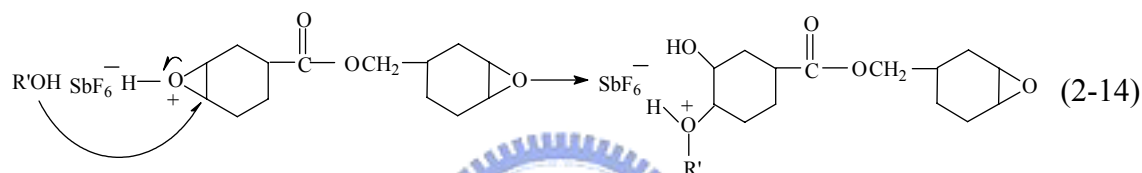
Equations (2-12) and (2-13) depict the two processes involved in the initiation of photoinitiated cationic polymerization. The H^+SbF_6^- is the strong Brønsted acid protonation which may induce the cationic polymerization of epoxide resin to produce oxiranium ion as presented in Eq. (2-12). The cationic polymerization then takes place by attacking protonated epoxide on another epoxide resin as shown in Eq. (2-13).



(2) Reaction Mechanisms for Polyol Monomer:

Cationic polymerization of the resin samples containing polyol monomer is the similarly depicted by Eqs. (2-11) and (2-13). The growing oxiranium ion chain, the product of Eq. (2-12), undergoes nucleophilic attack by the polyol to generate protonated ether as shown in Eq. (2-14). Penczek *et al.* [72] demonstrated that in the presence of polyols, the attack of the hydroxyl at the propagating oxonium ion chain end takes place more rapidly than usual ring opening mechanism. According to this, hydroxyl group of the polyol intercepts the oxonium ion terminus of the growing polyether chain. Deprotonation of hydroxyl groups of the polyol caused by the

epoxide monomer, the products of Eq. (2-14) [73], results in the termination of the growing polymer chain and transfers to the monomer to start new chains as shown in Eq. (2-15). Repetition of above process generates a hydroxyl end group for continuing the termination and transfer processes. This mechanism is expected to occur to some extent during cationic ring-opening polymerization initiated by Brønsted acids because terminal hydroxyl groups are always formed as end groups shown in Eq. (2-16). Therefore, the presence of polyols has considerable effect on the cationic ring-opening polymerization of UV-curable epoxide resins [74].

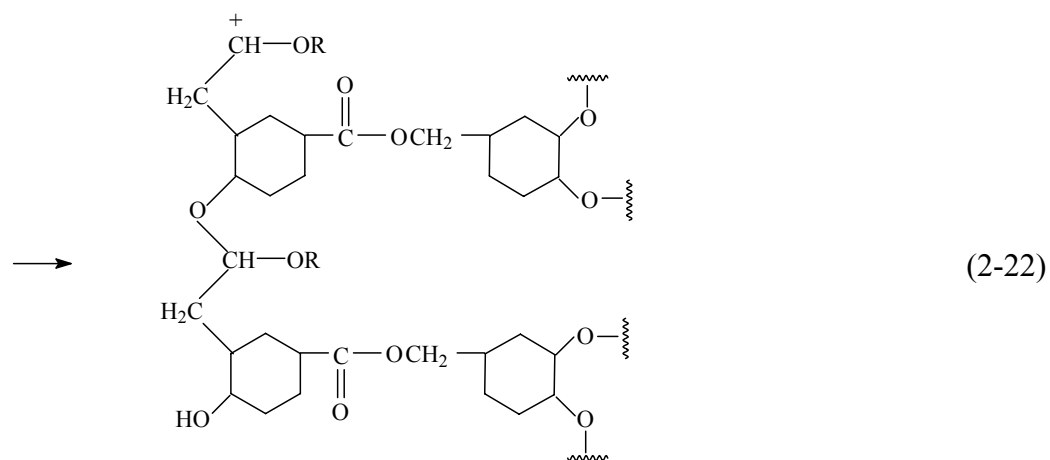
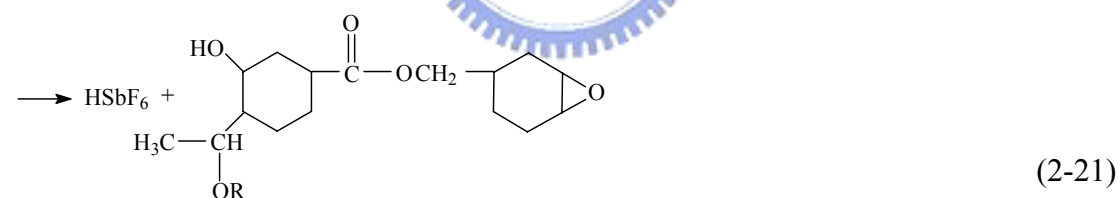
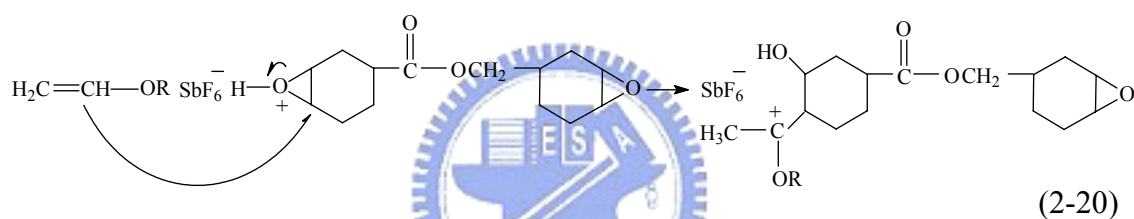
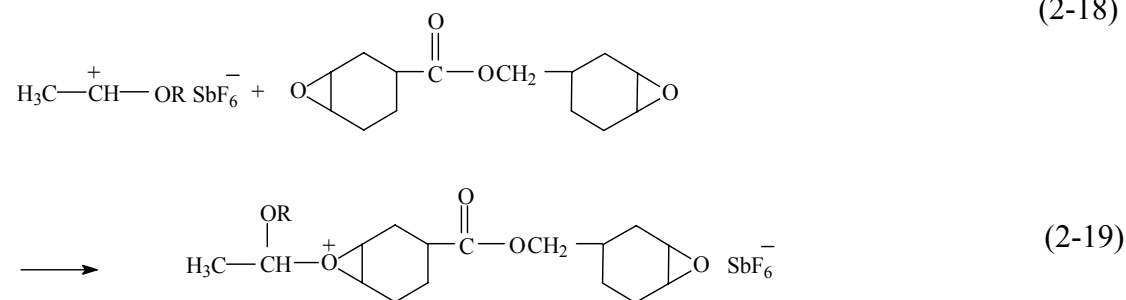
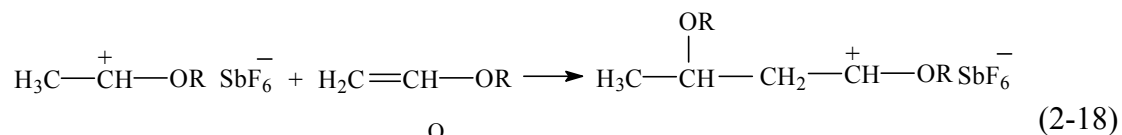
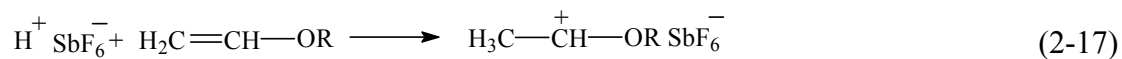


(3) Reaction Mechanisms for Vinyl Ether Monomer:

Vinyl ether monomers possess a much more pronounced tendency toward cationic polymerization and do not undergo free-radical polymerization because they contain electron-rich centers, *e.g.*, the highly nucleophilic double bonds caused by

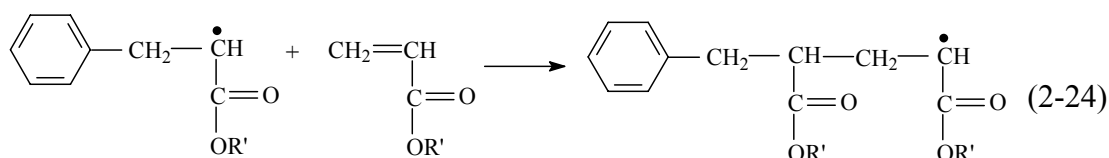
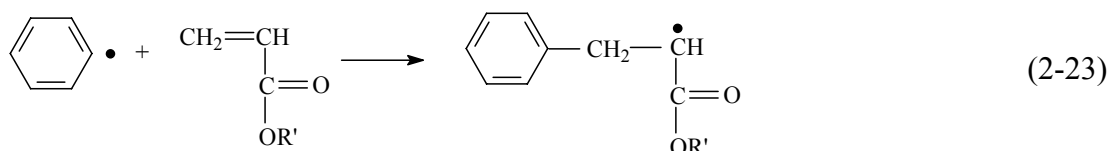
onium ions and alkoxy groups [62,75]. Vinyl ether monomers, featured by a combination of π -donor ($C=C$) and n -donor ($R-O^+(R)_2$, onium ions), contain two nucleophilic sites [76]. The polymerization mechanisms for resin samples containing vinyl monomer are the same as shown in Eqs. (2-11) to (2-13). From Eq. (2-17), the formation of active species for the initiation of cationic polymerization takes place by the attack of nucleophilic on a vinyl ether group to generate the alkoxy-carbenium ion. In Eqs. (2-12) and (2-17), only the attack by protons is shown because they are the most prominent species involved in the initiation. The rates of both reactions are expected to be fast. The carbocation, formed by the initial protonation of the vinyl ether groups, can induce polymerization of either other vinyl ether or an epoxide group as shown in Eqs. (2-18) and (2-19) [50,77]. Cationic polymerization of the protonated epoxide of Eq. (2-19) and oxiranium ion can take place by the nucleophilic attack of vinyl ether group as shown in Eq. (2-20). It results in the termination of the growing polymer chain and transfers to the monomer that thereafter can form start new chains shown in Eq. (2-21). The two possible reactions, the propagating oxiranium ions are converted into alkoxy-carbenium ions and *vice versa*, are shown in Eqs. (2-19) and (2-20). Similar crossover reactions can be written for any reactive chain end generated during the course of the polymerization and the positions of these equilibration are dependent on the relative stabilities of the two types of reactive species and the corresponding reactivities of the two monomers. Repetition of this process regenerates an ether end group that continues the termination and transfer processes. This mechanism is expected to occur to some extent during the cationic epoxide ring-opening polymerizations initiated by Brønsted acids because terminal alkoxy groups always form as the end groups as shown in Eq. (2-22). Cationic polymerizations of vinyl ether adhesive resin system are shown in Eqs. (2-13) and

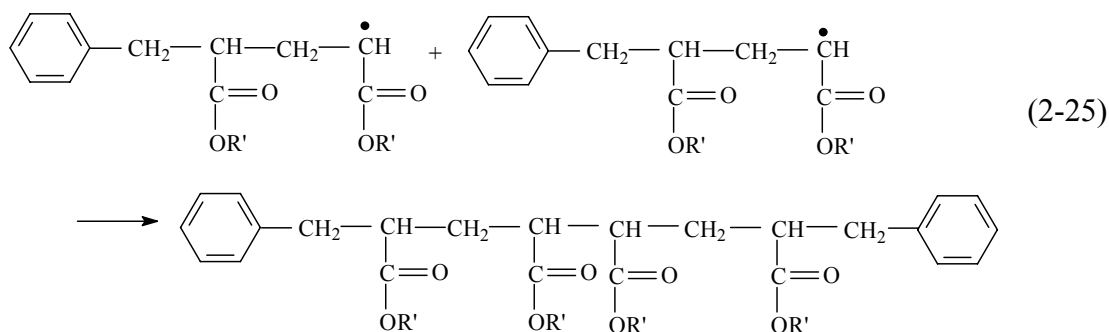
(2-20) either does not occur or takes place very slowly due to the relatively high stability of the oxiranium ion compared to that of carbocation.



(4) Reaction Mechanisms for Acrylate Monomer:

Fast polymerization is particularly easy to obtain in the resin samples containing acrylate monomers due to the existence of electron-deficient double bonds. Acrylate is often with the structure of $\text{H}_2\text{C}=\text{CHCOOR}$ in which R is an arbitrary group that does not significantly affect the mechanism of the polymerization. The phenyl free radicals produced by the photolysis of the cationic photoinitiator has sufficient energy to initiate the free-radical polymerization [78]. During cationic polymerization, photoinitiator and dicycloaliphatic epoxide may also react with acrylate monomer to undergo the free-radical polymerizations. The mechanisms are depicted in Eqs. (2-11) to (2-13) and Eqs. (2-23) to (2-25). The free-radical polymerization can be divided into three classes: the photochemical event leading to the first monomer radical, the propagation, and the termination process of the reaction as shown in Eqs. (2-23) to (2-25) [79]. Phenyl radical (see Eq. (2-11)) can react with acrylate monomer to induce grafting in accord with a homopolymerization reaction shown in Eq. (2-23). The addition of acrylate monomer to a macroradical results in a larger macroradical, as shown in Eq. (2-24) and termination occurs when the macroradicals are recombined as shown in Eq. (2-25).





2.7.3. Effects of Silane Coupling Agents on Adhesion Strengths

Silane coupling agents are commonly adopted as the surface modification species and primarily serve as adhesion promoters in composite materials to achieve strong bonding of polymers on metals, glass, minerals *etc.* [80]. Silane coupling agent typically possesses alkoxy groups (OR) and an organo-functional group (R'). The alkoxy groups hydrolyze in the aqueous environment and form covalent bonds with hydroxyl groups on the surface as well as with other hydrolyzed silane molecules. The organo-functional group may also react with the matrix resin [81-82]. A properly chosen organo-functional group for a specific application increases the interfacial strength significantly. In some cases the adhesion enhancement is due to the formation of covalent linkages with the polymer *via* chemical interactions to produce so-called interpenetrating polymer network (IPN) [83]. The widespread usage of organic-functional silanes prompts an in-depth study of the mechanisms of adhesion reinforcement. In this study, the organo-functional group was chosen according to its reactivity and compatibility with the photoinitiator. Silane coupling agents with organo-functional groups of amine [84], epoxy [85], methacrylic [86], acrylic [87] and vinyl [88,89] are utilized for adhesion enhancement. Depending on the method of application, a silane coupling layer normally consists of several monolayers. There are basically four different methods of applying silane coupling agents: deposition

from aqueous solutions, deposition from organic solutions, integral blend method and deposition as a primer [90]. Among these, deposition from organic solutions was used in this work.

2.7.4. Effects of Tertiary Amines on Etiolation

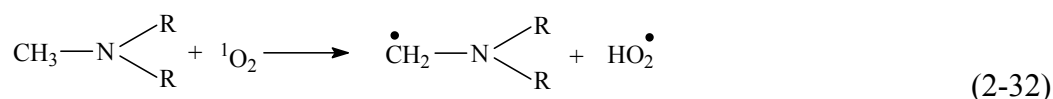
Transparency becomes an important property of UV-curable resins for direct encapsulation of advanced OLEDs such as TOLEDs and FOLEDs. A common detriment to transparency of UV-curable resins is the etiolation phenomenon resulted from the poor resistance to subsequent UV irradiation. Etiolation of UV-curable resins is induced by: (i) residual photoinitiators that promote the photo-yellowing reactions [91-93]; (ii) hydrogen-atom was abstracted by the residual photoinitiator [94]; (iii) oxidization caused by the presence of functional groups containing residual free radicals in resins [95]; and (iv) hydroperoxidation resulted from the formation of conjugated unsaturated carbonyl products with strong UV absorption at the wavelength of 275 nm [96].

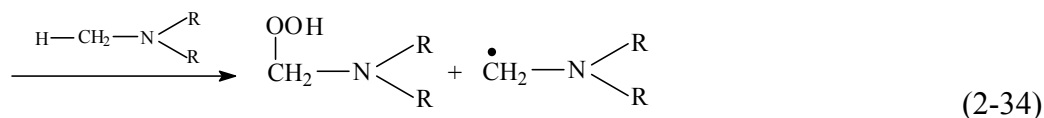
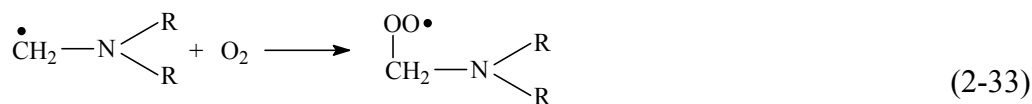
The etiolation of resin samples was resulted from the residual free radicals generated by photolysis of sulfonium salt photoinitiator, polymer or photosensitizer. The radicals react with oxygen in air to produce free radicals *via* the oxidation reaction shown in Eq. (2-26) [97]. As depicted by Eqs. (2-27) and (2-28), the free radicals further react with polymer (RH) and other free or phenol radicals to form hydroperoxide (ROOH) and ester, respectively. It is known that the emergence of hydroperoxide induces the etiolation of resins [79,98-99]. The ROOH then decomposes into alkoxy and hydroxide radicals in accordance with Eq. (2-29) [100,101] and subsequently reacts with RH to form alkyl radical (Eqs. (2-30)). The alkyl radicals are continuously formed by the repetition of reactions shown in Eqs. (2-26) to (2-31). The more residual free radicals generated in the resin samples, the

more hydroperoxide were produced and the severer etiolation occurred in the UV-curable epoxide resins.



Etiolation suppression of UV-curable resins utilizing monoacrylate of a cyclic carbamate [102], monoacrylate of a cyclic urethane [102] and amine acrylate [96,103] have been reported. Etiolation of UV-curable resin improved by the addition of tertiary amines could be explained by the oxygen scavenging processes as depicted by Eqs. (2-32) to (2-34). During UV irradiation, singlet oxygen was produced by a triplet energy transfer from photosensitizer (*i.e.*, the free radical initiators such as BPO) to ground-state oxygen [104]. The singlet oxygen may react with tertiary amines *via* an electron transfer process to produce α -aminoalkyl radicals in accordance with Eq. (2-32) [105]. The α -aminoalkyl radicals depicted by then react with oxygen to produce α -hydroperoxyamine (HOOCH₂NR₂) and α -aminoalkyl radical *via* the reactions shown by Eqs. (2-33) and (2-34) [46,101].





Tertiary amines are common thermal accelerators in epoxy resins to reduce curing temperatures and promote thermal conversions. One of the special features of tertiary amines is that they may react with carbonyl compounds, singlet oxygen and other species *via* an electron transfer process to improve the low ionization potential property [102].

2.8. Adhesion Strengths of Polymer Resins

Adhesion strength of polymer resins is resulted from the formation of chemical bonds between main chain of polymer resin and the substrate. Attraction resulted from van der Waals force of molecules in polymer resin and substrate is another source of adhesion [103]. In addition, crosslinking in resin inhibits the sliding between molecule chains so as to enhance the adhesion strength. However, the resin becomes stiff when crosslinking density is too high. The interfacial stress thus cannot be released and fracture may occur along the resin/substrate interface.

In order to enhance the adhesion strength, functional groups are commonly selected to promote interfacial chemical bonds or specific interactions that may produce hydrogen bonds. In general, chemical bonds is much more effective than hydrogen bonds in the adhesion enhancement. Some useful functional groups for adhesion enhancement are briefly described below [104].

(i) Carboxyl groups promote the adhesion on metals, glass, and polymers. They can be incorporated into resins by copolymerization with carboxyl monomers, or

using additives containing carboxyl groups.

- (ii) Hydroxyl, methylol and nitrogen-containing groups promote the adhesion on various organic and inorganic substrates.
- (iii) Epoxide groups promote adhesion on various organic and inorganic substrates containing active hydrogens such as hydroxyl, carboxyl, amino and amide groups.
- (iv) Highly reactive isocyanate groups promote adhesion on substrate surfaces containing hydroxyl, carboxyl, amino or amide groups.
- (v) Phosphoric acid group can be incorporated into a polymer by reacting phosphoric acid with a polymer containing an epoxide group. Such a functional group promotes adhesion on metal and ceramic substrates.
- (vi) Sulfonic acid group can be incorporated into a polymer by copolymerizing with sulfoethyl methacrylate. Such copolymers improve adhesion on a variety of substrates.

Furthermore, several compounds are known to promote adhesion by chemical coupling between resin and substrates. These include silanes, esters of phosphoric, phosphonic, or phosphorous acid, chromium complexes and titanates.

There are a variety of adhesion test methods, *e.g.*, single lap joint tests (thin substrates), thick substrate shear test, double lap joint tests, strap joint test, scarf joint of overlap test, shear joint tests, T-peel test, flexible-to-rigid peel test, pull-off, test butt joint tests and pull-out tests of tension pull tests [105]. These test methods in general determine the adhesion strength from the force required to pull a resin sample off the substrate surface (or a part from the substrate surface). In this work, pull-off test was adopted to evaluate the adhesion strengths of resin samples on various substrates.

In addition to the value of adhesion strength, the location of the breakage/fracture

is also important when reporting the data of adhesion test. The locations of breakage/fracture can be classified as follows [106]:

- (i) Substrate breaking: breakage occurs in substrate;
- (ii) Cohesive breaking: breakage occurs in the resin matrix;
- (iii) Interface breaking: breakage occurs along the resin/substrate interface;
- (iv) Mixture breaking: A combination of above types of breakages.

2.9. Underfill for Flip-chip IC Packaging

The pursuit of high speed and high performance of electronic products raises the size and device density of IC chips. Power consumption increases accordingly and, for the development of encapsulation resins for IC chips, the ability for the resins to satisfactorily dissipate heat is essential. Underfill was originally served as sealant and mechanical support for flip-chip (FC) joints on IBM mainframe computer modules in 1964 [107]. The early work led to the discovery that thermo-mechanical fatigue could be reduced by filling resin in between the solder bump joints. The underfill technology hence becomes essential for the improvements of reliability, in particular to the assembly of flip-chip ICs on organic boards in which the CTE mismatches are significant. The underfill is a polymeric adhesive that serves to reduce the strain of the solder joints between the die and the substrate. Thus, the application of underfill would enhance the reliability performance of flip-chip on board assembly by at least one to two orders of magnitude over that of a nonunderfilled one.

Epoxide resin is one of the most popular organic materials for encapsulation due to its relatively low price, excellent processing ability, and low viscosity. Its deficiencies include low thermal conductivity and high CTE. According to their publications, it has been shown that in general the dielectric properties of polymers and blends are depended on their structure, crystallinity, morphology, and the

presence of inorganic fillers or other additives such as silica [108-110], silicone carbide (SiC) [111-112], alumina (Al₂O₃) [112-113], aluminum nitride (AlN) [114-116] and boron nitride (BN) [117]. However, the dielectric constants of SiC, Al₂O₃, AlN, *etc.* are relatively high as shown in Table 2-5, and are undesirable for electronic packaging that always requires low dielectric properties. At present, most of flip-chip interconnections are underfilled by silica-filled epoxy resins that have been used in IC industry for almost 30 years because of their good mechanical and electrical properties, low cost and much easier to process than inorganic encapsulants. The advantages provided by epoxy/silica composites have received a lot of attentions in electrical insulation applications such as outdoor high-voltage installations for the replacement of ceramic insulators [118].

Table 2-5. Dielectric properties of inorganic fillers.

Filler	Dielectric constant (at 1 MHz)	Tangent loss ($\times 10^{-4}$, at 1 MHz)
SiC	40 ~ 42	500 [119]
Al ₂ O ₃	8.5 ~ 8.9	2 ~ 3 [119]
AlN	8.8 ~ 8.9	1 ~ 5 [119]
SiO ₂	4	2 [120]
hBN	3.9	< 2 [121]

The signal integrity, as it propagates through the package, is a direct function of the conductor's resistivity, dielectric constant and the loss tangent. It is important to recognize that the dielectric constant and tangent loss can be strong functions of the frequency. In general, the dielectric tangent loss is not a strong function of frequency for ceramic packages, while the tangent loss is generally large and can have strong resonances at higher frequencies for plastic packages, especially above 1 GHz. In addition, underfill adhesion is crucial to the integrity and reliability of the assembly. It

has been shown that high adhesion strength at interface between die and underfill is strongly correlated with solder joint fatigue life and alleviated fillet crack problem [122].

Hexagonal boron nitride, hBN, has a crystal structure similar to graphite ($a = 0.25$ nm, $c = 0.67$ nm) [123] except for differences in the stacking sequence of layers. hBN is a naturally lubricious material in its powder form and is often called white graphite. It is also an electrical insulator and exhibits excellent resistance to oxidation, performs exceptionally well at high temperatures (to 3000°C), and is resistant to corrosive attack. Most of the applications of hBN are associated with thermal dissipation, lubrication, hot-pressed shaping, and pyrolytic shaping [121].

Most of the studies related to hBN focused on its thermal conductivity [123-128]. Liu *et al.* [129] filled BN in cyclic butylenes terephthalate (CBT) and poly (butylenes terephthalate) (PBT) resins and investigated its effects on CTE, T_g and storage modulus of composites. However, no dielectric properties were reported in their study. Dielectric constant of hBN (~ 3.9) is similar to that of SiO_2 (~ 4.0) at 1 MHz. This work intended to evaluate the applicability of these two types of fillers for underfill resin preparation by comparing various physical properties of the composite resin samples. In this work, dielectric properties of hBN-epoxy resin composites in the frequency ranging from 0.1 to 1 GHz were presented. In addition, the effects of hBN filler on the conversion of thermal polymerization of resins, which are rarely reported, were also studied in this work.

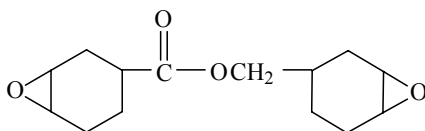
Chapter 3

Experimental Methods

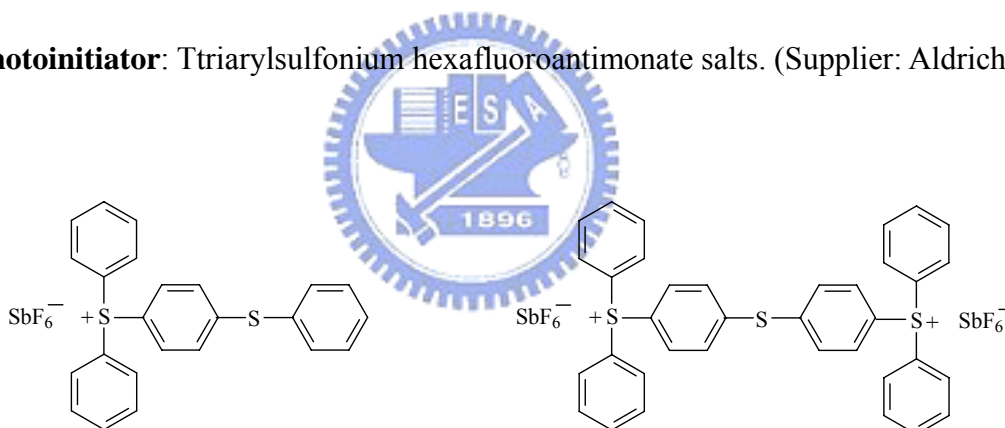
3.1. Experimental Methods of Sealing Resins for the OLED Packaging

3.1.1. Materials

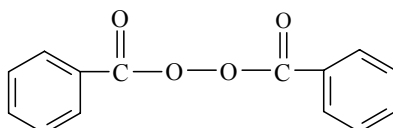
- (1) **Oligomer:** 3,4-Epoxy cyclohexylmethyl 3,4-epoxycyclohexanecarboxylate
(Supplier: Aldrich).



- (2) **Photoinitiator:** Ttriarylsulfonium hexafluoroantimonate salts. (Supplier: Aldrich)



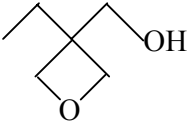
- (3) **Thermal initiator:** Benzoyl peroxide (BPO) (Supplier: Fluka).



- (4) **Monomers:** 3-ethyl-3-oxetanemethanol (EOM), tri(propylene glycol) (TPPG), polycaprolactone triol (PCAT), bis(4-vinyloxy)butylisophthalate (BVBP) and 1,6-Hexanediol diacrylate (HDDA). The types and chemical structures of

monomers are listed in Table 3-1. All monomers were purchased from Aldrich Co.

Table 3-1. The types and chemical structures of monomers.

Monomer	Type	Structures
3-ethyl-3-oxetanemethanol (EOM)	polyol	
Tri(propylene glycol) (TPPG)	polyol	$\text{H}(\text{OC}_3\text{H}_6)_3\text{OH}$
Polycaprolactone triol (PCAT)	polyol	$\text{C}_2\text{H}_5\text{C}[\text{CH}_2\text{O}[\text{CO}(\text{CH}_2)_5\text{O}_n]\text{H}]_3$
Bis(4-vinyloxy)butylisophthalate (BVBP)	vinyl ether	$[\text{CO}_2(\text{CH}_2)_4\text{OCH}=\text{CH}_2]_2$
1,6-Hexanedol diacrylate (HDDA)	acrylate	$\text{CH}_2=\text{CHCOO}(\text{CH}_2)_6\text{OOCH}=\text{CHCH}_2$

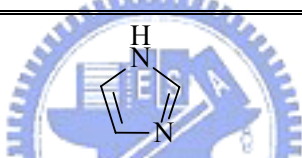
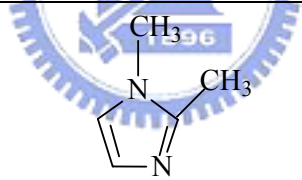
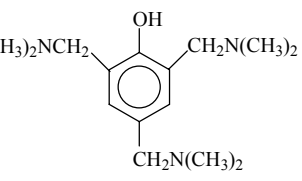
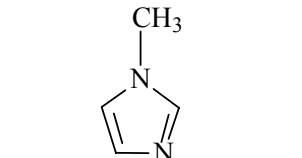
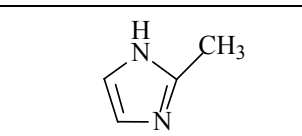
(5) **Silane coupling agents:** vinyltrimethoxysilane, 3-glycidoxypropyltrimethoxysilane, 3-aminopropyltrimethoxysilane, 3-acryloxypropyltrimethoxysilane and 3-methacryloxypropyltrimethoxysilane. All silane coupling agents were supplied by Aldrich and their chemical structures are shown in Table 3-2.

(6) **Tertiary amines:** the chemical structures, designated names and providers of the five tertiary amines under studying are listed in Table 3-3.

Table 3-2. Structures and designated names of organo-functional silanes.

Organo-functional silane	Chemical structure	Designated name
vinyltrimethoxysilane	$(\text{CH}_3\text{O})_3\text{SiCH}=\text{CH}_2$	Vinyl
3-glycidoxypropyltrimethoxysilane	$(\text{CH}_3\text{O})_3\text{Si}(\text{CH}_2)_3\text{OCH}_2\text{CH} \begin{array}{l} \diagup \text{O} \diagdown \\ \text{---} \end{array} \text{CH}_2$	Epoxy
3-aminopropyltrimethoxysilane	$(\text{CH}_3\text{O})_3\text{Si}(\text{CH}_2)_3\text{NH}_2$	Amino
3-acryloxypropyltrimethoxysilane	$(\text{CH}_3\text{O})_3\text{Si}(\text{CH}_2)_3\text{OOCCH}=\text{CH}_2$	Acrylic
3-methacryloxypropyltrimethoxysilane	$(\text{CH}_3\text{O})_3\text{Si}(\text{CH}_2)_3\text{OOC}(\text{CH}_3)=\text{CH}_2$	Methacrylic

Table 3-3. Chemical structures and designated names of tertiary amines.

Tertiary amine	Chemical structure	Designated name	Supplier
Imidazole		1-amine	Aldrich
1,2-dimethylimidazole		2-amine	Aldrich
2,4,6-tris(dimethylamino-methyl)phenol	$(\text{CH}_3)_2\text{NCH}_2$  $\text{CH}_2\text{N}(\text{CH}_3)_2$	3-amine	TCI
1-methylimidazole		4-amine	Aldrich
2-methylimidazole		5-amine	Aldrich

3.1.2. Experimental flow

Experimental flow of this work is shown in Fig. 3-1. Sample preparation and characterization methods are described as follows.

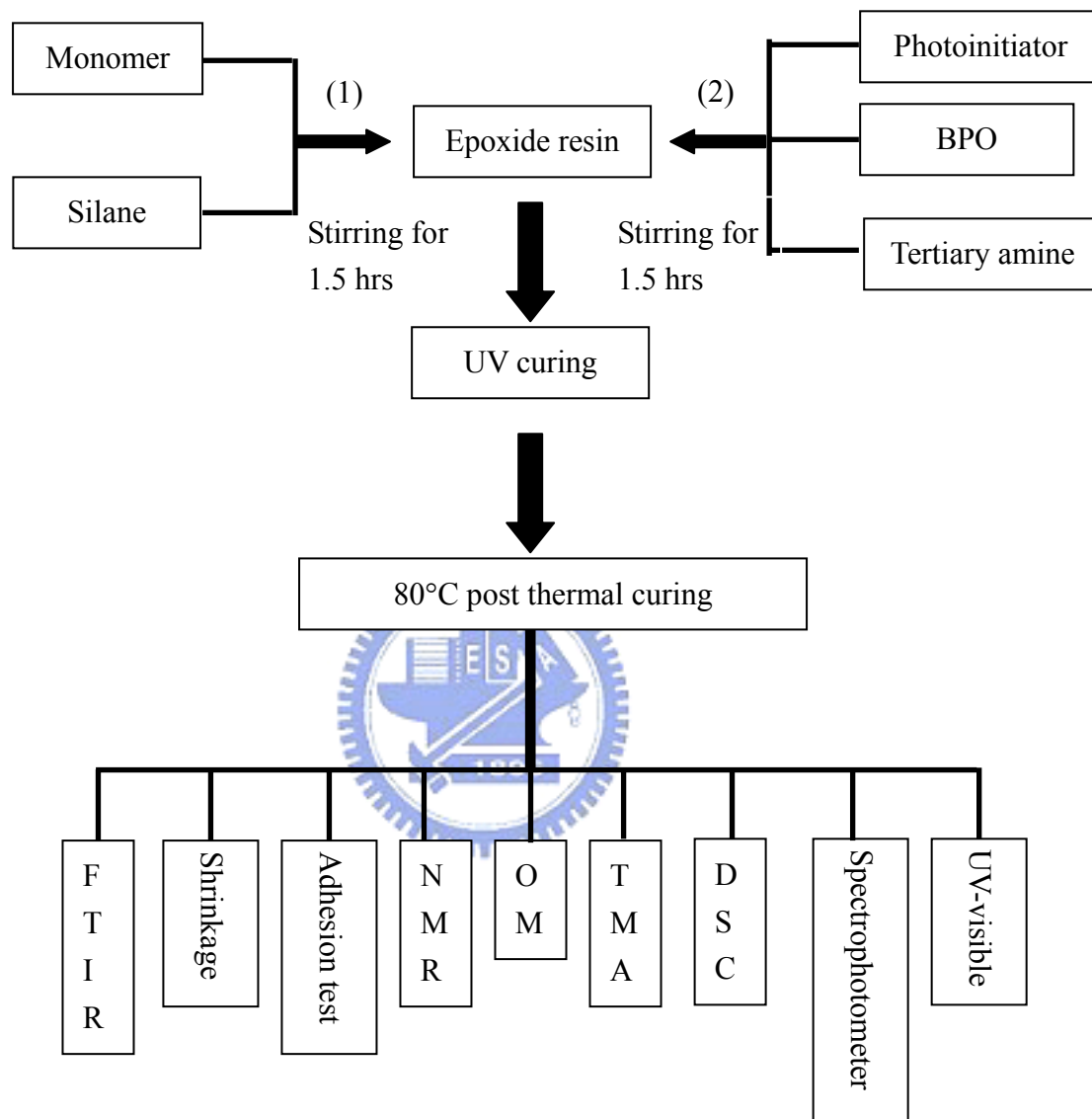


Figure 3-1. Experimental flow.

The resin samples were prepared by first mixing dicycloaliphatic epoxide and polyol monomer at the ratio of 4:1 by weight and 1.0 wt.% of silane coupling agent together then stirring for 1.5 hrs (step (1) shown in Fig. 3-1). 1.5 g of photoinitiator and different amounts of BPO were added into above mixture and stirred for another

1.5 hrs (step(2) shown in Fig. 3-1). Characterizations were performed in order to identify the optimum content of BPO in epoxide resin matrix as 2.0 wt.%. The following samples were prepared by fixing the dicycloaliphatic epoxide, photoinitiator and BPO contents and sequentially changed monomer types, silane types or tertiary amines types in the resins. The whole resin mixtures were stirred for another 2 hrs to complete the resin samples preparation.

3.1.3. Characterization Methods

(1) **Measurement of Shrinkage:** The adhesives samples were dispensed onto glass substrates at the size of 10 mm × 10 mm × 3 mm and then UV cured for 25 min. The volume shrinkage of sample was determined by measuring the density change of each resin sample before and after UV curing. The shrinkage of samples was calculated according to the following Eq. (3-1) [49]:

$$\text{Shrinkage (\%)} = \frac{1/d_{\text{before}} - 1/d_{\text{after}}}{1/d_{\text{before}}} \times 100\% \quad (3-1)$$

where d_{before} = the density of sample before curing, d_{after} = the density of a resin after curing. The densities of the cured samples were determined by the displacement method by using a Mettler AX105DR density determination kit. The weights of the adhesives samples were assumed to be constant at the temperature of 25°C. Surface morphologies of adhesives were observed by optical microscopy (U-LH100-3, Olympus).

(2) **FTIR Characterizations:** The FTIR samples were prepared by coating the resin samples, silanes and silanes blended with photoinitiator on KBr discs and cured in the UV oven for various time spans. The samples were then transferred to a Nicolet

Protégé 460 Fourier-transform infrared spectrometer (FTIR) for structure analysis.

The UV conversion of the samples was determined from absorbance at 910 cm^{-1} and 975.4 cm^{-1} from FTIR spectra. Since slight difference in thickness existed among all the samples and the thickness of samples might change during UV curing, an internal standard band method was hence chosen in order to compensate the change in sample thickness. The absorption band at 1728 cm^{-1} for C=O of dicycloaliphatic epoxide was adopted as an internal standard band for calculation. The conversion of samples was calculated according to the following Eq. (3-2):

$$\text{UV Conversion} = \left(1 - \frac{[A]_{\text{Et}}/[A]_{\text{rt}}}{[A]_{\text{E0}}/[A]_{\text{r0}}} \right) \times 100\% \quad (3-2)$$

in which $[A]_{\text{Et}}$ = peak intensity of epoxy group in the normalized spectrum of the sample subjected to UV curing, $[A]_{\text{rt}}$ = peak intensity of C=O group in the normalized spectrum of the sample subjected to UV curing, $[A]_{\text{E0}}$ = peak intensity of epoxy group in the normalized spectrum of the sample prior to UV curing and $[A]_{\text{r0}}$ = peak intensity of C=O group in the normalized spectrum of the sample prior to UV curing.

(3) **NMR Characterizations:** Samples of silanes blended with photoinitiator and tertiary amines blend with BPO were further dissolved in CDCl_3 then characterized by INOVA 500 MHz nuclear magnetic resonance (NMR) spectrometer to reveal their ^{13}C - and ^1H -NMR spectra after they were cured by UV radiation.

(4) **Kinetics of Thermal Curing:** Kinetics of resin samples by thermal curing was determined by using a differential scanning calorimeter (DSC, Perkin Elmer, Diamond) at a heating rate of $100^\circ\text{C}/\text{min}$. The samples were hermetically sealed in aluminum pans and isothermally scanned at 80°C for 1 hr in an ambient purged with nitrogen at gas flow rate of $20\text{cc}/\text{min}$. The extent of the reaction or, the thermal

conversion, as a function of time was determined by integrating the isothermal curves by using the relationship given below [130]:

$$\text{Thermal Conversion (\%)} = \frac{100}{\Delta H_T} \int_0^t \frac{dH}{dt} dt \quad (3-3)$$

where ΔH_T is total enthalpy change calculated from the integral of dH/dt from $t = 0$ to $t = \infty$.

(5) **Thermal Properties:** Thermal properties including coefficient of thermal expansion (CTE) and glass transition temperature (T_g) of resin samples were measured by using a TA 2940 thermal mechanical analyzer (TMA). A tension probe was adopted to detect the expansion of sample with 1 mm × 4 mm × 25 mm in sizes during heating from room temperature to around 150°C at a heating rate of 5°C/min. The value of CTE was calculated from the plot of dimension change *versus* temperature in the range of 30 to 60°C. The point where a significant change of slope was also identified from the plot and the onset temperature corresponding to such a change was termed as the T_g of the resin sample.

(6) **Transmittance:** Agilent 8453 UV-visible spectrometer was utilized to measure the transmittance of resin sample coated on glass substrate subjected to UV and post-baking treatments.

(7) **Yellowness Indices and Color Parameters:** The yellowness of specimens was evaluated in accordance with the ASTM D 1925-70 test standard by using a spectrophotometer (Minolta, CM-508i) in conjunction with the On Color software (Version 5.3.0.7 QC-Basic, Cyber Chrome, Inc.). First, the reflectance of samples was measured in the visible-light wavelengths ranging from 400 to 700 nm. Reflectance data were taken in each 20-nm wavelength interval from an 8-mm² area of specimen

and a white color standard (*i.e.*, a double A white paper). By utilizing the CIE (Commission International d'Eclairage) standard [131], the CIE values corresponding to resin sample (L^* , a^* and b^*) and the white standard (L^*_{std} , a^*_{std} and b^*_{std}) could be calibrated [132], respectively. It is noted that L^* parameter is the value or the degree of lightness in the Munsell system, while a^* and b^* coordinates designate the positions on red or green ($+a^*$ = red, $-a^*$ = green) and yellow or blue ($+b^*$ = yellow, $-b^*$ = blue) axes, respectively. The color parameter (ΔE^*_{ab}) [133] and yellowness index (ΔYI) [134] of the resin sample were calculated according to Eqs. (3-4) and (3-5) by utilizing above parameters

$$\Delta E^*_{ab} = \sqrt{(\Delta L^*)^2 + (\Delta a^*)^2 + (\Delta b^*)^2} \quad (3-4)$$

and

$$\Delta YI = \frac{1.28X - 1.06Z}{Y} \times 100 \quad (3-5)$$



where $\Delta L^* = L^* - L^*_{std}$, $\Delta a^* = a^* - a^*_{std}$, $\Delta b^* = b^* - b^*_{std}$ and the (X, Y, Z) are the tristimulus values calculated from the color reflectance spectra [133] obtained by using a 2° observer.

(8) Adhesion Strengths: In the part regarding the adhesion of resins containing polyol, vinyl ether and acrylate on glass substrates, the glass blocks were first ground into a truncated shape with the sizes illustrated in Fig. 3-2(a). Each of resin samples was then applied onto the $7 \times 7 \text{ mm}^2$ surface area and another glass plate at the size of $10 \text{ mm} \times 10 \text{ mm} \times 3 \text{ mm}$. Both of the glasses were purchased from Liehcher Co. Ltd (Taiwan). The two glass parts were then glued together to form the adhesion test samples. Adhesion strengths of epoxide resins containing vinyl, epoxy, amino, methacrylic and acrylic silane groups on glass to ITO glass substrates were evaluated

in similar way. ITO glass substrates with dimensions of 10 mm × 10 mm × 0.7 mm was supplied by Merck Display Technologies Ltd. (Taiwan). The ITO overlayer had the thickness = 200 nm and sheet resistance = 10 Ω/□. After applying the adhesive resin on this area, the glass block was glued to the glass plate and ITO glass separately to form the adhesion test specimens. The specimens were cured in a UV oven (CL-1000M, UVP USA) with wavelength ranging from 314 to 340 nm at a power of 40 W for 25 min, then post-cured at 80°C for 1 hr to complete the hardening process. Two steel bars were then attached onto the two ends of the adhesion test sample and sent to a pull tester for adhesion strength measurement at the pull rate of 5 mm/min (see schematic illustration shown in Fig. 3-2(b)). The pull tester was Model-HT-8116 purchased from Hung Ta Instrument Co. Ltd. (Taiwan). For each type of resin sample, the pull test was repeated for five times.

The tertiary amines were added to UV-curable resins of which adhesion strengths on various types of substrates, namely, glass, ITO, PET, and stainless steel were evaluated according to ASTM D897 standard by using a pull tester. The PET substrates were formed by firmly gluing the PET films on glass plate. As to the adhesion test of resins on stainless steel, 2-mm thick plates were adopted as the substrates. The samples for adhesion strength measurement were prepared by first coating appropriate amount of resin sample on various substrates. A glass block with 10 mm × 10 mm × 8 mm in dimensions was then attached onto the substrate and sent to the ovens for UV curing followed by a post thermal baking. The UV curing was carried out in the UV oven (UC-1000) which was supplied by C-SUN with wavelength ranging from 254 to 360 nm at power of 80 W for various time spans followed by a post thermal baking at various temperatures for 1 hr. The thickness of thin-film samples was about 130 μm. For each type of resin samples, the average value of pull strengths taken from at least five samples was adopted as the adhesion

strength of that sample.

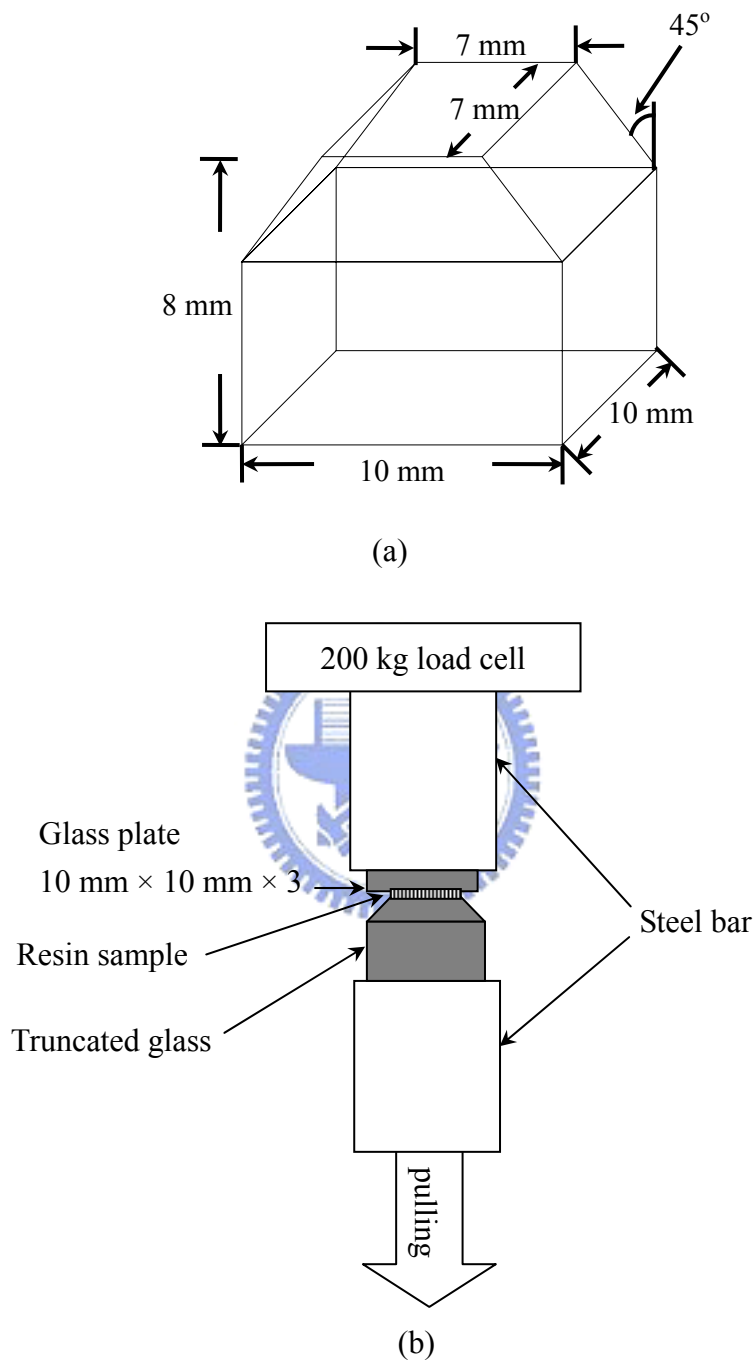


Figure 3-2. (a) The form and size of the truncated glass substrate and (b) the test scheme of adhesion strength.

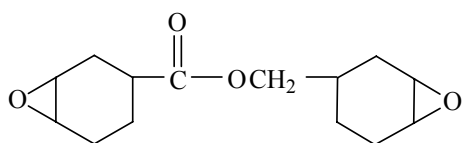
(9) **Hardness Test:** The hardness of resins was measured by using a D scale Shore hardness meter (BAREISS, Germany) according to ISO R868 (ASTM D 2240)

standard. The thickness of samples for hardness measurement was at least 6 mm.

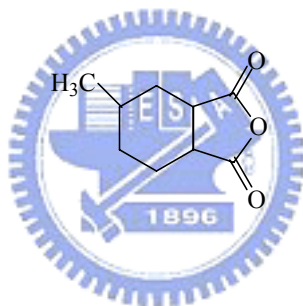
3.2. Underfill Resins for Flip-chip Interconnections

3.2.1. Materials

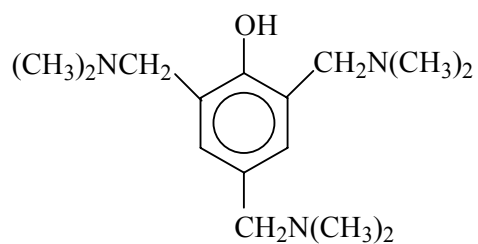
- (1) **Oligomer:** 3,4-Epoxy cyclohexylmethyl 3,4-epoxycyclohexanecarboxylate
(Supplier: Aldrich).



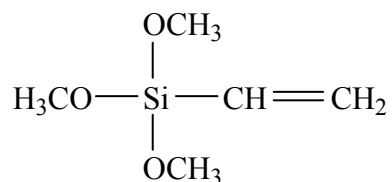
- (2) **Hardener:** hexahydro-4-methylphthalic anhydride (HMPA) (Supplier: Aldrich).



- (3) **Curing agent:** 2,4,6-Tris(dimethylaminomethyl)phenol (Supplier: TCI).



- (4) **Coupling agent:** γ -glycidoxypropyltrimethoxysilane (Supplier: Aldrich).



(5) **Inorganic filler:** The inorganic fillers include SiO₂ and hBN. SiO₂ was quartz-based with an average particle size of 4 μm; density = 2.65 g/cm³, dielectric constant = 3.8 ~ 4, and CTE = 12.3 ppm/°C (Supplier: Japanese High Purity Chemicals). HBN was supplied by National Nitride Technologies Co., Taiwan, and possessed an average particle size from 2 - 4 μm; density = 2.1 g/cm³, tap density = 0.35 g/cm³, dielectric constant = 4, and CTE = 1 ppm/°C.

3.2.2. Sample Preparation

3,4-epoxycyclohexylmethyl 3,4-epoxycyclohexanecarboxylate was used as the epoxide resin of which molecular weight and epoxy equivalent weight (EEW) are 252.3 g/mole and 133 g, respectively. The hardener is hexahydro-4-methylphthalic anhydride (HMPA). The chemicals were used as received. The purity of HMPA exceeds 97%. The ratio of epoxy to hardener was 1:1 based on the EEW and the hardener. 2,4,6-Tris(dimethylaminomethyl)phenol (0.5 wt.%) was used as the curing catalyst and γ-glycidoxypropyltrimethoxysilane (1.0 wt.%) was used as the coupling agent.

The composite resin was prepared by first stirring the mixture of epoxide resin, hardener, curing catalyst, and coupling agent for 2 hrs. The hBN filler was added into the organic mixture *via* a milling process using a triple roller mill (EXAKT, Germany). SiO₂ filler was added into the organic mixture in a stepwise manner and then stirred for 2 hrs. The curing of all the composite resin samples was carried out at 150°C for 1 hr. The composite resins containing hBN and SiO₂ fillers are henceforth

referred to as hBN-resins and SiO₂-resins, respectively.

3.2.3. Dielectric Properties

Dielectric constants (ε) and tangent loss ($\tan\delta$) of composite resins were measured with a Hewlet Packard 4291B impedance analyzer, which contains a HP 16453A test fixture, at frequencies ranging from 1 MHz to 1.0 GHz [121]. The disc-like sample, about 3 mm in thickness and 15 mm in diameter, was inserted between the electrodes and the measurement was carried out in accordance with the ASTM D150 test standard. The dielectric properties of the samples were calculated using the following Eqs. (3-6) and (3-7):

$$\varepsilon = \frac{\dot{Y}_m}{j\omega C_o(1 + E_{edge})}, \quad (3-6)$$

$$\tan\delta = D. \quad (3-7)$$



In the above, \dot{Y}_m is the measured admittance of sample, C_o is the capacitance of parallel electrodes with spacing equal to the sample thickness, $\omega = 2\pi f$ and is the angular frequency where f is the measured frequency in Hz, $E_{edge} = 434t^{0.825}\varepsilon^{-0.554}$ (t is sample thickness) and is the compensation coefficient resulting from the edge effect of the HP 16453A test fixture, and D is the dissipation factor.

3.2.4. Curing Kinetics of Resins

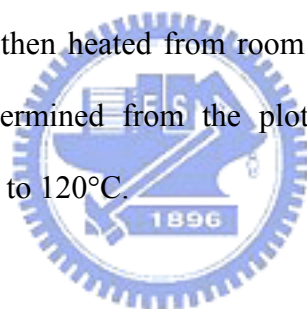
A differential scanning calorimeter (DSC, TA 2970) operating at a heating rate of 100°C/min was utilized to analyze the curing kinetics of the resin samples. Samples containing 9.2, 11.2, 13.1, 15.0, 20.0, and 25.7 vol.% hBN filler were individually sealed in DSC pan. The samples were scanned isothermally at 150°C in

an ambient purged with nitrogen gas at 50 cc/min. The extent of reaction (*i.e.* conversion as a function of time) is determined by integrating the isothermal curves using Eq. (3-3) [135].

The T_g 's of the samples were determined by DSC. The samples were heated in the DSC cell at a heating rate of 5°C/min from 30 to 250°C to obtain the curing profiles and the transition points of the profile were adopted as the T_g values of the composite resins.

3.2.5. Coefficient of Thermal Expansion (CTE)

The CTE values of the samples were measured with a TMA (TA 2940). The cured samples were cut with a diamond saw into squares (5 mm × 5 mm × 3 mm), placed in the TMA cell, and then heated from room temperature to 30 to 250°C at 5°C/min. The CTE was determined from the plot of thermal expansion *versus* temperature in the range of 30 to 120°C.



3.2.6. Thermal Conductivity

Thermal conductivity (κ) of the samples was measured by using equipment at Microelectro-mechanical Systems of Electronics Research and Service Organization of Industrial Technology Research Institute (ERSO/ITRI) in Taiwan. The test assembly is shown schematically in Fig. 3-3 [136]. The resin sample of dimensions 30 mm × 30 mm × 6 mm was inserted between two copper blocks separately maintained at low (initially 80°C) and high temperatures. During measurement, the energy transfer rate at the low-temperature Cu block, $\frac{\Delta Q}{\Delta t}$, was calculated according to Eq. (3-8)

$$\frac{\Delta Q}{\Delta t} = \rho C_p V \frac{dT}{dt} \quad (3-8)$$

where ρ , C_p , and V are density, specific heat, and volume of the Cu block, respectively, and dT/dt is the heating rate of the low-temperature Cu block, which is obtained from the slope of temperature change *versus* time plot. Fourier's law can be expressed by Eq. (3-9) where A and Δx are the cross-sectional area for heat transfer and thickness of the sample, respectively, and ΔT is the temperature differential between the two Cu blocks.

$$\frac{\Delta Q}{\Delta t} = \kappa A \frac{\Delta T}{\Delta x} \quad (3-9)$$

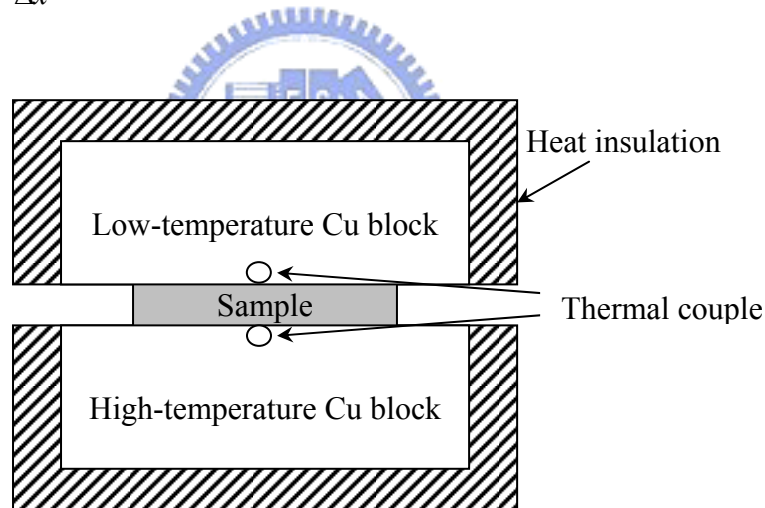


Figure 3-3. Test assembly of thermal conductivity measurement.

The thermal conductivity of the sample was calculated according to the Eq. (3-10) derived from Eqs. (3-8) and (3-9):

$$\kappa = \frac{\rho C_p V \Delta x}{A \Delta T} \cdot \frac{dT}{dt} \quad (3-10)$$

3.2.7. Morphology

The morphologies of composite resins containing hBN- and SiO₂ fillers were examined by a scanning electron microscopy (SEM, Hitachi S-4700).

3.2.8. Adhesion Strengths

Adhesion strengths of resin samples were measured according to ASTM D897 test standard. The glass block was first polished into a truncated shape with top surface with dimensions 5 mm × 10 mm. After applying the resin sample onto this area, the glass block was glued to various types of substrate materials including Al₂O₃, eutectic PbSn solder, Si wafer, and epoxy-based printed circuit board (PCB) to form the pull test specimens. Two steel bars were then attached to the two ends of the pull test samples and transferred to a pull tester (HT-8116, Hung Ta Instrument Co., Taiwan) operating at a pull rate of 5 mm/min for adhesion strength measurement. At least five samples were tested for each set of designated sample conditions and the average of data was termed as the adhesion strength of that sample.

3.2.9. Viscosity Measurement

The viscosities of the hBN-resins were measured at room temperature with a Brookfield viscometer (RVDV-III+) using a #6 spindle at a rotating speed of 5 rpm.

Chapter 4

Results and Discussion

4.1. Effects of Monomer Types on Adhesion Strengths of UV-Curable Resins

4.1.1. Kinetics of Photo-Polymerization of Resins

Kinetics of the photo-polymerizations was studied by FTIR spectroscopy to assess the polymer formation. Since the absorption intensity of epoxy group on dicycloaliphatic epoxide at the position of 910 cm^{-1} by ring vibration was decreased during cationic polymerization and the conversion of polymerization was hence calculated according to the intensity change of epoxy group and the result was presented in Fig. 4-1. Furthermore, the slopes of the linear portions of the plots shown in Fig. 4-1 are directly proportional to the rates of polymerization (slope = $R_p/[M_o]$) [77, 137]. It was found that the rates of polymerization are 0.09, 0.34 and 0.14 sec^{-1} for HDDA, BVBP and TPPG adhesives, respectively. Therefore the cationic polymerization reaction rates are in the order of: $\text{HDDA} < \text{TPPG} < \text{BVBP}$. The BVBP adhesive possesses the highest reaction rate since its mechanisms of cationic polymerization include the reactions depicted by Eqs. (2-11) to (2-13) and (2-17) to (2-22). Equations (2-11) to (2-13) and (2-14) to (2-16) describe the mechanisms for TPPG adhesive and hence it exhibits a slower reaction rate in comparison with that of BVBP adhesive. As to HDDA adhesive, it has the slowest reaction rate since only dicycloaliphatic epoxide executes the cationic polymerization and the polymerization of HDDA monomer with photoinitiator is *via* free-radical polymerization.

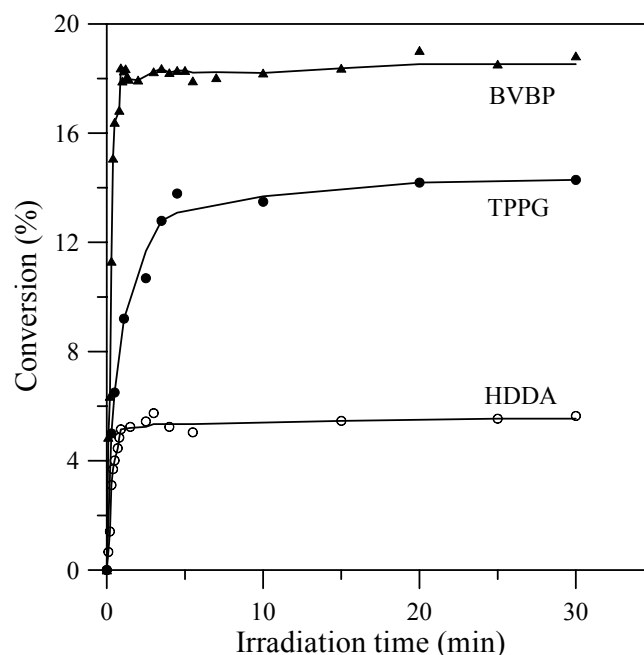


Figure 4-1. Conversion versus the time of UV irradiation for various monomers.

On the other hand, the absorption band at $802\text{-}817\text{ cm}^{-1}$ characterizes the $\text{CH}=\text{CH}$ - twisting motion of the acrylate group of HDDA which demonstrates the reaction rate of free-radical polymerization. The conversion rates of acrylate and epoxy groups of HDDA adhesive in Fig. 4-2 that reveal the rates of polymerization of these two functional groups are 0.39 and 0.09 sec^{-1} , respectively. According to the result, the rate of free-radical polymerization is faster than the rate of cationic polymerization which is similar to the study of Decker *et. al.* [138]. Due to UV irradiation, the acrylate monomer was polymerized *via* free-radical mechanism, while the dicycloaliphatic epoxide was polymerized *via* cationic mechanism. The acrylate mixed with cationic photoinitiator and epoxy resin thus generated an interpenetrating network [5]. It has been reported that the rate *via* free-radical polymerization of acrylate is faster than the cationic polymerization of the epoxy resins and other monomers [139], we hence observed the shortest curing time for the resin containing acrylate monomer. Both of the resins containing vinyl ether and polyol monomers

were cured *via* cationic mechanism. However, unlike polyol monomer, vinyl ether monomer also reacts with photoinitiator and this makes the reaction rate of vinyl ether fast than that of polyol but slower than the rate of acrylate.

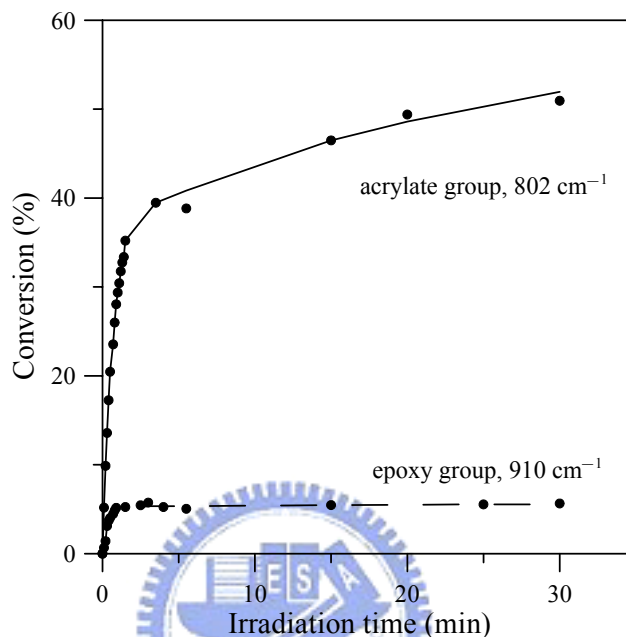


Figure 4-2. Conversion rate *versus* UV irradiation time for acrylate and epoxy groups in HDDA.

4.1.2. Effects of UV Curing Times on Shrinkages of Resins

Polymerization leads to an increase in density of the material. If the polymerization were coupled with other chemical reactions, the increasing of density may be compensated or at least reduced shrinkage [140]. Shrinkage, or volume reduction of the resins, which occurs during the curing process may affect its adhesion strength because high shrinkage might induce a considerable amount of internal stress that pulls the adhesive resin away from substrate [141-142]. Figure 4-3 shows the shrinkage of various resin systems cured at different UV irradiation time. The slope of each plot corresponds to the photo-polymerization reaction rate of resin containing a particular type of monomer. A sharper slope means slower reaction rate and *vice versa*.

The slope for resin containing HDDA turned to be flat after curing for 25 min, which means reaction has almost finished. For the resins containing BVBP and TPPG, the reactions terminated at 35 and 40 min, respectively. Figure 4-3 shows that the curing times for the resins containing HDDA and BVBP are shorter than that containing TPPG. The experimental results above also demonstrate a feasible way to measure the degree of curing of resins affected by the type of monomer.

Figures 4-4(a) to 4-4(c) show the morphology of epoxide resin containing various types of monomers after UV curing. The degree of shrinkage can be readily seen from the morphology change of sample surfaces. From Figs. 4-3 and 4-4, it was found that shorter curing time implies larger shrinkage and *vice versa*. As shown in Fig. 4-4(a), the resin containing TPPG exhibits the smoothest surface with the smallest degree of shrinkage and the longest curing time. The degree of shrinkage is in the order of: TPPG < BVBP < HDDA.

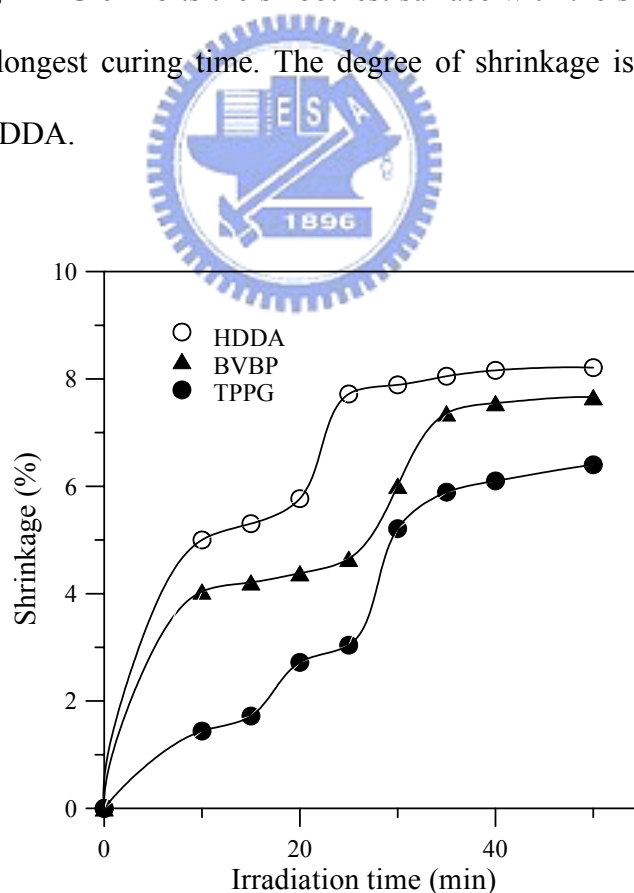


Figure 4-3. Shrinkage change *versus* UV curing time of resin containing TPPG, BVBP and HDDA monomers.

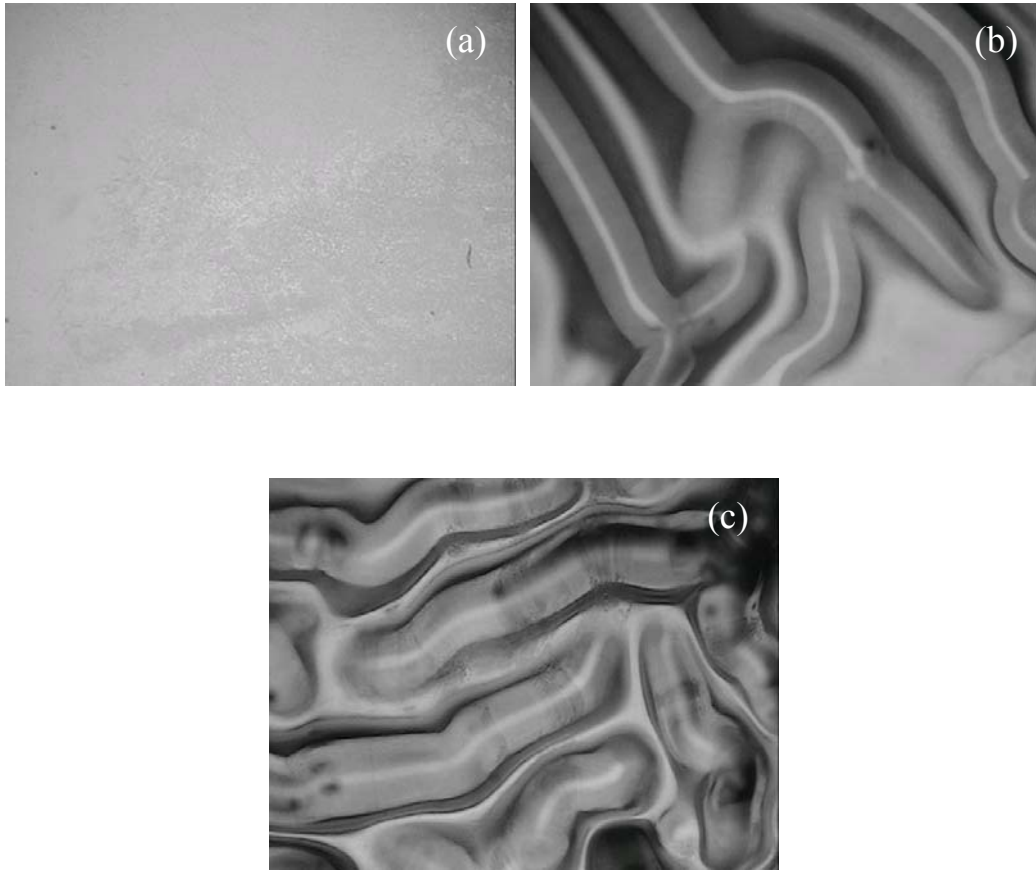


Figure 4-4. Surface morphology of epoxide resins containing (a) TPPG (b) BVBP and (c) HDDA after UV curing (Magnification = 20×).

The type of monomer implies different reaction mechanism during UV curing. The epoxy resin hence exhibited different adhesion property when it was cured at different conditions. In the aspect of curing time, fast curing induces high internal stresses. This would result high shrinkage and poor adhesion strength. As shown in Fig. 4-5, adhesion strength of TPPG, BVBP and HDDA resin systems is 153.4, 28.1 and 20.1 kg/cm², respectively. Adhesion strength of the resins, if designated according to the monomer type, is thus TPPG > BVBP > HDDA. The resin containing the TPPG monomer, which exhibits the minimum shrinkage, also possesses the highest adhesion strength. Such a result was also reported by the study of Tilbrook *et al.* [57]. Furthermore, cationic polymerization of TPPG and BVBP generates the hydroxyl groups, but there is no hydroxyl group generated after the free-radical polymerization

of HDDA. The hydroxyl groups are able to form hydrogen bonds on the glass substrate and hence the cationic polymerization provides better resin adhesion property in comparison with the free-radical polymerization.

During the experiment, we also observed the self-curing behavior of resin containing acrylate monomer. Such a phenomenon indicated that free radicals were formed by photolysis of cationic photoinitiator in the resin containing acrylate monomer.

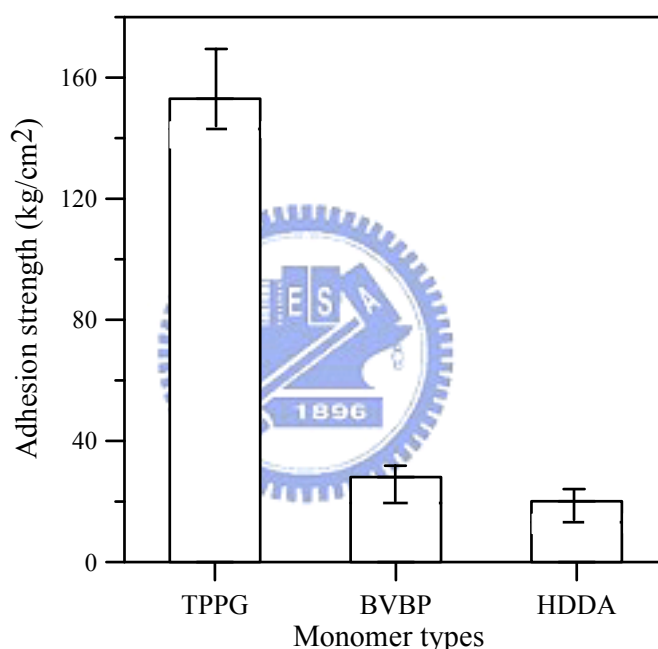


Figure 4-5. Adhesion strength and scatter range for the various monomers.

4.1.3. Effects of *R* Values

This work also studied the effects of *R* value on the adhesion strength of epoxide resin containing polyol monomer since it possesses the highest adhesion strength as the mixture of epoxy resin and polyol at equal proportion, the *R* value is defined as [49]:

$$R = \frac{\text{epoxy/epoxy equivalent weight (g)}}{\text{polyol/hydroxyl equivalent weight (g)}} \quad (4-1)$$

The R value is an important parameter in modifying the properties of epoxy resin when formulating with polyols and has to be larger or equal to unity Tilbrook *et al.* [57]. The mixtures with low R values are in general flexible and soft. Increase of polyol equivalent weight would increase the flexibility, extensibility, and softness of resins, while decrease of polyol equivalent weight would increase the hardness and cure rate of resins [57].

As shown in Fig. 4-6, after UV curing for 25 min, the resin exhibits the highest adhesion strength of 153.4 kg/cm² at $R = 3$. When $R = 2.5$, excess polyol induced partial curing and hence decreased the adhesion strength due to insufficient curing time to achieve complete crosslinking. Similar result was also reported by Tilbrook *et al.* [57]. Furthermore, poor adhesion strength was observed in the samples containing less amount of polyol. It should be resulted from less crosslinking density due to the shortage of hydroxyl group. The resin samples with $R > 3$ means less polyol content in the resins. Under same radiation condition, it would result in over curing with exceeding energy to crosslink. The results above imply that appropriate polyol content is essential to obtain satisfactory adhesion strength for photo-curable epoxy resins.

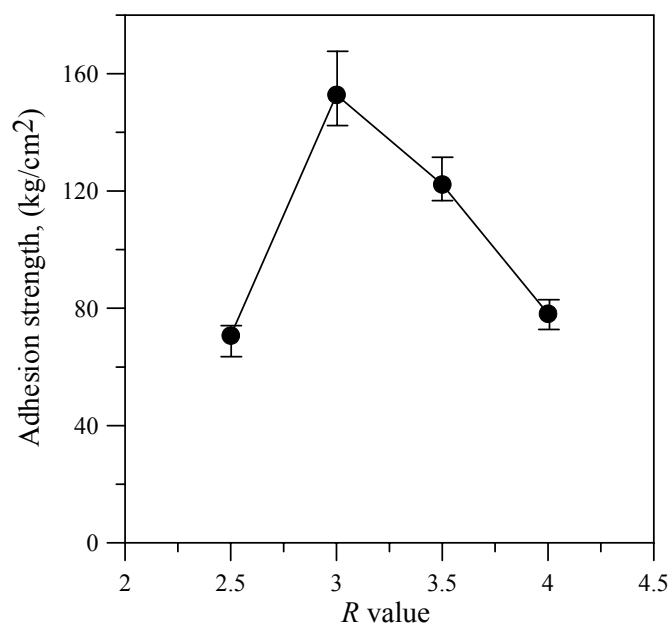


Figure 4-6. The *R*-value *versus* adhesion strength of resins containing polyol monomer.

4.1.4. Effects of the Number of Hydroxyl Functional Groups

The presence of hydroxyl groups has an important effect on the cationic ring-opening polymerization of epoxides. As shown in Table 4-1, the numbers of hydroxyl group on polyol monomers, EOM, TPPG and PCAT are 1, 2 and 3, respectively. Figure 4-7 plots the adhesion strength of resins *versus* numbers of hydroxyl group on polyol monomers. Average adhesion strength of epoxide resins containing EOM, TPPG, and PCAT on glass substrate is 73.6, 153.4 and 126.9 kg/cm², respectively. For EOM monomer, it would result in over curing with excessive energy to crosslink at the same UV curing condition. The PCAT monomer contains three hydroxyl groups that may induce partial curing. It hence lowers the adhesion strength due to insufficient curing time to achieve complete crosslinking. This implies that appropriate amount of hydroxyl groups of monomer is also a critical factor to the adhesion strength of photo-curable epoxy resins. Table 4-1 shows that the minimum shrinkage of EOM, TPPG, and PCAT is 6.40, 1.72 and 4.00 %, respectively. Figures 4-4(a), 4-8(a) and 4-8(b) showed the morphologies of epoxide resin containing

various types of poly monomers after UV curing. As shown in Figs. 4-8(a) and 4-8(b), the pull-off surfaces of the resins containing EOM and PCAT indicate larger shrinkages in comparison with the resin containing TPPG. The degree of shrinkage was found to be in the order of: TPPG < PCAT < EOM. According to the results above, the resin containing TPPG possesses the highest adhesion strength due to the lowest degree of shrinkage.

Table 4-1. Number of hydroxyl group (-OH) of various poly monomers.

Polyol	Number of hydroxyl groups	Minimum shrinkage (%)
EOM	1	5.84
TPPG	2	1.72
PCAT	3	4.00

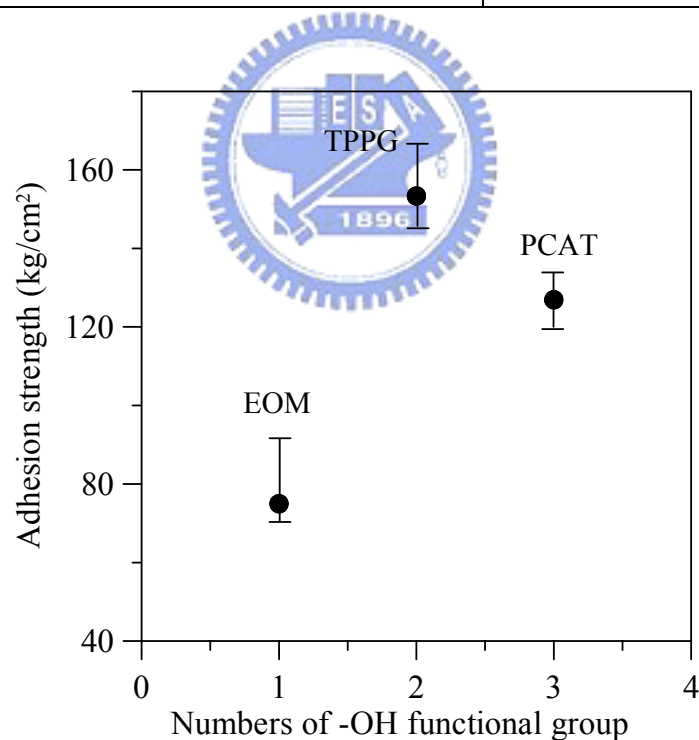


Figure 4-7. Adhesion strength *versus* numbers of hydroxyl group of polyol monomers.

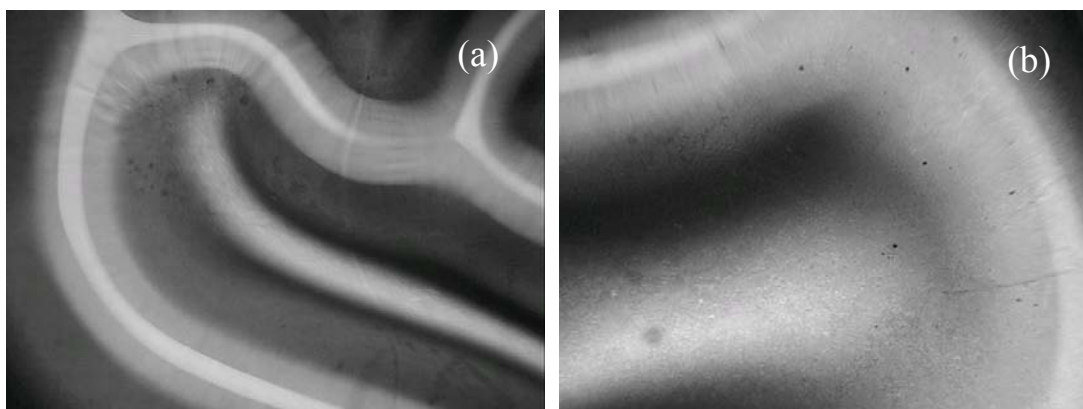
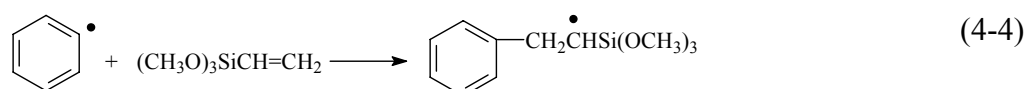
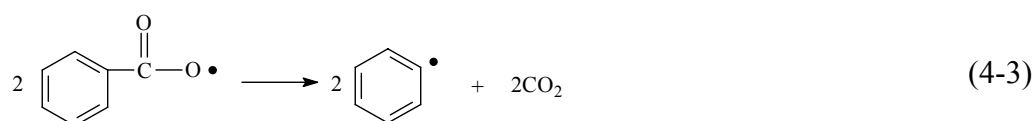
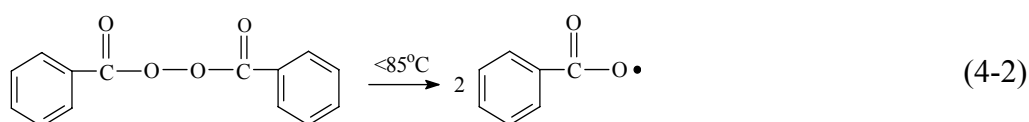
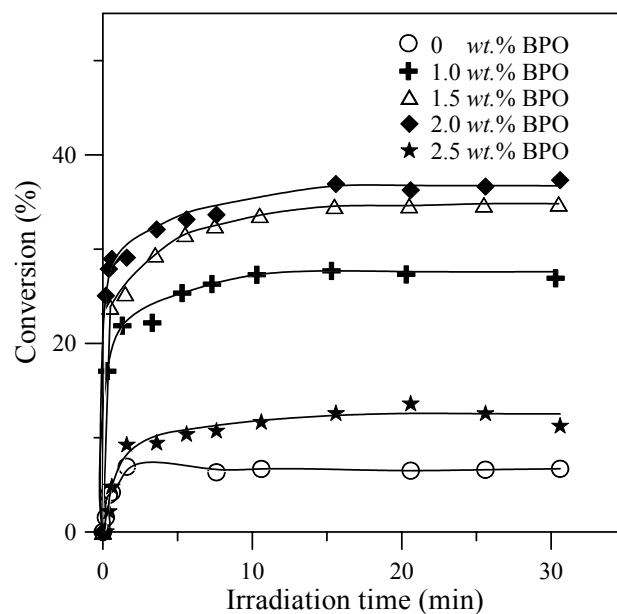


Figure 4-8. Surface morphology of epoxide resins containing (a) EOM (b) PCAT after UV curing (Magnification = 20×).

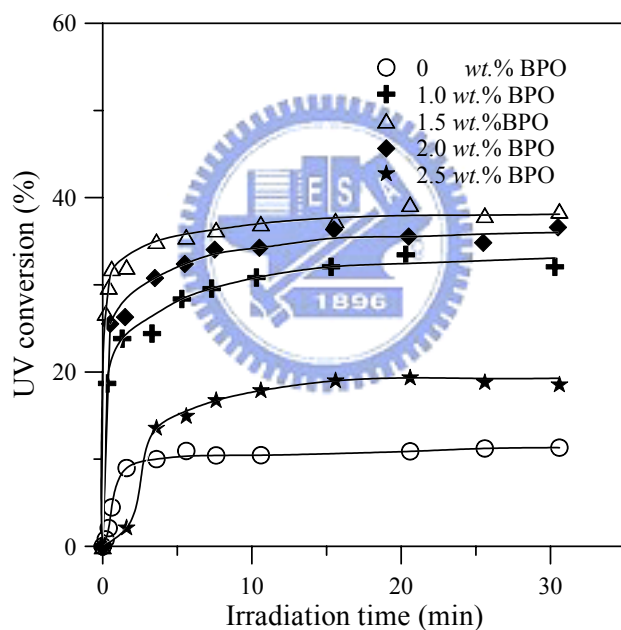
4.1.5. The Effects of BPO and UV Reactivity

Benzoyl peroxide (BPO) is a common free-radical photoinitiator and/or thermal initiator added in UV-curable resins. The radicals for polymerization are produced *via* the thermal or photochemical decompositions of BPO. Equations (4-2) and (4-3) show the initiating reactions of BPO when heated or irradiated by UV light [136]. In this work, vinyl silane was added into the resin samples in order to improve their adhesion strength on glass [143]. However, BPO reacted with the $-C=C-$ bond on vinyl silane *via* free-radical photo-polymerization as shown in Eq. (4-4). As revealed by $^1\text{H-NMR}$ spectra presented in Figs. 4-9(a) and 4-9(b), the peaks corresponding to hydrogen atom on double bonds of vinyl group at $\delta = 6.125\text{-}6.022$ of $^1\text{H-NMR}$ spectrum disappear after UV curing. This evidences the reactivity of $-C=C-$ bonds on silane with phenyl radicals.





(a)



(b)

Figure 4-10. Conversions of resin samples evaluated by absorbance change of peak corresponding to (a) $-\text{SiCH}=\text{CH}_2$ group located at 975.4 cm^{-1} and (b) epoxy group at 910 cm^{-1} of FTIR spectra versus the UV irradiation times.

Increasing trend of UV conversions of epoxy group shown in Fig. 4-10(b) also implies that the addition of BPO up to about 2.0 wt.% benefits the photo-polymerization of resins. Dursun *et al.* reported that onium salts (On^+) such as

triarylsulfonium and diaryliodonium salts (cationic photoinitiators) may serve as electron acceptors in redox reaction relating to free radicals [144]. At appropriate reduction potentials, the presence of onium salts may initiate the oxidation of free radicals to produce cationic species according to Eq. (4-5). The cationic species are able to induce the polymerization of monomers and the so-called free-radical-promoted cationic polymerization is thus established. It has been reported benzoin and its derivatives might serve as the free radical sources for cationic photo-polymerization [145]. This explains the promotion of photo-polymerization in UV-curable epoxide resins by the addition of BPO since it is one of the derivatives of benzoin.



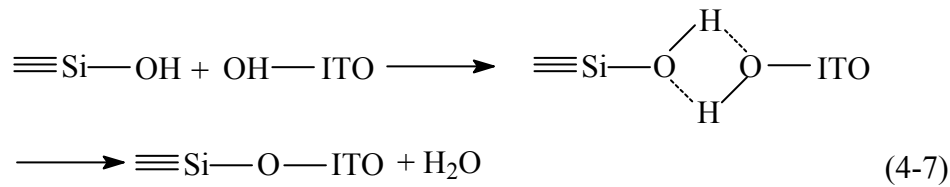
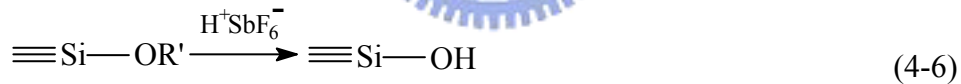
4.2. Effects of Organo-Functional Silanes on Adhesion Strengths of UV-Curable Resins

4.2.1. Chemical Reaction of Silane Containing Alkoxy Groups

Most of the studies relative to the chemical reaction of silane containing alkoxy group ($-\text{SiOCH}_3$) focused on the hydrolysis of alkoxy group to produce $-\text{Si-OH}$ [104,146] so as to improve the adhesion of polymeric materials on inorganic surfaces. In this work, silanol was formed as alkoxy group of silane underwent UV irradiation. FTIR and NMR analyses were utilized to explain the chemical reactions of silanes blended with photoinitiator. Figure 4-11 shows the FTIR spectra of vinyl group silane and silane blended with photoinitiator after UV curing for 60 min. Prior to UV curing, the alkoxy group of silane presents a peak at 1088 to 1076 cm^{-1} . During UV curing, the alkoxy group of silane reacts with H^+SbF_6^- to generate $-\text{Si-OH}$, as evidenced by the peak at 953 cm^{-1} . The other four silanes studied in this work exhibit the same

result. On the other hand, a comparison of ^{13}C -NMR spectra for the specimens of vinyl group silane and the silane blended with photoinitiator subjected to UV curing shown in Figs. 4-12(a) and 4-12(b) that reveal the peak at $\delta = 50.437$ ppm corresponding to alkoxy group of silane vanished after UV curing. Decomposition of alkoxy group of silane by cationic photoinitiator to form $-\text{Si}-\text{OH}$ has been reported elsewhere [147]. Also, the peak at $\delta = 3.569$ ppm in ^1H -NMR spectrum shown in Fig. 4-12(c) corresponds to H atoms on alkoxy groups of silane which disappeared when silane was blended and subsequently underwent UV curing, as show in Fig. 4-12(d).

Apparently, the Brønsted acid generated during UV curing attacks the alkoxy group of the silane and the acid converts the alkoxy groups into silanols, as depicted by Eq. (4-6). The ITO glass surface was treated electrochemically to generate hydroxyl groups [148-150] that reacted with silanol to produce hydrogen bonding, as shown in Eq. (4-7). This is similar to the hydrolysis of silane in order to enhance the adhesion to metals such as steel [151], copper [84] and aluminium [152].



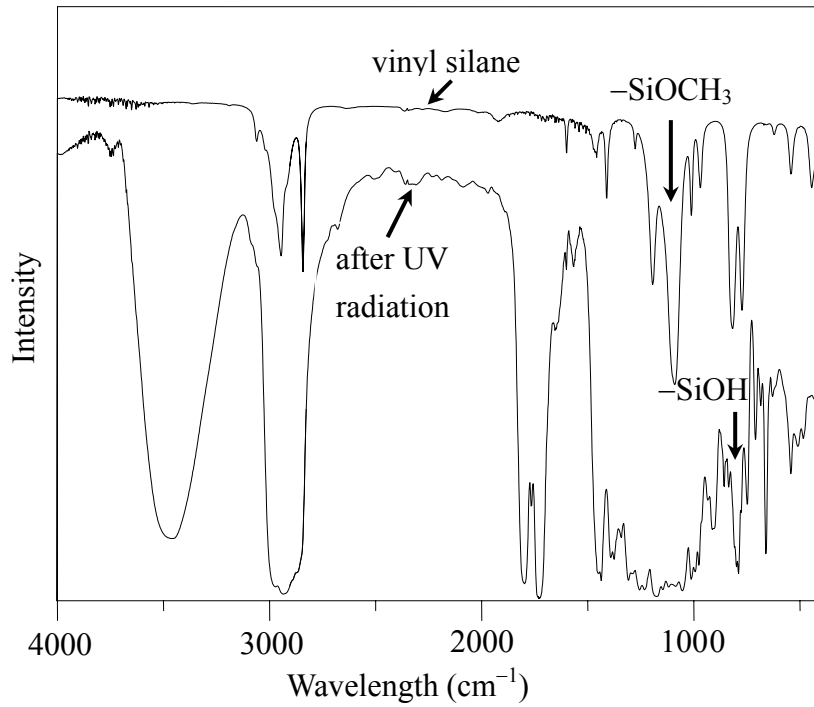


Figure 4-11. FTIR spectra of vinyl group silane and silane blended with photoinitiator after UV curing for 60 min.

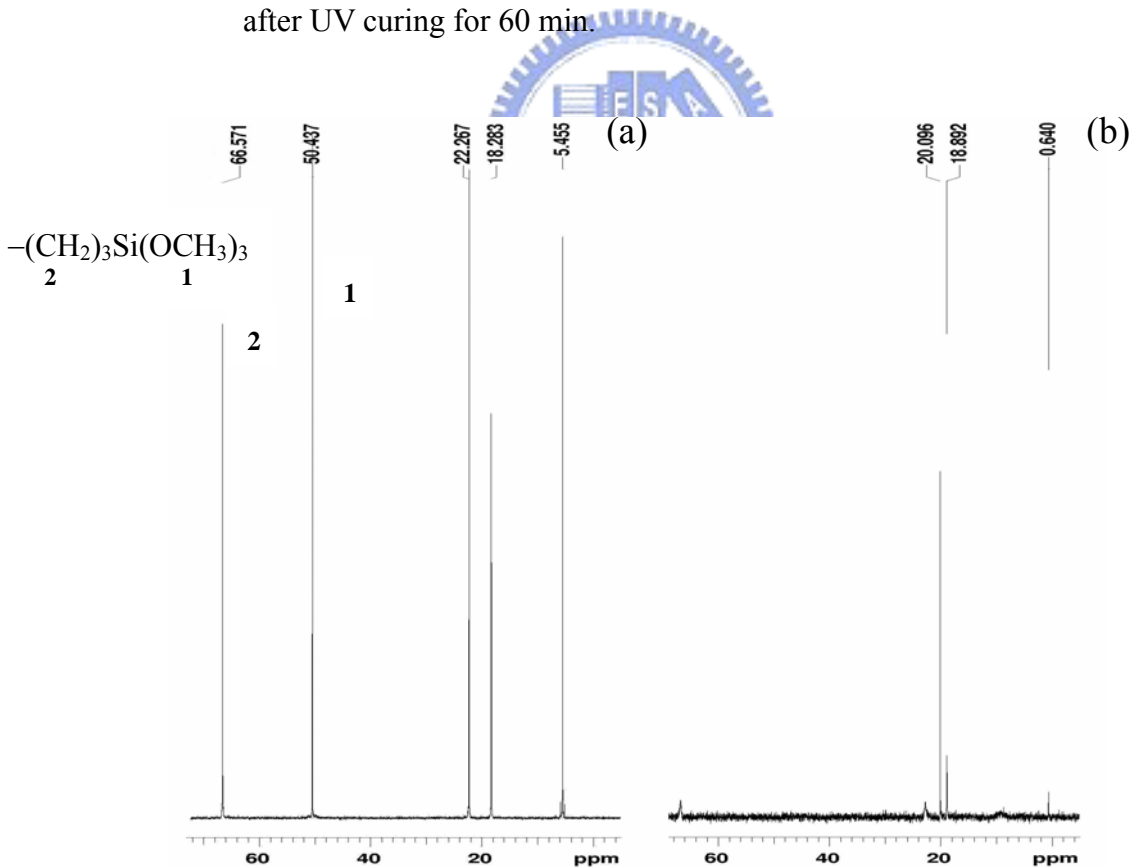


Figure 4-12. ^{13}C -NMR spectra of (a) the alkoxy group of vinyl silane and (b) vinyl silane blended with photoinitiator after UV curing. ^1H -NMR spectra of (c) the alkoxy group of vinyl silane and (d) vinyl silane blended with photoinitiator after UV curing. (continue)

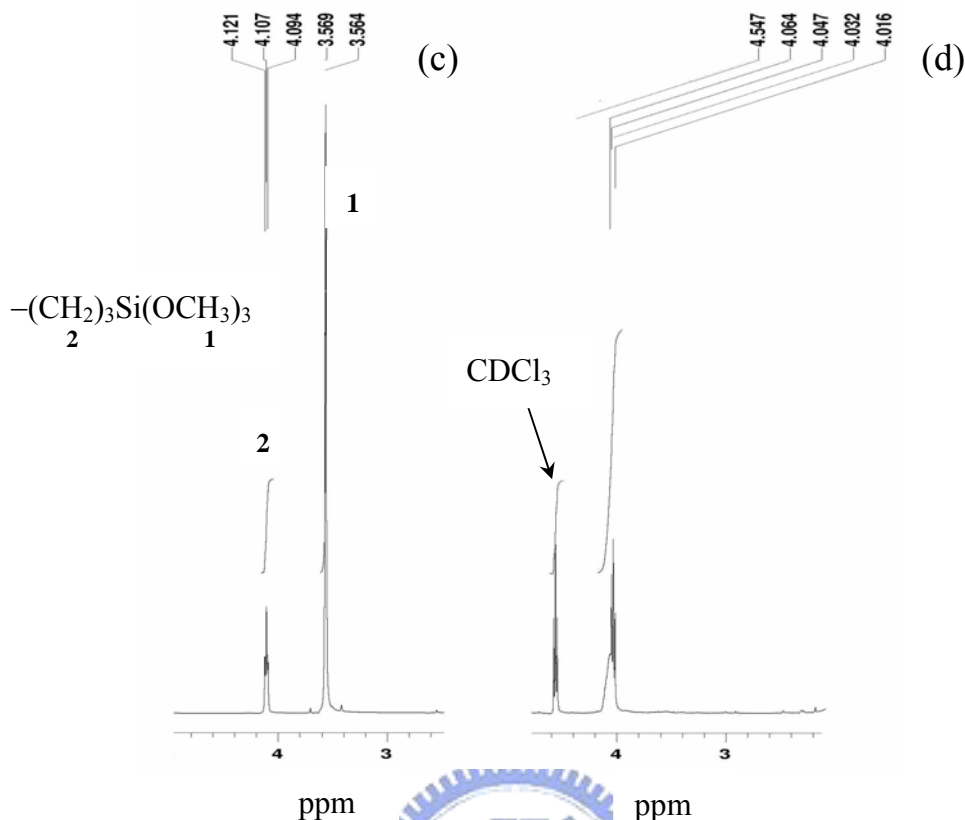


Figure 4-12. ^{13}C -NMR spectra of (a) the alkoxy group of vinyl silane and (b) vinyl silane blended with photoinitiator after UV curing. ^1H -NMR spectra of (c) the alkoxy group of vinyl silane and (d) vinyl silane blended with photoinitiator after UV curing.

4.2.2. The Reactions of Organo-functional Group on Silane and Cationic Photoinitiator

The reactions of organo-functional group on silane coupling agent and cationic photoinitiator affect the adhesion strength of resin on ITO glass. This work focused on the effect of UV curing time of the samples prepared by mixing 1 g of cationic photoinitiator and 0.5 g of selected silane coupling agent. Table 4-2 shows the UV curing times for different silanes blended with photoinitiator. The lengths of UV curing time were in the order: amino > vinyl > methacrylic > acrylic > epoxy. The UV curing time of epoxy silane is the shortest because a cationic photoinitiator was used in this work. The silanes containing acrylic, methacrylic, and vinyl groups can

undergo free-radical polymerization. Different C=C double bond structures in these organo-functional groups imply different UV reactivities. The free-radical polymerization reaction was relatively slow in comparison to the cationic polymerization in the system due to the low production rate of initiating radicals during the photolysis of the onium salt [52]. Meanwhile, the UV reactivity was in the order: acrylic > methacrylic > vinyl \approx allyl > double bond in the main chain. Acrylic group silane exhibits the highest UV reactivity because its $-\text{COOR}$ group is electrophobic [153]. It can decrease the density of electron cloud on the C=C bond and makes it easier to bond with the free radicals. The UV reactivity of methacrylic group silane is lower than that of acrylic group since it possesses electrophilic $-\text{CH}_3$ group [153] which increases the density of electron cloud. The vinyl group silane has the lowest UV reactivity because of the high density of electron cloud on the C=C bond and lack of substituent group. Different functional groups with the C=C double bond affect differently the crosslinking density of the network and the length of curing time of resin [154-155]. As to the amino-functional silane, it inhibits the UV curing reaction and thus resin sample could not be cured, as described by Plueddemann [80].

From the ^{13}C -NMR spectra shown in Figs. 4-13(a) and 4-13(b), the peaks of epoxy group silane at $\delta = 50.269$ and 43.885 ppm disappeared after UV curing. There are two signals appearing in peak 2 of Fig. 4-13(a) and their locations are too close to be differentiated as to which one is methoxy carbon and which one is epoxy carbon. However, the peak at 43.885 ppm corresponds to epoxy carbon and it disappeared after UV irradiation, which means epoxy silane had reacted with H^+SbF_6^- . For the ^1H -NMR spectra shown in Figs. 4-13(c) and 4-13(d), the peaks of epoxy group silane at $\delta = 2.6-3$ and $3.2-3.5$ ppm disappeared after UV curing, and the peaks at $\delta = 4.8868$ and 4.046 ppm are generated by the photoinitiator. The reaction of epoxy silane with H^+SbF_6^- produces oxiranium ion as depicted by Eq. (4-8) [156].

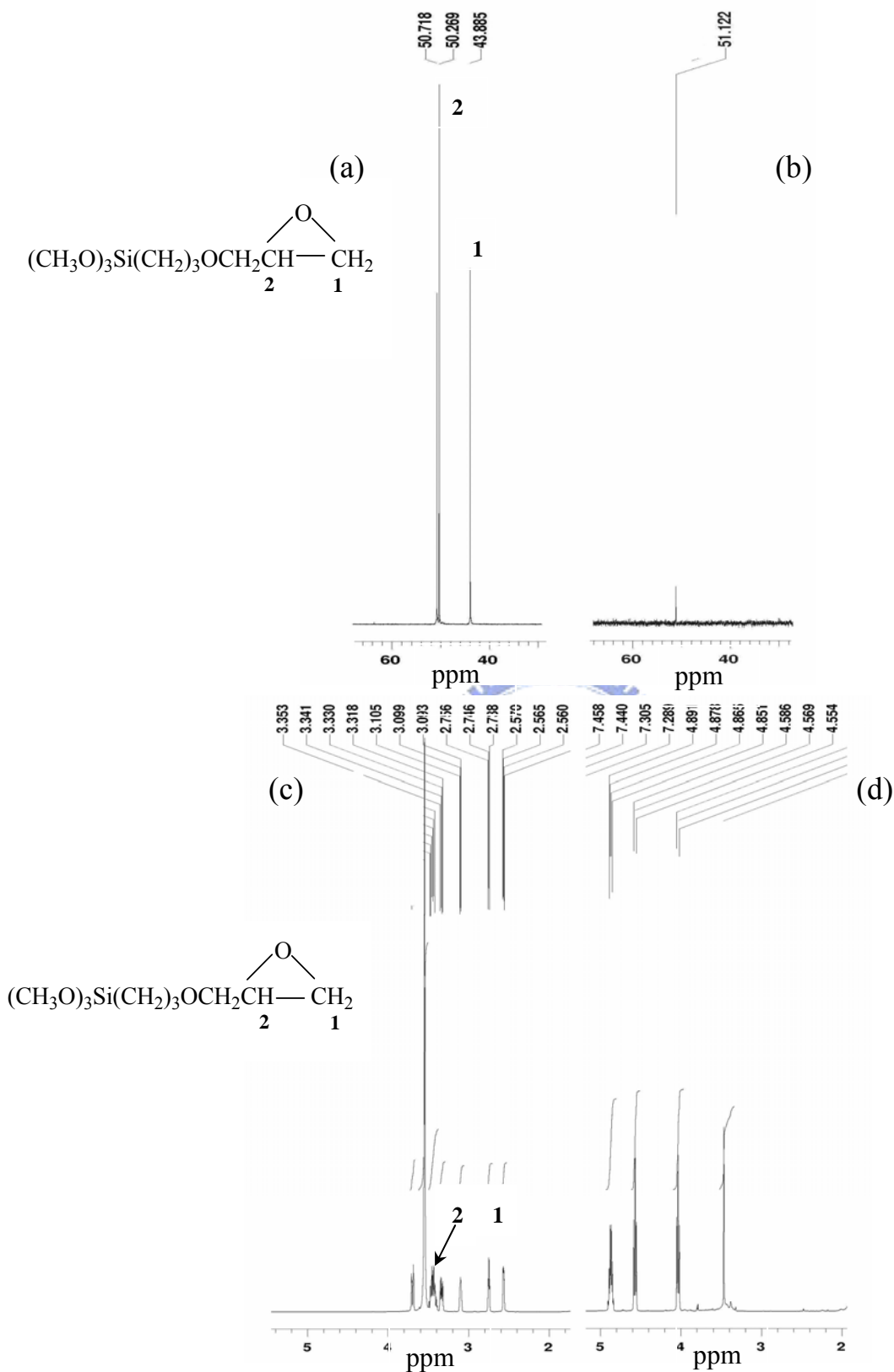
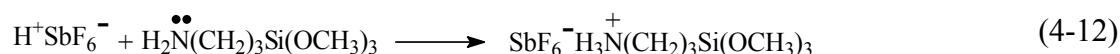
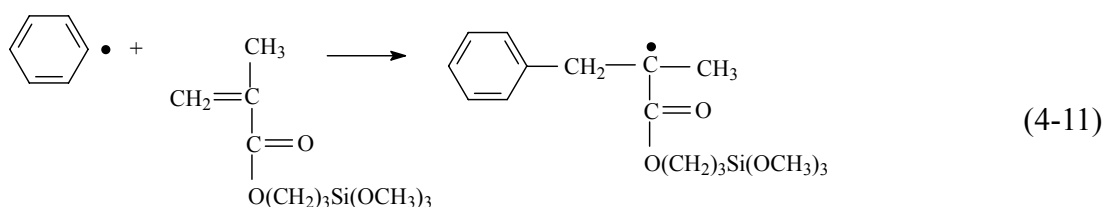
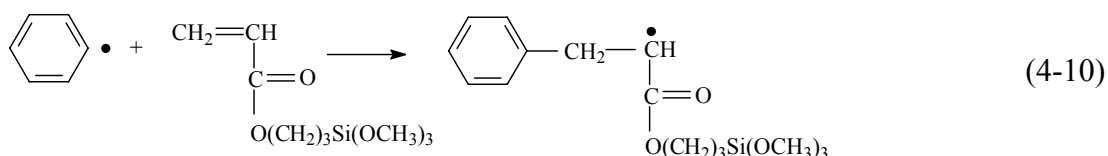
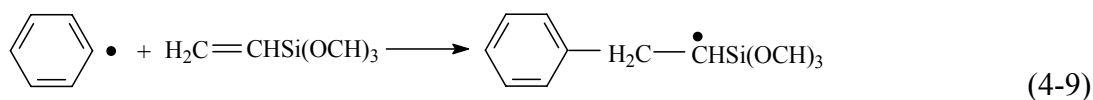
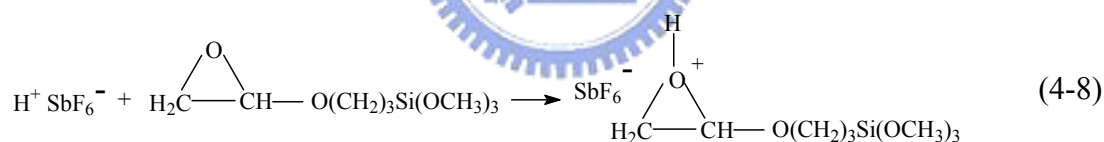


Figure 4-13. ^{13}C -NMR spectra of (a) the epoxy silane and (b) epoxy silane blended with photoinitiator after UV curing. ^1H -NMR spectra of (c) the epoxy silane and (d) epoxy silane blended with photoinitiator after UV curing.

According to Eq. (2-11), phenyl radical was produced by the photoinitiator during UV irradiation and the radical would bond to the double bonds present in the monomer [47]. Organofunctional groups of vinyl, acrylic and methacrylic silanes all possess C=C double bonds which can undergo free-radical polymerization as described by Eqs. (4-9) [157], (4-10) [78], and (4-11) [158]. The chemical structures for the three types of silanes, vinyl, acrylic and methacrylic, were evidenced by the ¹H-NMR spectra shown in Figs. 4-14(a), 4-15(a) and 4-16(a), respectively. The peaks of double bonds of vinyl, acrylic and methacrylic groups are at $\delta = 6.125$ - 6.022 and 5.944 - 5.873 ppm, $\delta = 6.4$ - 6.1 and 5.827 - 5.928 ppm and $\delta = 6.091$ and 5.941 ppm, respectively. After UV curing, the C=C double bonds of these three types of silanes reacted with phenyl radical and hence the corresponding peaks disappeared as presented in Figs. 4-14(b), 4-15(b) and 4-16(b), respectively. Furthermore, the H atoms on the phenyl group of the photoinitiator result in the peak at $\delta = 7$ - 8 ppm.



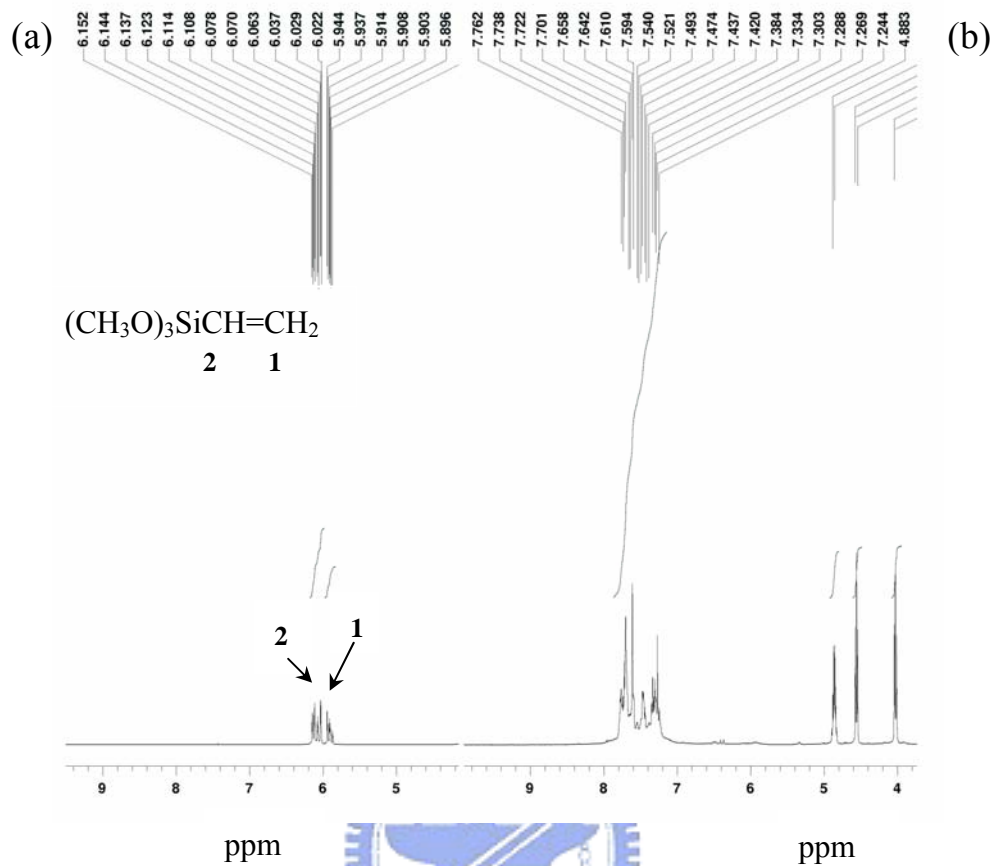


Figure 4-14. ^1H -NMR spectra of (a) vinyl silane and (b) vinyl silane blended with photoinitiator after UV curing.

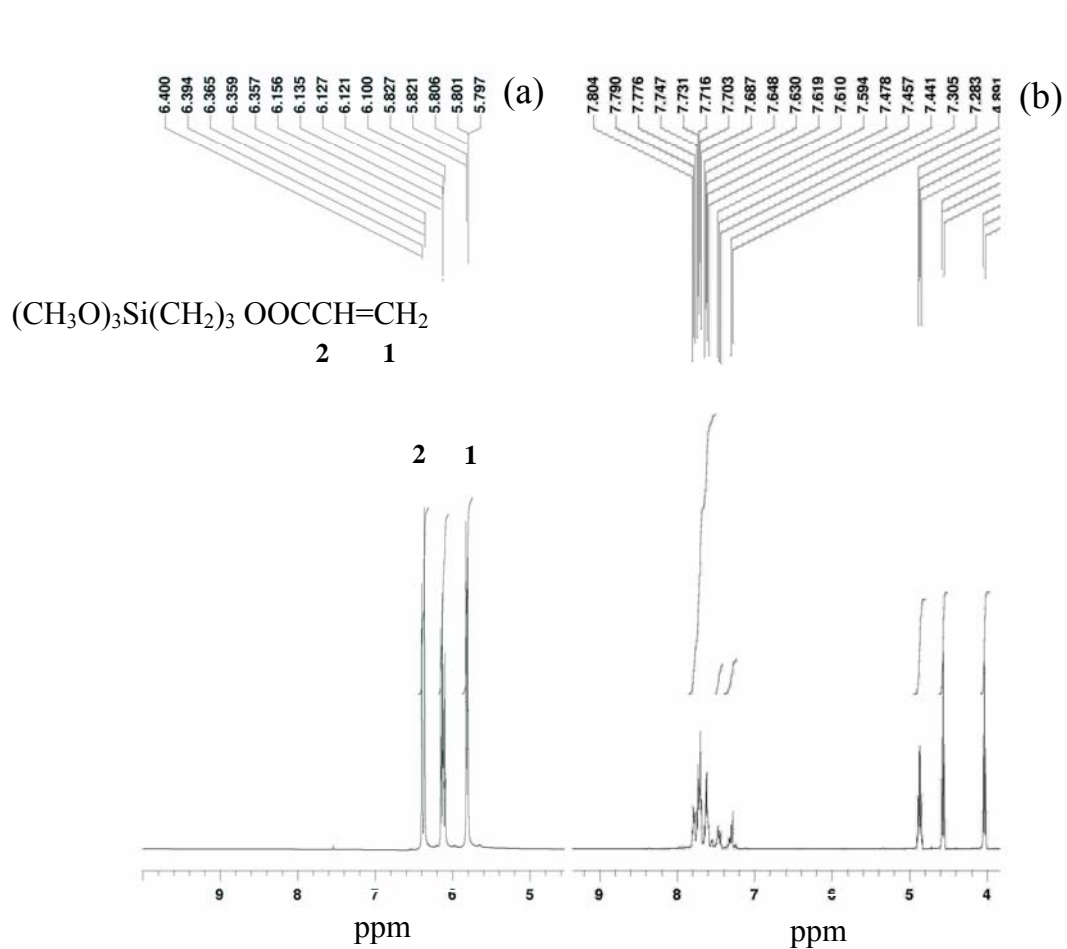


Figure 4-15. ^1H -NMR spectra of (a) acrylic silane and (b) acrylic silane blended with photoinitiator after UV curing.

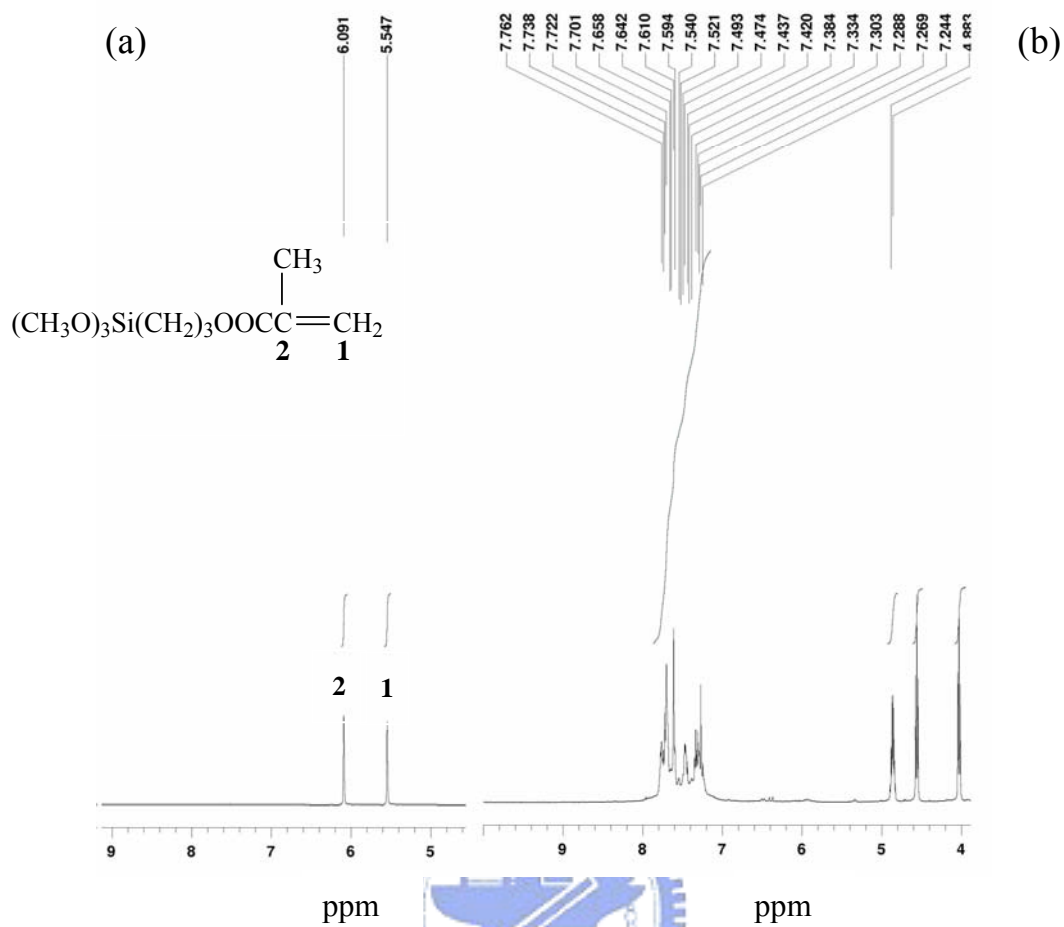


Figure 4-16. $^1\text{H-NMR}$ spectra of (a) methacrylic silane and (b) methacrylic silane blended with photoinitiator after UV curing.

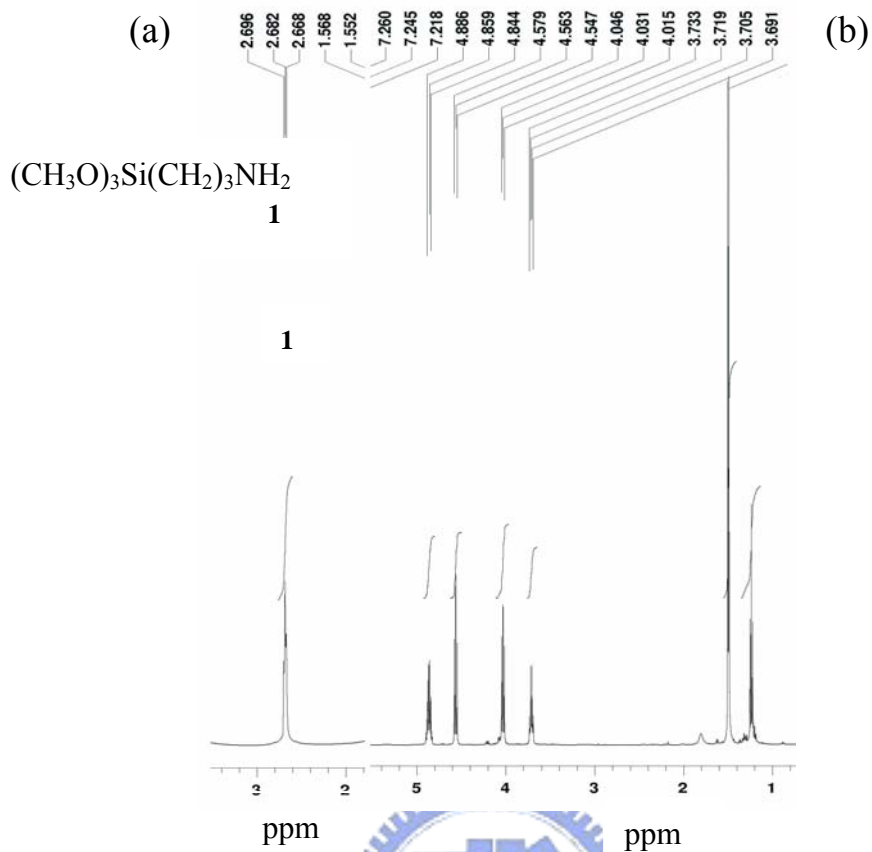


Figure 4-17. ^1H -NMR spectra for (a) amino silane and (b) amino silane blended with photoinitiator after UV curing.

Figures 4-18(a) to 4-18(f) show morphology of epoxide resin containing various types of silanes after UV curing and the degree of shrinkage can be readily seen from the morphology change of specimen surfaces. Referring to Fig. 4-18 and Table 4-2, it is found that a shorter curing time implies a larger shrinkage and *vice versa*. As shown in Fig. 4-18(a), the resin containing vinyl group exhibits the smoothest surface with the smallest degree of shrinkage and the longest curing time. The degree of shrinkage was found to be in the order: vinyl < methacrylic < acrylic < epoxy < sample free of silane additive < amino.

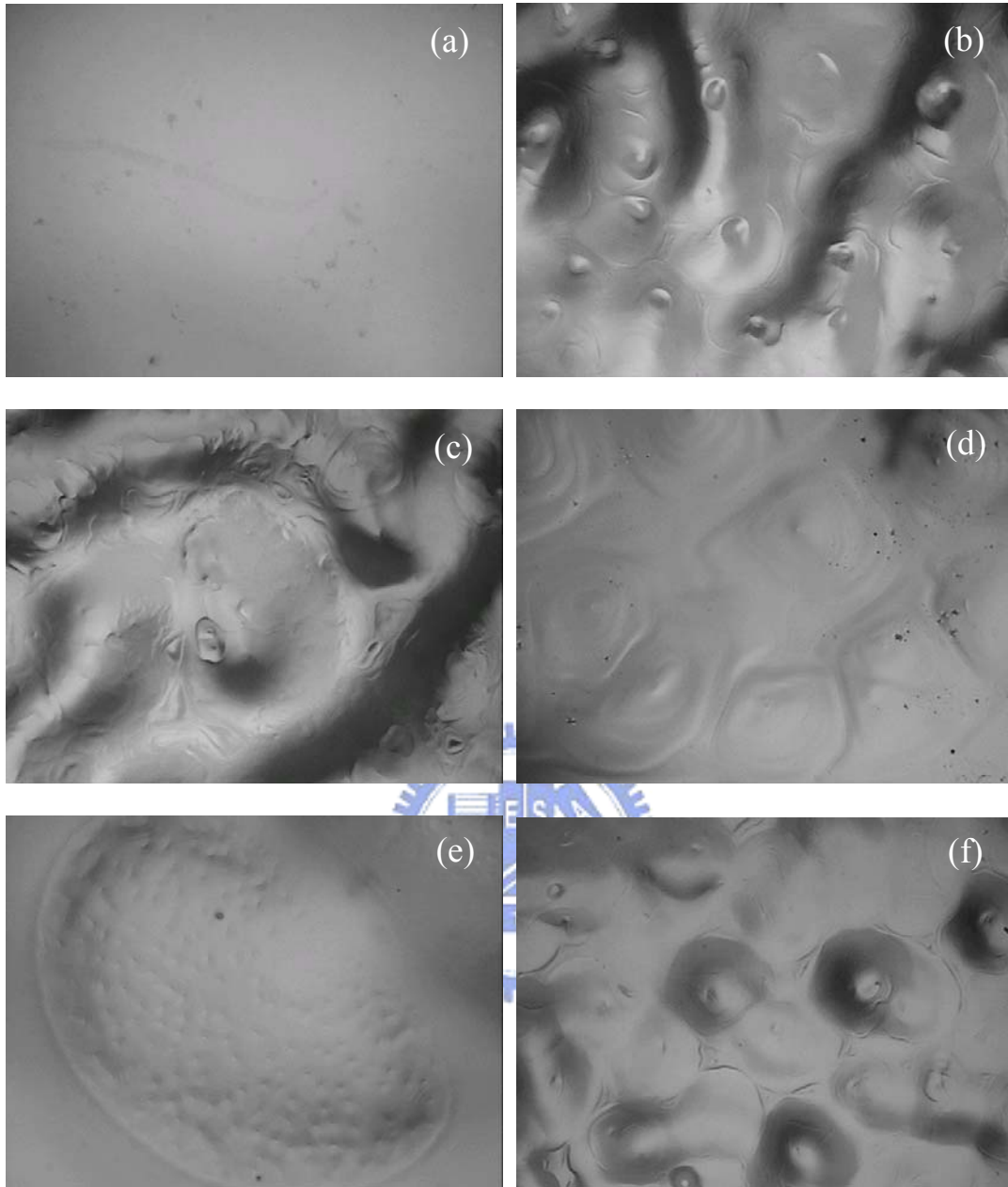


Figure 4-18. OM images of epoxide resins containing: (a) vinyl, (b) epoxy, (c) amino, (d) acrylic, (e) methacrylic silanes and (f) free of silane additive after UV curing (magnification = 20 \times).

Table 4-2. Curing times of samples containing various silanes.

Silane type	Curing time (min)	Polymerization method	Organo-functional group
Vinyl	60	Free radial	-CH=CH ₂
Epoxy	5	Cationic	
Amino	(Uncurable to be cured)		-NH ₂
Acrylic	8	Free radial	-OOCCH=CH ₂
Methacrylic	45	Free radial	-OOC(CH ₃)=CH ₂

4.2.3. Effects of Silane Functional Groups on Adhesion Strengths

Shrinkage of the resin occurred during the curing process may affect its adhesion strength because it may induce internal stress that pulls the adhesive resin away from substrate [141,142]. Figure 4-19 shows the adhesion strengths of five adhesive resins blended with different type of silanes and resin without silane evaluated by a pull test. The adhesion strengths to ITO glass were found to be in the order: vinyl > methacrylic > acrylic > epoxy \approx sample free of silane additive > amino and the values are 79.77, 78.18, 59.39, 36.78, 35.57 and 22.77 kg/cm², respectively. The trend of adhesion strengths is similar to that reported by Priola *et al.* [152] who studied the adhesion of BGEDA resins containing vinyl, methacrylic, and acrylic silanes to steel sheet [152]. The results of adhesion study also evidenced that a reduction in resin shrinkage implied a decrease of internal stress that would benefit the adhesion strength of resins.

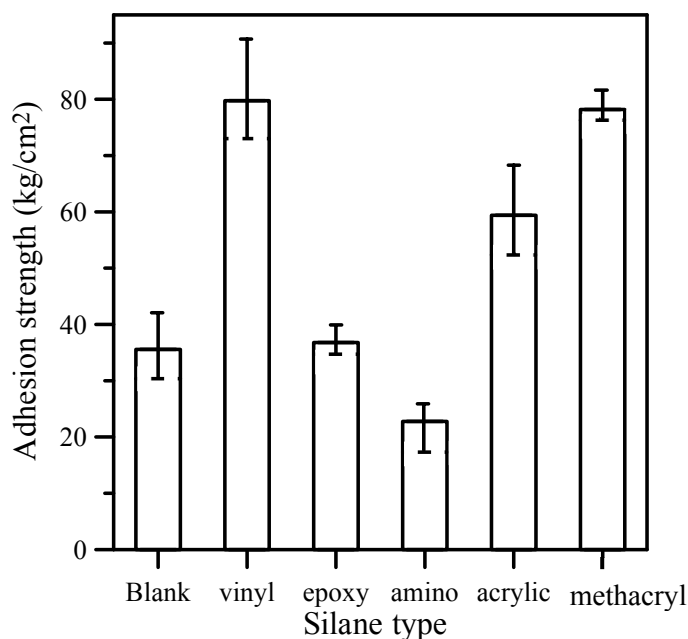


Figure 4-19. Adhesion strength of epoxide resins containing various types of silanes to ITO glass.

4.2.4. Effect of Weight Percentage of Vinyl Group Silane on Adhesion Strengths

According to the results of pull test, the adhesive resin containing vinyl group silane exhibited the highest adhesion strength. Subsequent study was hence focused on the adhesion property to ITO glass for such resin containing different weight percentages of vinyl group silane. From the results of pull test shown in Fig.4-20, one can readily see that the resin sample containing 1.0 wt.% of vinyl group silane possesses the highest adhesion strength of 91.42 kg/cm². When the weight percentage of silane was further increased, a decreasing trend in adhesion strength of the resin was observed. Silanol, produced from the UV-irradiated alkoxy, reacted with the hydroxyl groups of ITO glass to generate Si-O-ITO bonds and some H₂O as shown in Eq. (4-6). Meanwhile, Si-O-Si bonds and H₂O are generated from the reaction between silanol groups [160-161]. As a result, there was more H₂O generated *via* these reactions when more silane was added in the resin. As a matter of fact, the addition of 1.0 wt.% of silane giving the highest adhesion strength among all of the

samples is in good agreement with the report of Gupta and Dhuldhoya [162]. Furthermore, an excessive amount of silane might dilute the concentration of resin and decrease the adhesion strength, which was reported by Gu, *et al.* [84] who studied the adhesion of epoxide resin containing γ -aminopropyltrimethoxysilane.

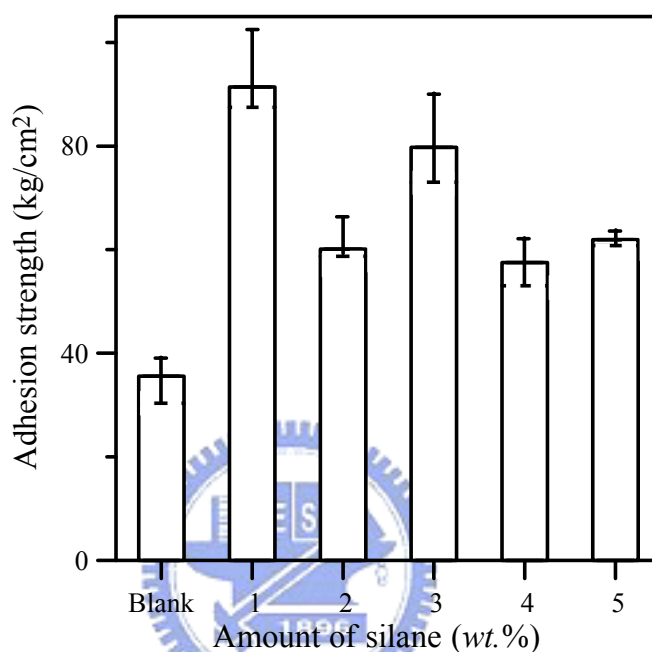


Figure 4-20. Adhesion strengths of epoxide resins containing different weight percentages of vinyl silane to ITO glass.

4.3. Effects of Tertiary Amines on UV-Curable Epoxide Resins

4.3.1. UV Conversions of Tertiary Amines

During UV curing, the strong Brønsted acid ($H^+SbF_6^-$), a derivative of photoinitiator, may induce cationic polymerization in epoxide resins to produce oxiranium ion. The cationic polymerization takes place by attacking the protonated epoxide on another epoxide resin. The peak height of absorption band at 910 cm^{-1} corresponding to the epoxy group hence changes with the UV irradiation time and amine amount. Figure 4-21 presents the UV conversions of resin samples containing various amounts of 3-amine calculated based on the change of such a peak height. It

can be seen that the UV conversion decreases with the increase of 3-amine content up to 1.0 wt.%. The resin sample could no longer be UV-cured when the amount of 3-amine exceeded 1.0 wt.% and similar results were observed in the resin samples containing the other four types of amines. The nitrogen atom of amines owning a lone pair of electrons may react with H^+SbF_6^- to produce ammonium salts [159] and consequently inhibit the photo-polymerization process of adhesive resins [163]. The excess amount of imidazole or tertiary amines is hence not allowed in the UV-curable epoxide resins.

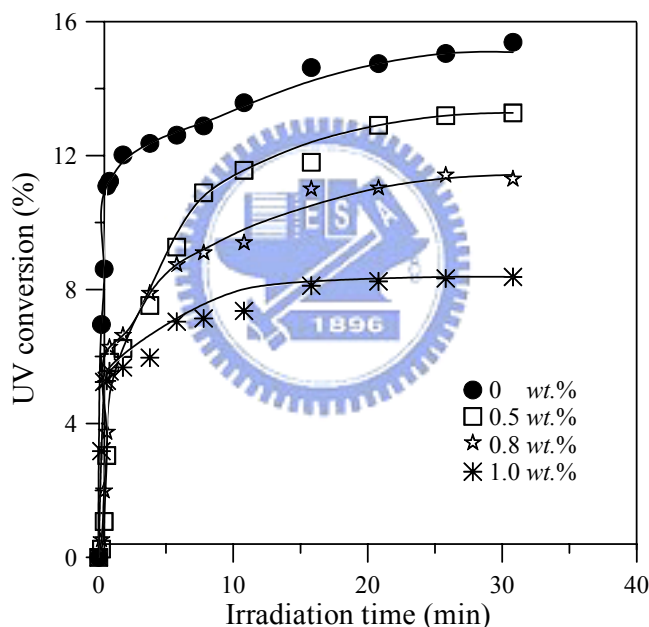


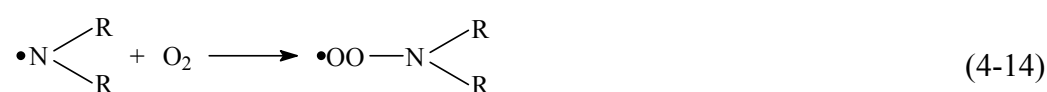
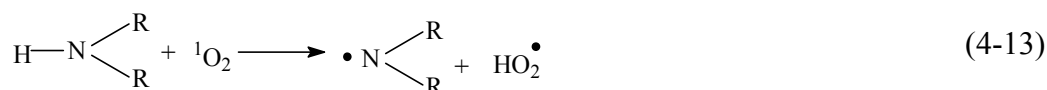
Figure 4-21. UV conversion versus the irradiation time of resin samples containing various amounts of 3-amine.

4.3.2. Tertiary Amines React with BPO under UV Irradiation

The tertiary amines reacted with BPO because singlet oxygen was produced by a triplet energy transfer from photosensitizer (*i.e.*, the free radical initiators such as BPO) to ground-state oxygen during UV irradiation [164]. The result of reaction was described by FTIR spectroscopy for assessing. The 4-amine mixed with BPO, which

of the absorption intensity of CH₃-N- on 4-amine at the 1232 cm⁻¹ disappeared after UV irradiation as shown in Fig. 4-22. In addition, Fig. 4-23 is ¹H-NMRs of spectra of 4-amine mixed with BPO before UV irradiation and after irradiation. The CH₃-N- on 4-amine took place a chemical shift from δ 3.284 ppm of ¹H-NMR spectrum to δ 3.757 ppm after UV irradiation and there was same result as 4-amine were replaced by 2- or 3-amines. The mechanisms of singlet oxygen reacted with 2-, 3- and 4-amines are *via* an electron transferring process to produce α-aminoalkyl radicals in accordance with Eq. (2-32) [101]. The α-aminoalkyl radicals of 2-, 3- and 4-amines, depicted by Figs. 4-24(b) to 4-24(d) then reacted with oxygen to produce α-hydroperoxyamine (HOOCH₂NR₂) and α-aminoalkyl radical *via* the reactions shown by Eqs. (2-33) and (2-34).

As Figure 4-25 presented, 1-amine reacted with BPO of which absorption intensity of NH- on 1-amine at the 1136 cm⁻¹ disappeared after UV irradiation and there was same result as 1-amine was replaced by 5-amine. The aminyl radicals of 1- and 5-amines, presented in Figs. 4-24 (a) and 4-24(e), reactions of singlet oxygen with 1- and 5-amines were shown in Eq. (4-13) which further reacted with oxygen to produce HOONR₂ and aminyl radical *via* the reactions shown by Eqs. (4-14) and (4-15). The oxygen scavenging processes was depicted by Eqs. (2-32) to (2-33) and Eqs. (4-13) to (4-14) are able to inhibit the oxidation in the backbone structure of resins [4].



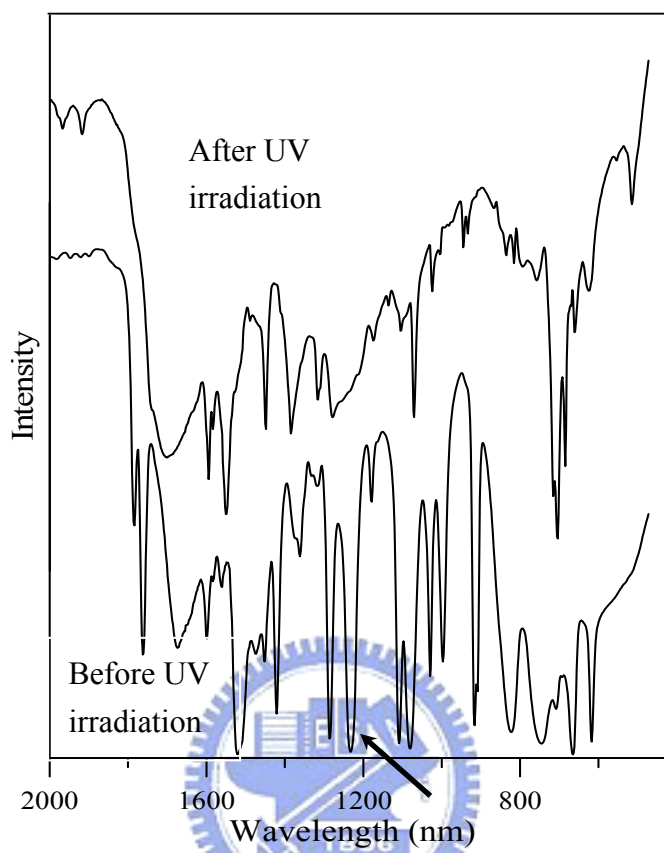
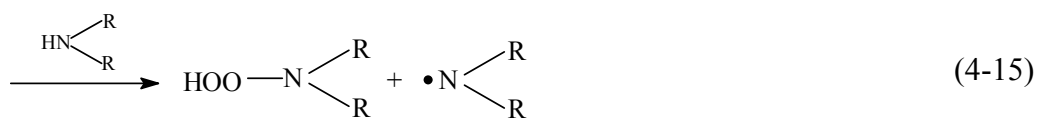


Figure 4-22. 4-amine mixed with BPO before and after UV irradiation.

and (b) after irradiation.

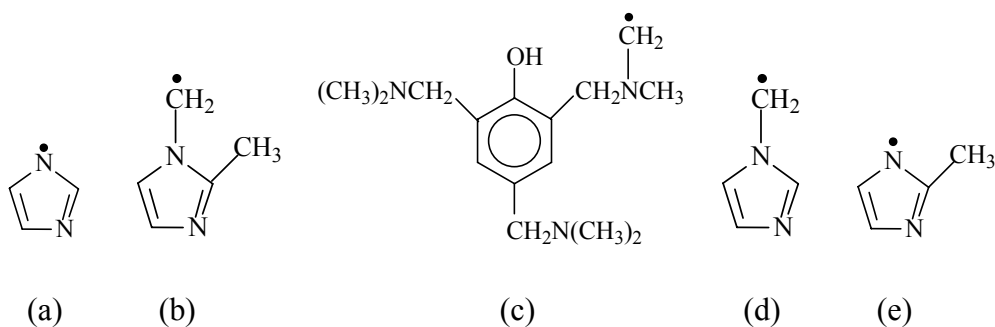


Figure 4-24. Structure of radicals generated by reactions of singlet oxygen with (a)1-amine, (b) 2-amine, (c) 3-amine, (d) 4-amine and (e) 5-amine.

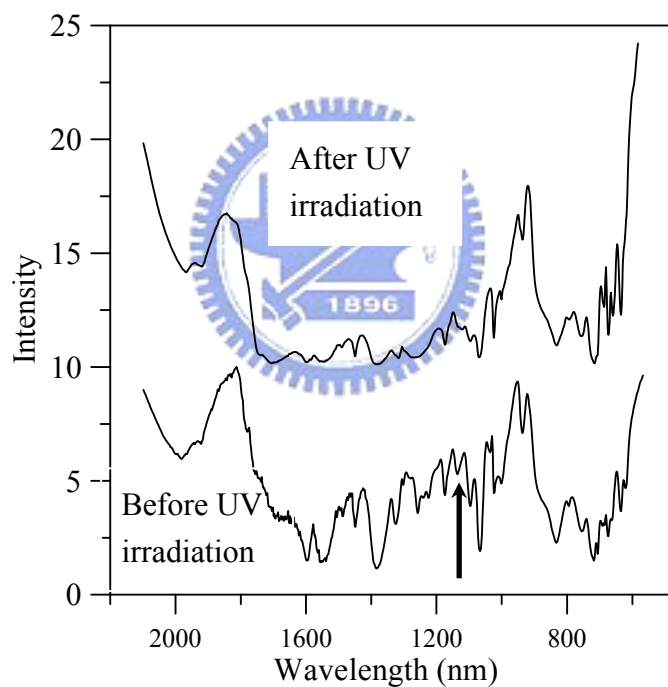
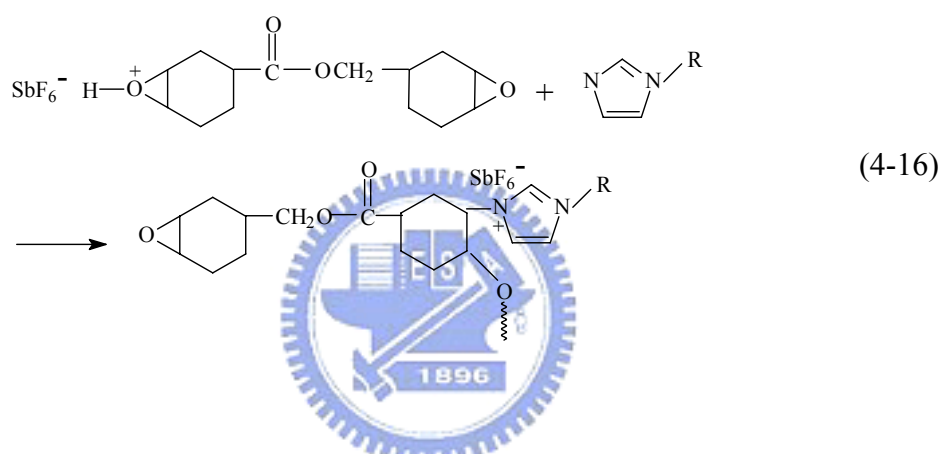


Figure 4-25. 1-amine mixed with BPO before and after UV irradiation.

4.3.3. Effect of Tertiary Amines on Thermal Conversions

Thermal polymerization of all types of samples was resulted from the photolysis of photoinitiator that produced H^+SbF_6^- to attack epoxide resin and consequently induce the polymerization [165]. The cycloaliphatic epoxide resins are highly

sensitive to acid-catalyzed cationic polymerization at room temperature. During the photo-polymerization process, the attack of H^+SbF_6^- produces oxiranium ions in accordance with the reaction depicted by Eq. (2-12). The oxiranium ions then react with the amines to induce cationic thermal polymerization according to the reaction shown in Eq. (4-16). It has been reported that triarylsulfonium salts is developed as the photoinitiator and cationic catalyst during cationic thermal polymerization [166,167].



Thermal conversion of the resin samples containing various types of amines was subjected to 10-min UV curing followed by post-curing at 80°C for 1 hr, which was studied by DSC isothermal scanning method. As seen in Fig. 4-26, the resin sample containing 3-amine exhibits the fastest thermal conversion while the sample containing 5-amine possesses the slowest conversion rate. The differences of crosslinking density in resins could be attributed to the reactivity of amines during thermal polymerization.

The highest conversion resulted from the addition of 3-amine indicates that such a tertiary amine is able to provide the fastest thermal polymerization in UV-curable epoxide resins. This is attributed to the following facts: (1) the presence of phenol hydroxyl groups that may offer further reactive sites containing active-hydrogen

of –OH to react with oxirane of resin [96, 167] and (2) the nitrogen in 3-amine may react with oxirane. For instance, it is known that phenol-compounds such as poly(*p*-vinylphenol) and 2,3,6-tris(dimethylaminomethyl) may serve as the curing accelerators of epoxy resins due to its faster thermal polymerization and better crosslinking capability in comparison with imidazole amine [168]. The ring-opening rate of epoxides containing amine-type curing agents could thus be enhanced by the presence of phenol compounds [169] so that high thermal conversion was observed in the resin sample containing 3-amine [170].

Imidazole exhibits distinct curing behaviors when the substituents at 1- and 2-positions are different [7]. The thermal reactivity of methyl substituent (CH₃–) at the 1-position of 2- and 4-amines are faster than that of pyrrole-type nitrogen substituent (NH–) at 1-position of 1- and 5-amines since the methyl substituent tends to push electrons towards the active nitrogen [7]. It is easier for methyl substituent to release electrons in comparison with hydrogen substituent (H–), which implies a richer electrons and better reactivity of 3-position nitrogen on 4-amine in comparison with 3-position nitrogen on 1-amine. Therefore, thermal conversion of resin containing 4-amine is faster than that of resin containing 1-amine. There is no effective steric hindrance for 1- and 4-amines due to the existence of hydrogen substituent at the 2-position; on the contrary, methyl substituent at the 2-position provides effective steric hindrance for 2- and 5-amines and hence promotes the thermal polymerization. Thermal polymerization of 1-amine is faster than that of 2-amine since there is pyrrole-type nitrogen on 1-position and no steric hindrance at 2-position. The 5-amine exhibits the slowest thermal polymerization owing to the pyrrole-type nitrogen substituent at 1-position and methyl substituent at 2-position. The thermal polymerization of resin samples rated according to the amine type is hence in the order of: 3-amine > 4-amine > 1-amine > 2-amine > 5-amine.

The values of T_g and CTE of the resin samples containing 1.0 wt.% of various types of amines obtained by TMA are presented in Table 4-3. The sample containing 3-amine possesses the highest T_g (72.3°C) and lowest CTE (70.8 ppm/°C). This is attributed to the highest crosslinking density resulted from the fastest thermal polymerization among the amines under study.

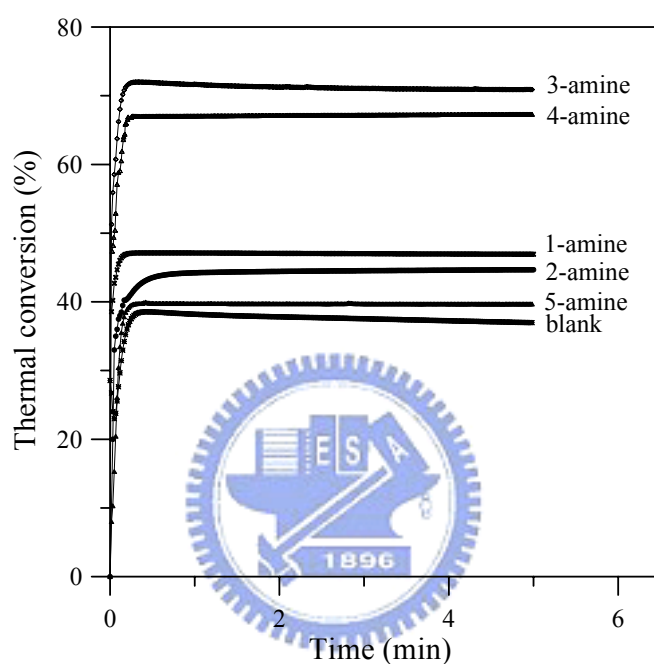


Figure 4-26. Thermal conversion of resin samples containing various types of amines subjected to post-curing at 80°C.

Table 4-3. CTE and T_g of resin samples containing various types of amines.

Amine type	T_g (°C)	CTE (ppm/°C)
(Blank)	67.3	157.9
1-amine	70.6	109.8
2-amine	68.8	124.9
3-amine	72.3	70.8
4-amine	71.3	85.8
5-amine	68.1	139.7

4.3.4. Effect of Tertiary Amines on Adhesion Strengths

Figure 4-27 (a) compares the resin-on-glass adhesion strengths of samples containing 3- or 5-amines UV-cured in air ambient or airtight environment. The airtight environment was accomplished by wrapping the samples tightly with Scotch tape. It can be seen that, regardless of resin types, the adhesion strengths of samples cured in air ambient are much higher than those cured in airtight environment. Hence sufficient oxygen supply is required in order to complete the UV curing of epoxide resins containing tertiary amines.

Figures 4-27(b) and 4-27(c) respectively present the adhesion strengths of resin-on-glass and resin-on-ITO samples. Rated according to amine type, the adhesion strength of resin-on-glass is in the order of: 3-amine (199 kg/cm^2) > 4-amine (181 kg/cm^2) > 1-amine (136 kg/cm^2) > 2-amine (124 kg/cm^2) > 5-amine (170 kg/cm^2) > blank resin (151 kg/cm^2) and the adhesion strength of resin-on-ITO is similarly in the order of: 3-amine (182 kg/cm^2) > 4-amine (162 kg/cm^2) > 1-amine (130 kg/cm^2) > 2-amine (106 kg/cm^2) > 5-amine (147 kg/cm^2) > blank resin (136 kg/cm^2). We however note that the adhesion strength data presented in Figs. 4-27(b) and 4-27(c) do not represent the true adhesion strengths on these substrates for the samples containing 1-, 2-, 3-, and 4-amines since subsequent examination of fracture morphologies revealed that the failure of these four types of specimens occurs *in* the resin matrix rather than *at* the resin/substrate interfaces [105]. Hence the adhesion strengths of resin samples containing 1-, 2-, 3-, and 4-amines on glass and ITO substrates must be higher than those presented in Figs. 4-27(b) and 4-27(c). For these four types of specimens, the adhesion strengths presented in Figs. 4-27(b) and 4-27(c) in fact correlated with the mechanical strengths of resin bulks. In this work the hardness of resin samples was measured in order to reveal such a correlation.

Figure 4-27(d) shows that the Shore D hardness of the samples containing 1-, 2-,

3-, and 4-amines. It can be seen that the values of hardness are arranged in the same order of adhesion strengths presented in Figs. 4-27(b) and 4-27(c) as well as the thermal conversion (*i.e.*, 3-amine > 4-amine > 1-amine > 2-amine) presented in previous section. Such results not only evidence the correlation between adhesion strengths and mechanical strengths of the resins containing 1-, 2-, 3-, and 4-amines, it also demonstrates that crosslinking density of resin affects its bulk fracture strength. Apparently, fast thermal conversion not only implies high crosslinking density, it also provides high adhesion strength so that the resin containing 3-amine exhibits the highest adhesion strengths in comparison with other types of resin samples prepared in this study.

The fractures of resin free of amine and resin containing 5-amine occurred at the resin/substrate interfaces. The resin contained 5-amine reacted with fewer oxygen in air ambient due to its relatively slow thermal conversion rate in comparison with the resins containing other four types of amines (see Fig. 4-26). The resin sample free of amine exhibited the lowest adhesion strength since neither oxygen reaction nor thermal cationic polymerization occurred in it.

The adhesion strengths of resin samples on PET and stainless steel are presented in Figs. 4-27(e) and 4-27(f), respectively. The purpose of adhesion test related to PET was to evaluate the applicability of our resin samples on advanced flat panel displays (FDPs) such as flexible organic light-emitting devices (FOLEDs). As to stainless steel, recently poly-Si TFT on stainless steel foil has been demonstrated [171-172] owing to the advantages of steel such as high mechanical strength, durability, flexibility, and thermal stability [173]. Fabrication of OLEDs on stainless steel substrate containing TFT is hence plausible and thus we evaluate the adhesion strengths of encapsulation resins on stainless steel. In these two types of samples, the fractures all propagate along the resin/substrate interfaces and the adhesion strengths for resin-on-PET and

resin-on-stainless steel samples, if rated according to the amine type, were in the order

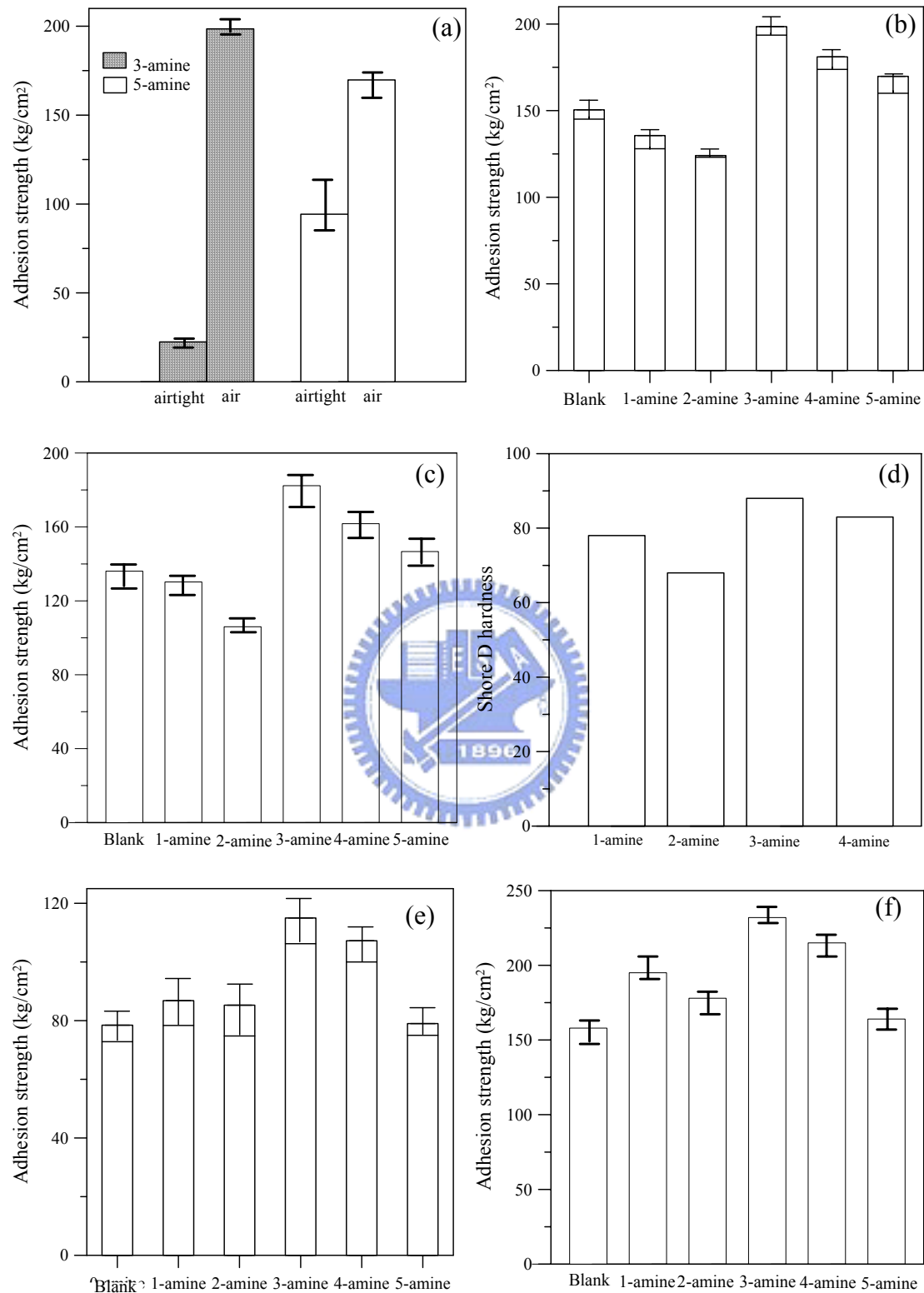


Figure 4-27. (a) Adhesion strengths of resins containing 3-amine and 5-amines cured in air ambient and airtight environment. Adhesion strengths of resins contained various types of amines on (b) glass and (c) ITO substrates (d) shore D hardness of resins contained 1- to 4-amises. Adhesion strengths of resins contained various types of amines on (e) PET and (f) stainless steel substrates.

of: 3-amine (115/232 kg/cm²) > 4-amine (107/215 kg/cm²) > 1-amine (87/195 kg/cm²) > 2-amine (85/178 kg/cm²) > 5-amine (79/164 kg/cm²) > blank resin (78/158 kg/cm²).

Previous analyses revealed the addition of 3-amine provides satisfactory curing behaviors and thermal properties for the UV-curable epoxide resins. In conjunction with the good adhesion properties reported in this section, it is speculated that the resin containing 3-amine would possess great potentials for the packaging applications of opto-electronic products.

4.3.5. Effects of BPO Contents on Amine-free Samples on Etiolation

Table 4-4 and Fig. 4-28 respectively present the ΔE^*_{ab} , ΔYI and transmittance change as function of BPO content of resin sample free of tertiary amines. It can be seen that ΔE^*_{ab} and ΔYI increase along with the higher amount of BPO and the transmittance decreases with the increase of BPO content in the visible-light wavelength range. Further, the values of ΔL^* cited in Table 4-4 defines the transparency of samples and the higher ΔL^* means the higher transparency. The decrease of ΔL^* 's with the increase of BPO content shown in Table 4-4 hence implies the degradation of transparency of resin samples containing BPO as presented in Fig. 4-28. The results above clearly indicate that addition of BPO deteriorates the etiolation and transparency properties of UV-curable epoxide resins though it did benefit the photo-polymerization process.

Table 4-4. ΔL^* , Δa^* , Δb^* , ΔE^*_{ab} and ΔYI of resin samples with different BPO content.

BPO (wt.%)	ΔL^*	Δa^*	Δb^*	ΔE^*_{ab}	ΔYI
0	-12.27	2.08	20.95	24.36	45.84
1.0	-14.81	2.57	24.73	28.94	54.26
1.5	-15.55	2.88	26.31	31.19	59.09
2.0	-16.28	3.52	29.03	33.12	63.06
2.5	-25.09	8.43	30.13	40.11	75.94

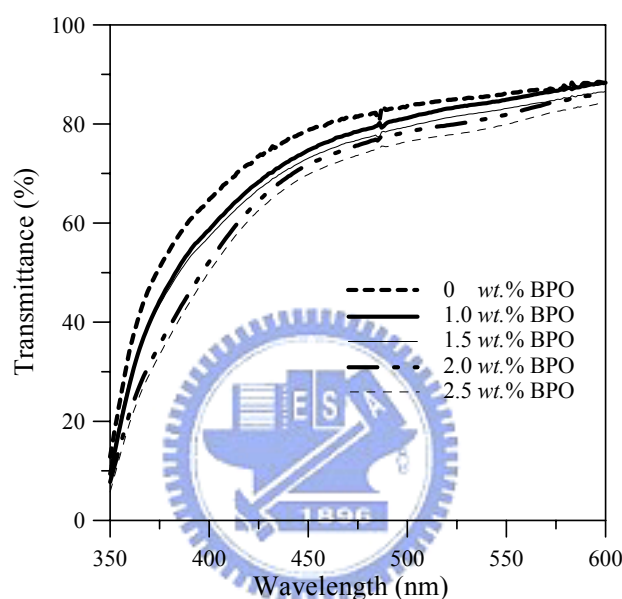


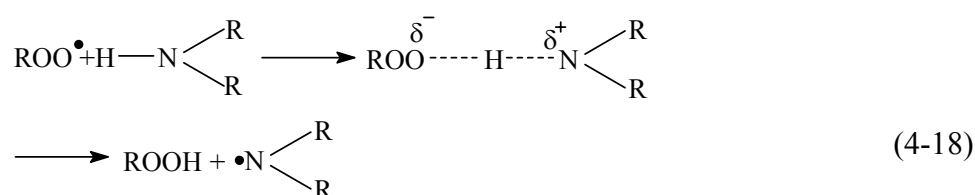
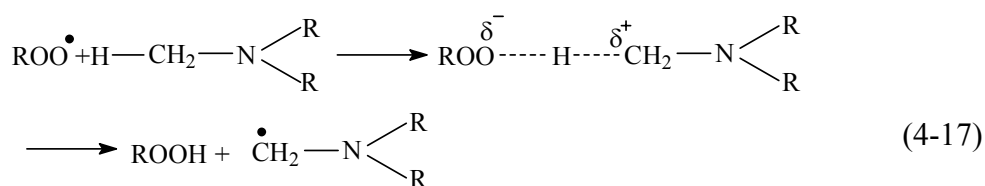
Figure 4-28. The transmittance changes *versus* the BPO contents of resin samples.

4.3.6. Effects of UV Irradiation Times on Etiolation

In this part of study, the etiolation of resin samples containing 2.0 wt.% of BPO and 1.0 wt.% of tertiary amine subjected to various UV irradiation time spans were evaluated. Figure 4-29 presents the variation of ΔE^*_{ab} and ΔYI as a function of UV irradiation times for resin matrix and resin samples containing various types of tertiary amines. Among all samples, resin matrix with free tertiary amine exhibits the highest ΔE^*_{ab} and ΔYI since it abounds with phenol radicals to react with oxygen. The lowest ΔE^*_{ab} and ΔYI are observed in the resin containing 3-amine since there are few phenol radicals to react with oxygen, which indicates that the reactivity of amine with

oxygen affects the values of ΔE^*_{ab} and ΔYI . Angiolini *et al.* [174] reported that higher reactivity implies less yellowing and *vice versa*. It is found in our previous study [175] that the reactivity of amine is in the order of: 3-amine > 4-amine > 1-amine > 2-amine > 5-amine and, therefore, the values of ΔE^*_{ab} and ΔYI of resins are in the order of: 3-amine < 4-amine < 1-amine < 2-amine < 5-amine. The best etiolation improvement provided by 3-amine is thus attributed to its highest reactivity among all the amines subjected to study in this work.

Our experiment found that the most appropriate UV irradiation time is about 10 min since excessive UV exposure produces more free radicals that would react with oxygen to deteriorate the etiolation of resins. Peroxy radicals (ROO \cdot) derived from BPO and photoinitiator in the resins subjected to excessive UV exposure might extract hydrogen from 2-, 3- and 4-amines to form hydroperoxide and α -aminoalkyl radicals as depicted by Eq. (4-17) [101]. The peroxy radicals similarly extracted hydrogen from 1- and 5-amines to form hydroperoxide and aminyl radicals in accordance with Eq. (4-18) [176]. The formation of hydroperoxide thus deteriorated the etiolation of UV-curable epoxide resins.



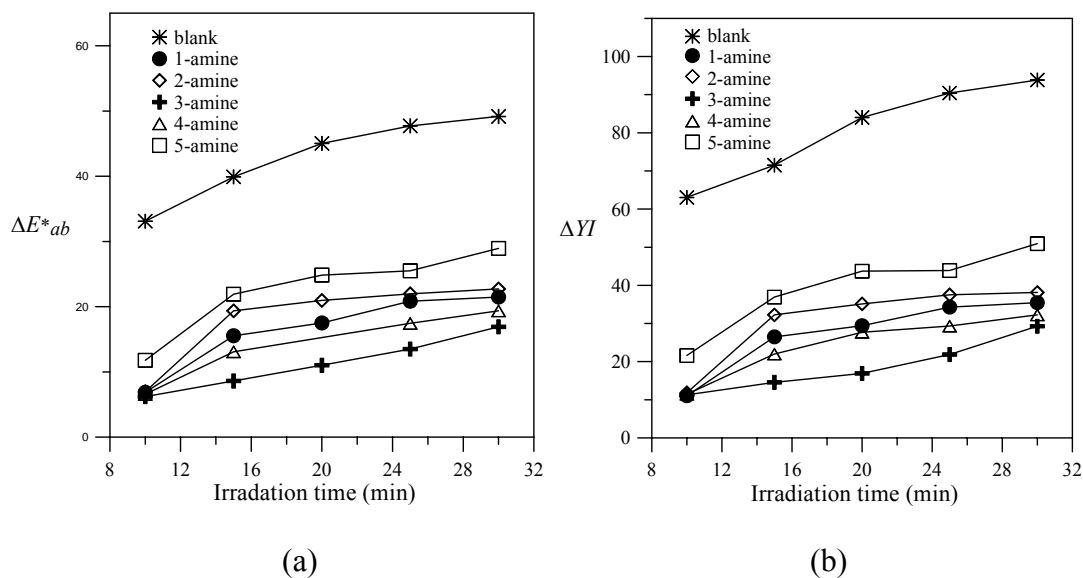


Figure 4-29. (a) ΔE^*_{ab} and (b) ΔYI values of resin samples containing various type of tertiary amines subjected *versus* the UV irradiation time.

4.3.7. Effects of Post Curing Temperatures on Etiolation

Effects of post-curing temperatures on ΔE^*_{ab} and ΔYI are respectively presented in Figs. 4-30(a) and 4-30(b). It shows that, regardless of resin types, etiolation worsens with the increase of post-curing temperatures. Apparently high thermal curing temperature accelerates the oxidation of resins and hence deteriorates the etiolation. Further, addition of 1-, 2-, 3- and 4-amines provides better resistance to etiolation in comparison with that of 5-amine.

4.3.8. Effects of Amine Types and Contents on Etiolation

In this part of study, the resin containing 2.0 wt.% BPO was adopted as the base resin matrix since it possessed the highest UV conversion. Different types and amounts of tertiary amines were then added into the base resin matrix and their effects on the etiolation were evaluated. Before the addition of amines, the ΔE^*_{ab} and ΔYI of base resin matrix is 33.12 and 63.06, respectively. After the addition of tertiary amines, substantial improvements of etiolation were obtained in all types of samples, as seen

in the measured results summarized in Table 4-5. For all samples, the values of ΔE^*_{ab} and ΔYI both decrease with the increase of amine content in resin samples. The most effective one is the sample containing 1.0 wt.% of 3-amine that exhibits the lowest ΔE^*_{ab} and ΔYI of 6.48 and 11.27, respectively. The best etiolation suppression provided by 3-amine thus could be attributed to its highest reactivity among all the amines subjected to study in this work.

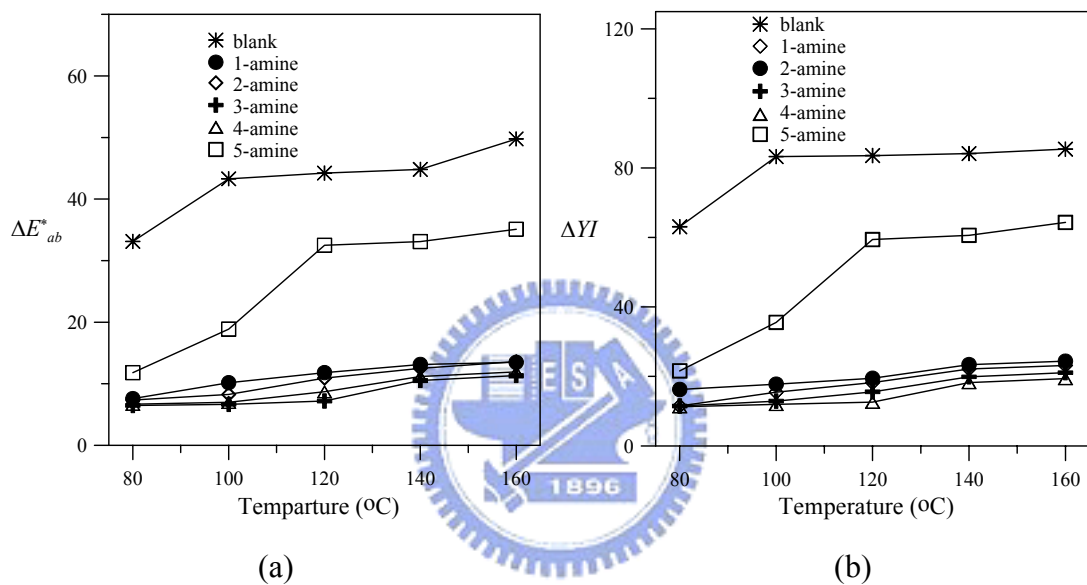


Figure 4-30. (a) ΔE^*_{ab} and (b) ΔYI values of resin samples containing various type of tertiary amines subjected *versus* the post-curing temperatures.

Furthermore, as shown in Table 4-5, the resin containing 3-amine exhibits the highest ΔL^* value and thus the highest transparency. Figure 4-31 shows the transmittances of resin samples containing various amounts of 3-amine. It is noted that the changes of transmittance with the amine content are similar for all five types of amines studied in this work. The increasing trend of transmittance again evidences the effectiveness of etiolation suppression by the addition of tertiary amine.

Table 4-5. ΔL^* , Δa^* , Δb^* , ΔE^*_{ab} and ΔYI of resin samples containing tertiary amines.

Amine type	Amount (wt.%)	ΔL^*	Δa^*	Δb^*	ΔE^*_{ab}	ΔYI
(None)	0	-15.55	3.52	29.03	33.12	63.06
1-amine	0.5	-6.37	-1.40	17.64	18.81	34.48
	0.8	-2.58	-1.40	8.93	9.40	12.13
	1	-2.19	-2.67	6.48	7.34	11.5
2-amine	0.5	-6.76	-1.09	18.24	19.48	36.10
	0.8	-4.02	-2.20	11.27	12.2	21.25
	1	-2.40	-2.04	6.89	7.58	11.84
3-amine	0.5	-4.73	-1.01	13.60	14.43	27.10
	0.8	-1.46	-1.26	6.38	6.67	12.46
	1	-1.12	-1.40	6.23	6.48	11.27
4-amine	0.5	-5.43	-0.42	16.36	17.71	33.59
	0.8	-1.56	-1.97	7.64	8.04	16.98
	1	-1.30	-1.77	6.30	6.67	11.47
5-amine	0.5	-17.67	1.30	23.19	29.18	49.44
	0.8	-10.85	-1.08	17.36	20.50	36.57
	1	-2.97	-1.84	11.26	11.79	21.59

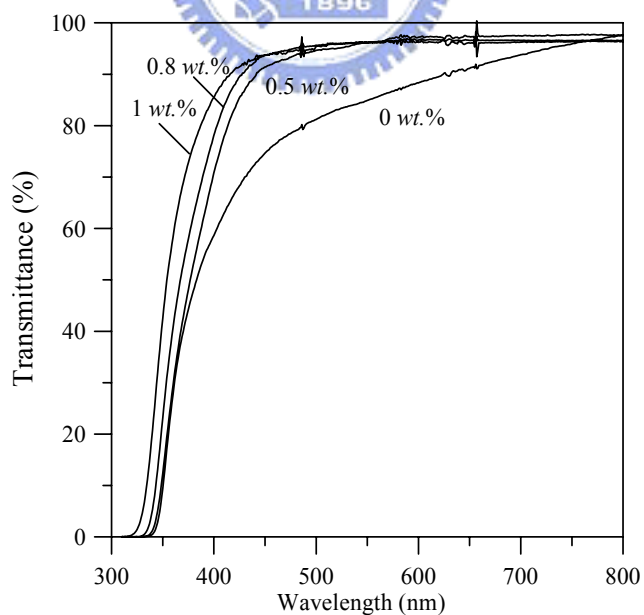


Figure 4-31. Transmittance of resin sample containing various amounts of 3-amine.

4.4. Study of Underfill Resins Containing hBN for Flip-chip Interconnection

4.4.1. Dielectric Properties

Figure 4-32 shows that the dielectric constants of all resin samples decrease with an increase in test frequencies. This trend is normally observed for polar resins that contain functional groups. An acid anhydride curing agent is commonly added in the unfilled resin to reduce viscosity. However, the hydroxyl group forms in the anhydride-cured epoxy resins after ring opening [177]. Though epoxy resins have no specific molecular unit to raise the dielectric constant before curing, secondary alcoholic hydroxyl groups might generate dielectric behavior after curing. The hydroxyl groups have an adverse effect on dielectric characteristics and also raise moisture absorption in the cured resins. Frommer *et al.* [178] reported that the dielectric constants of non-polar materials, such as PFTE, are nearly constant over a wide range of test frequencies. In contrast, for polar materials such as phenolic resins or plasticized PVC, the dielectric constant decreases with the increase in frequency; and, most thermoset resins tend to exhibit high dielectric constants due to their polar functionalities.

Figure 4-32 also shows that the dielectric constants of the composite resins increase with an increase of hBN content. The crystal structure of hBN is similar to graphite and mica in that they both have molecularly smooth basal planes and no surface functional group is available for chemical bonding or interaction. However, at the edge planes of the hBN platelets, there are amine and hydroxyl groups available for chemical bonding [117]. Therefore, an increase in dielectric constant was observed because a higher hBN-filler content results in more hydroxyl groups [179].

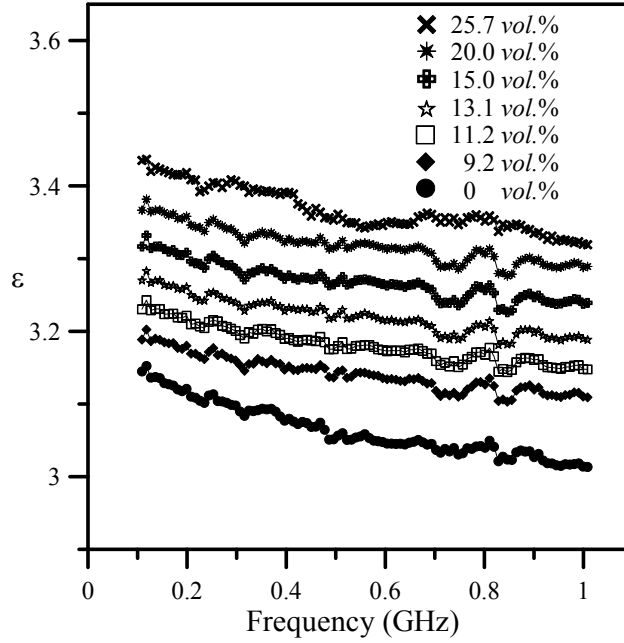


Figure 4-32. Dielectric constants of hBN-resins as a function of test frequency.

Figure 4-33 shows the variation of dielectric constants of hBN- and SiO₂-resins measured at 1 GHz. Since the surface of SiO₂ filler contains more hydroxyl groups at the same filler loading, the dielectric constant of the hBN-resin is lower than that of SiO₂-resin. This is evidence for the presence of polar groups in the filler and that interfacial polarization indeed affects the dielectric properties of composite resins [180].

The dielectric properties of composite material can be predicted according to Eqs. (4-19) and (4-20) [180-181].

$$\ln \varepsilon_c = \phi \ln \varepsilon_1 + (1 - \phi) \ln \varepsilon_2 \quad (4-19)$$

$$\ln(\tan \delta)_c = \phi \ln(\tan \delta)_1 + (1 - \phi) \ln(\tan \delta)_2 \quad (4-20)$$

where ε_c , ε_1 and ε_2 are the dielectric constants of the composite, filler, and resin matrix, respectively, and $(\tan \delta)_c$, $(\tan \delta)_1$ and $(\tan \delta)_2$ are the tangent loss of the composite, filler, and resin matrix, respectively; ϕ is the volume fraction of filler. As

shown in Fig. 4-33, the dielectric constants obtained by theoretically and experimentally are in good agreement for both types of composite resins. Furthermore, at the same filler loading, the measured dielectric constants of hBN- and SiO₂-resins are lower than those obtained by computation. Such phenomenon was also observed in PTFE/SiO₂ composites system and was attributed to a non-uniform dispersion of inorganic filler in resin matrix [120].

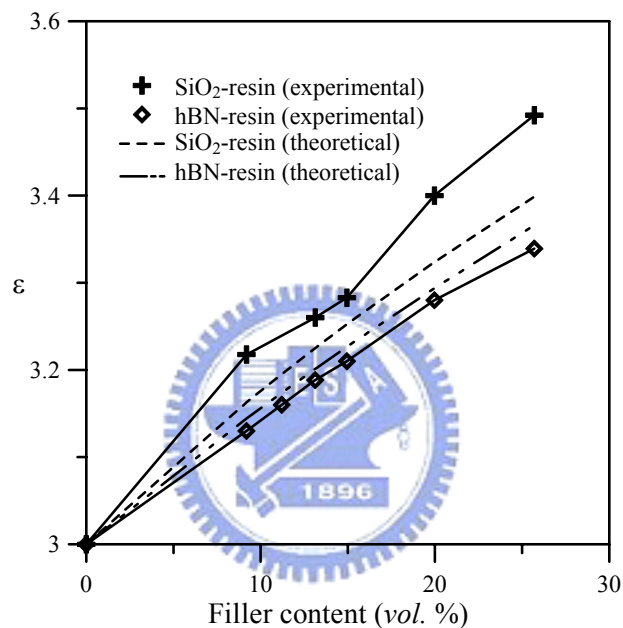


Figure 4-33. Dielectric constants of composite resins as a function of filler content measured at 1 GHz.

Figure 4-34 shows the $\tan\delta$ loss as a function of filler content for the two different composite resins measured at 1 GHz. At this testing frequency, the $\tan\delta$ values of SiO₂, hBN and dicycloaliphatic epoxide are known; *i.e.*, 0.005 [178], 0.0003 [182] and 0.016 (measured values), respectively. Figure 4-34 indicates that tangent loss property of the hBN-resin is always better (lower) than that of the SiO₂-resin. The lower values are a result of fewer polar hydroxyl groups at the hBN filler surface [182]. Figure 4-34 also shows that the $\tan\delta$ values of composite resins increase with an increase in filler content. Since $\tan\delta$ implies electrical energy dissipation during

signal propagation, there exists a limitation on the inorganic filler content for underfilled resins. Equation (4-20) predicts that addition of an inorganic filler will suppress the tangent loss. However, as shown in Fig. 4-34, the tangent losses of hBN- and SiO₂-resins both increase with an increase of inorganic fillers. Such a phenomenon might result from the absorption of moisture on the surface of fillers. Since the tangent loss of water is as high as 35 [183], the tangent losses of the composite resins increase with the amount of filler content.

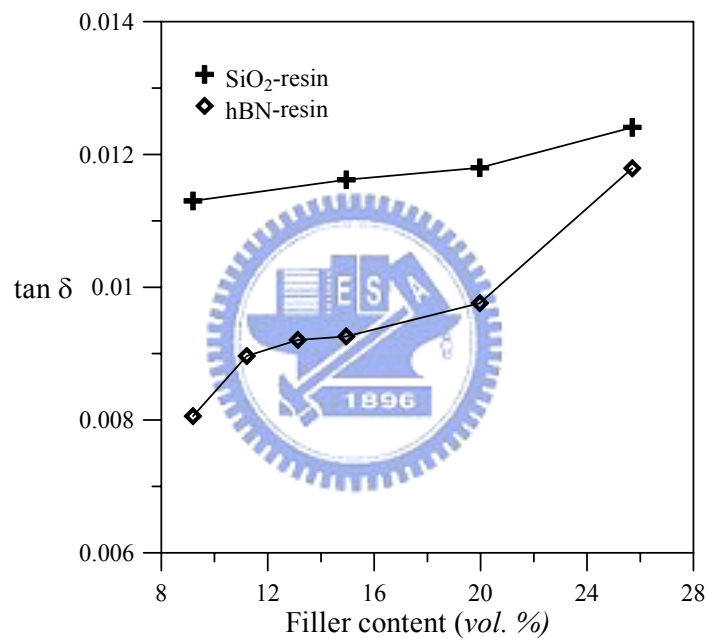


Figure 4-34. Tangent loss of composite resins as a function of filler content measured at 1 GHz.

4.4.2. Curing Kinetics

The heat flow as a function of time at 150°C for the hBN-resins was determined by DSC and the results are plotted in Fig. 4-35. All curves exhibit a peak depicting the initial reaction rate followed by a leveling-down tail where the slope becomes steeper as the filler content increases. The flat non-zero reaction rate tails reveal that there is a continuous post-curing reaction after the initial reaction. These tails imply the

existence of a diffusion-controlled reaction mechanism due to an increase in viscosity after the peak reaction. The onset of the diffusion-controlled process indicates that fast transportation of the molecules in the resin system is prevented by the increase of viscosity [173].

The ΔH_T values of resins containing various amounts of filler were calculated using Eq. (3-3) and the data in Fig. 4-35. The percentage conversion as a function of time for the composite resins is shown in Fig. 4-36. Figures 4-35 and 4-36 show that as the hBN filler content is increased, the time for completing resin curing decreases and conversion increases. Those results suggest that amine groups on the edge planes of hBN react with epoxy groups to accelerate polymerization [183-184]. In addition, crosslinking is enhanced, which is expressed in the T_g values of epoxide resins (Table 4-6).

Figure 4-37 depicts the isothermal DSC thermograms of hBN- and SiO₂-resins containing 25.7 vol.% filler. The shorter curing time of hBN-resin again evidences the existence of amine groups on hBN that promotes the polymerization of the epoxide resins.

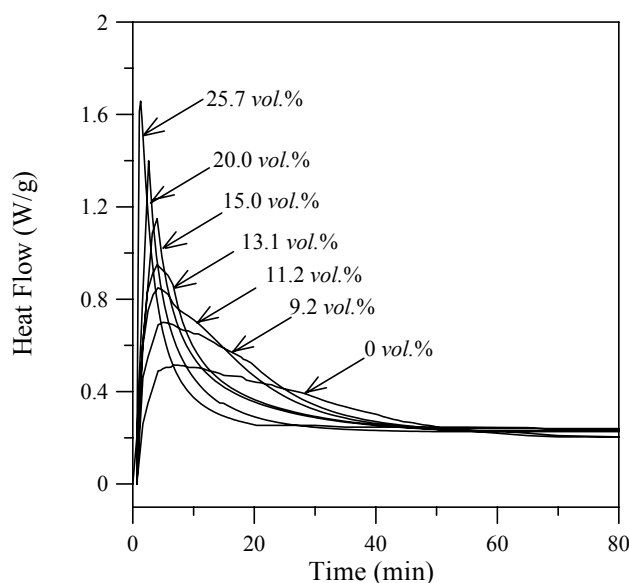


Figure 4-35. Isothermal DSC thermograms of hBN-resins obtained at 150°C.

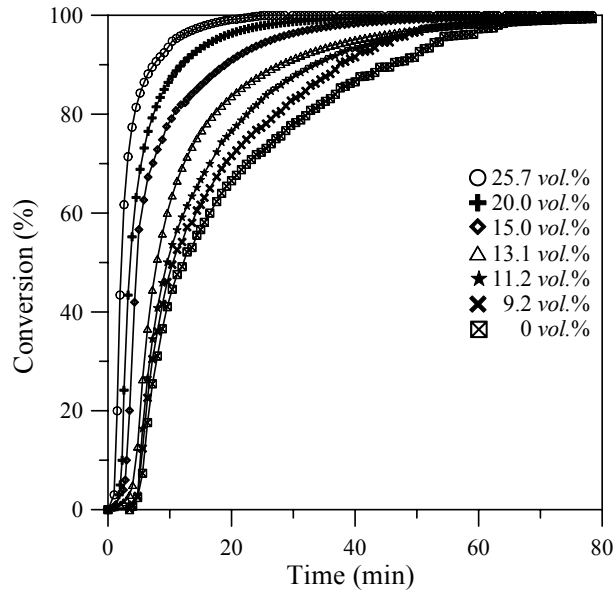


Figure 4-36. Conversion of hBN-resins.

Table 4-6. T_g of hBN-resins measured by DSC.

hBN (vol.%)	T_g (°C)
25.7	148
20.0	130
15.0	125
13.1	123
11.2	120
9.2	118
0	117

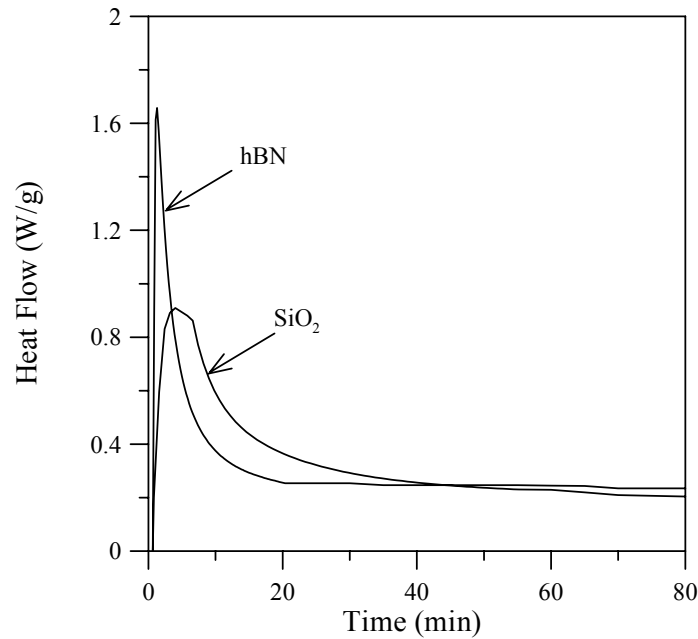


Figure 4-37. Isothermal DSC thermograms of hBN and SiO₂-resins containing 25.7 vol.% filler.

4.4.3. Effects on Coefficient of Thermal Expansion (CTE)

Figure 4-38 shows the variation of CTE with hBN-resin filler content. The addition of the inorganic filler effectively reduces the CTE of the organic resin, which indicates a mechanical interlock at the organic-inorganic interface that may constrain the CTE mismatch of the two components in composite resin. Figure 4-38 also shows that high hBN content (>15 vol.%) alleviates the reduction of CTE, which is similar to the behavior of the SiO₂-resin that was reported previously [128,185]. According to our measurement, the CTE of the SiO₂-resin at 25.7 vol.% is 40 ppm/°C, which is larger than 25.8 ppm/°C for the hBN-resin at the same filler content. This has been attributed to: (a) a non-uniform dispersion of SiO₂ filler in the resin matrix and (b) that quartz-SiO₂ filler possesses a higher CTE.

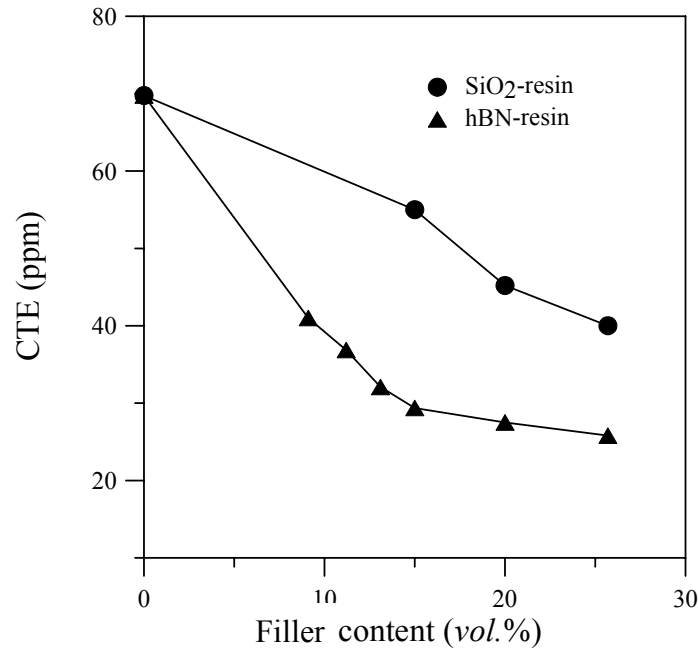


Figure 4-38. CTE as a function of hBN and SiO₂ content.

4.4.4. Effects on Thermal Conductivity

Heat dissipation becomes an important issue in microelectronic packaging since the increase of device density drastically increases the electrical energy consumption. In comparison with metals and ceramics, polymers possess lower thermal conductivity due to relatively low atomic density. Nevertheless, such a deficiency could be improved by adding into the organic matrix an inorganic filler with high thermal conductivity.

Figure 4-39 shows the variation of thermal conductivity with the filler content for hBN- and SiO₂-resins. The thermal conductivities of both types of resins are enhanced with the increase of filler content, and the addition of hBN exhibits a better effect on the thermal conductivity enhancement. For hBN-resin containing 25.7 vol.% filler, the thermal conductivity reaches 1.08 W/m²K, while for the SiO₂-resin with the same filler content, the thermal conductivity is about 0.43 W/m²K. This was attributed to the higher thermal conductivity property of hBN ($\kappa_{//} = 59$ W/m²K; $\kappa_{\perp} = 33$ W/m²K)

[128] relative to the SiO₂ filler ($\kappa = 2$ to 10 W/m²K). Furthermore, the shape and dispersion of fillers in the matrix might affect the thermal conductivity of composite resin. As shown in Fig. 4-40, the SEM of the hBN-resin system clearly exhibits a more uniform dispersion in resin matrix. It is noted that the surface area of filler increases with the increase of aspect ratio. The plate-like shape of hBN results better inter-filler contact in comparison with the spherical filler at the same volume loading [128]. As a result, a better thermal conductivity property is observed in the hBN-resin.

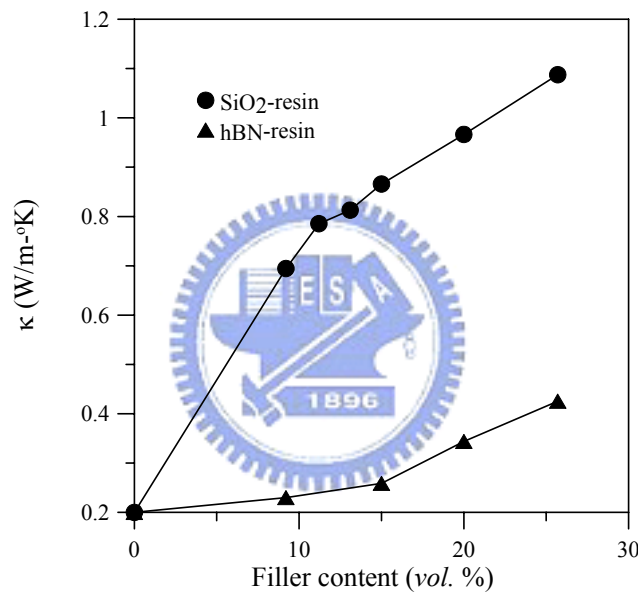


Figure 4-39. Thermal conductivity of an EMC with various volume fractions of filler.

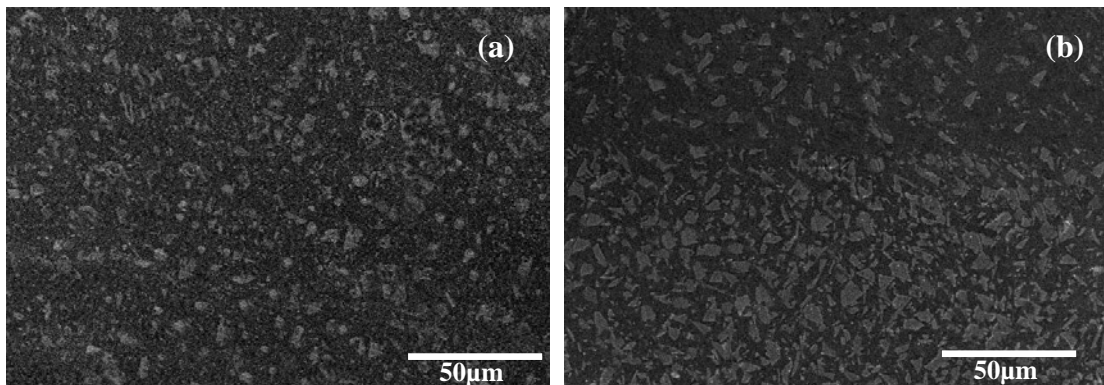


Figure 4-40. SEM morphology of (a) hBN-resin and (b) SiO₂-resin (filler content = 25.7 vol.%).

4.4.5 Effects on Adhesion Strengths

It is expected that encapsulation resins will make contact with IC chips, interconnect materials, and assembly substrates [186-187]. Therefore, we measured the adhesion strengths of composite resins on Si wafers, eutectic PbSn solders, Al₂O₃, and PCB, respectively. Adhesion strengths of hBN- and SiO₂-resins (filler content 25.7 vol.%) on various substances are summarized in Fig. 4-41. It is noteworthy that for the PCB specimen fracture propagation occurs along the resin matrix and for the other three types of specimens fracture occurs at the resin/substrate interface. Hence, the adhesion data for PCB substrate do not represent the true adhesion strength of the resin/PCB interface. For the other three substrates, the adhesion strength was in the order Al₂O₃ > Si wafer > PbSn solder.

Polarity is defined as the ratio of the polar component, γ^p , to the total surface free energy, γ^s . It is expected that an increase in the polarity of the substrate surface will result in higher wettability of the resin with the substrate [122]. Therefore, a stronger interfacial bond which will occur [10]. The polarities of Al₂O₃, Si wafer and PbSn solder are known to be in the order 0.79 [188] > 0.62 [122] > 0.32 [122], which is in consistent with the adhesion measurements. Figure 4-41 also shows that the adhesion strength of the SiO₂-resin on various substrates is higher than for the hBN-resin. This may be attributed to the fact that hydroxide moieties on the SiO₂ surface benefit the formation of interfacial bonding [180].

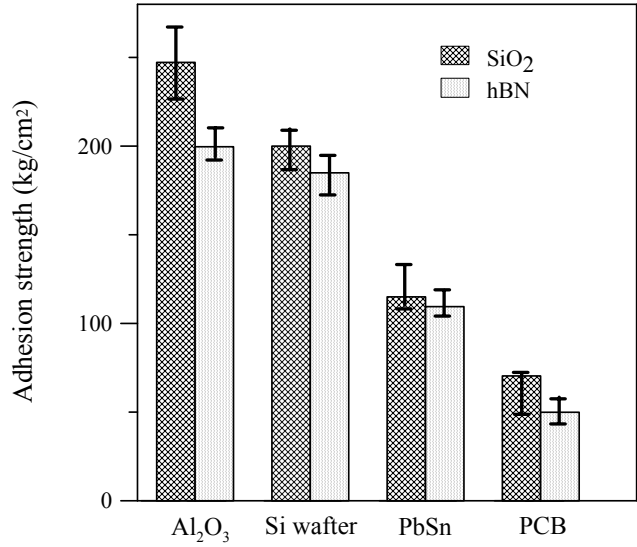


Figure 4-41. Adhesion strengths of hBN- and SiO₂-resins on various types of substrates.

The adhesion strengths as a function of filler content of hBN-resin on various substrates are given in Fig. 4-42. Existence of inorganic fillers would reduce the contact area of resin when applied on the substrate. The increase of filler content decreases the contact area of resin and hence the adhesion strength decreases accordingly.

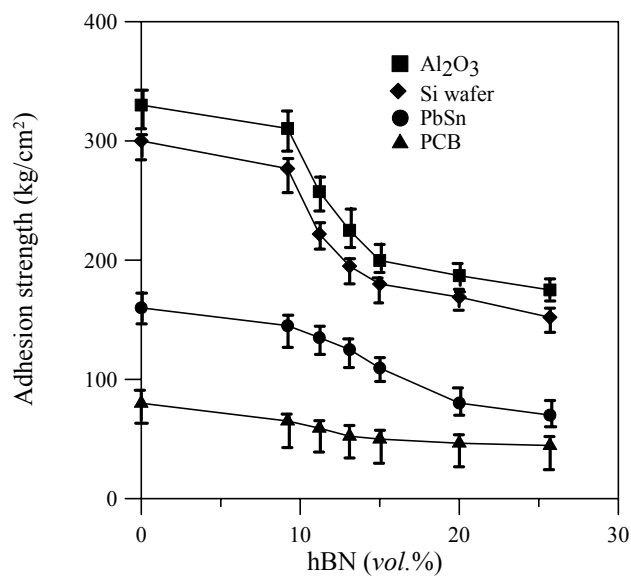


Figure 4-42. Adhesion strengths as a function of filler content of hBN-resin on various substrates.

4.4.6. Viscosity of hBN-Resin

Viscosity is the key property affecting the dispensation of encapsulation resins. The viscosity of hBN-resins increases with an increase of filler content (Table 4-7). It is noted that the resin samples become rather immobile when the hBN content is greater than 20.0 *vol. %*. Pujari *et al.* [189] reported that a large surface areas in non-spherical hBN appears to attract more polymer in the vicinity of the filler surface. As a result, a portion of the polymer has reduced flow consequently increasing the viscosity of composite resin.

Table 4-7. Viscosity of resins at various hBN loadings.

hBN (<i>vol. %</i>)	Viscosity (cPs)
25.7	2.85×10^4
20.0	1.95×10^4
15.0	6.67×10^3
13.1	4.67×10^3
11.2	3.00×10^3
9.2	2.33×10^3
0	230

Chapter 5

Conclusions

This work studies the properties and modifications of UV-curable epoxide resins applied to OLED packaging. Preparation and property characterizations of epoxide resins containing hBN (hexagonal boron nitride) as inorganic filler for underfill of flip-chip interconnection were also investigated. The main conclusions deduced from various parts of works are summarized as follows.

Part (i): **Effects of monomer types on adhesion strength of resins:**

- (1) Monomer types affected the shrinkage of UV-curable epoxide resins. High shrinkage deteriorated the adhesion strength since it induced a considerable amount of internal stress in the resin and thus pulled the resin away from substrate. This work found that the polymerization rates are in the order of: TPPG (poly type) < BVBP (vinyl ether type) < HDDA (acrylate type) and the shrinkages are in the order of: TPPG < BVBP < HDDA.
- (2) The R value and numbers of hydroxyl groups of polyol monomer affect the adhesion strength of UV-curable resins on glass substrate. Appropriate R value might improve the flexibility and softness of resin hence provides satisfactory adhesion strength. Furthermore, adequate numbers of hydroxyl group of monomers and UV curing times are important to achieve satisfactory adhesion strength for UV-curable epoxy resins. This work found that that the resin containing polyol monomer, *i.e.*, tri(propylene glycol), possesses the slowest polymerization rate (0.09 sec^{-1}), the smallest shrinkage (1.72%) and the highest adhesion strength on glass substrate (153.35 kg/cm^2) when R value = 3.
- (3) Addition of appropriate amount of BPO in UV-curable epoxide resins accelerates

the crosslinking density. The resin samples containing 2.0 wt.% BPO exhibited the fast UV conversion.

Part (ii): Effects of organo-functional silanes on adhesion strength of resins:

- (1) The surfaces of glass and ITO substrates generated hydroxyl groups that may react with silanol, a functional group formed by alkoxy group of silane when subjected to UV irradiation, to produce hydrogen bonding and thereby enhance the adhesion strength.
- (2) UV-curable epoxide resins containing various organo-functional silanes reacted with photoinitiator *via* different reaction mechanisms and hence resulted in different UV curing times. Longer UV curing time resulted in less shrinkage of the resin and hence higher adhesion strength. It was found that the time spans of UV curing were in the order of: amino (Uncurable to be cured) > vinyl > methacrylic > acrylic > epoxy. The degree of shrinkage was found in the order of: vinyl < methacrylic < acrylic < epoxy < sample free of silane additive < amino. The epoxide resin containing vinyl group exhibits the smallest degree of shrinkage and the highest adhesion strength on glass and ITO substrates. The enhancement of adhesion resulting from the addition of vinyl group silane in epoxide resin was attributed to the promotion of free-radical polymerization by photoinitiator.
- (3) The resin sample containing 1.0 wt.% of vinyl group silane exhibited the highest adhesion strengths on glass (153.35 kg/cm²) and ITO (91.42 kg/cm²) substrates. Further increase of silane content in the resin generated too much H₂O that would dilute the resin concentration and thus deteriorate the adhesion strength.

Part (iii): Effects of tertiary amines on UV/thermal curing, adhesion strength and etiolation of resins:

- (1) UV conversion decreases with the increase of tertiary amines content up to 1.0

wt.% in the epoxide resins. When the amount of tertiary amines exceeded 1.0 wt.%, nitrogen atom of amines owning a lone pair of electrons would react with $H^+SbF_6^-$ to produce ammonium salts and consequently inhibit the photo-polymerization of resins.

(2) The addition of imidazole and tertiary amines accelerated the thermal conversions of the UV-curable resins. The cycloaliphatic epoxide resins subjected to UV irradiation produced oxiranium ions and reacted with amines to induce cationic thermal polymerization. The thermal polymerization of resin samples rated according to the amine type was in the order of: 3-amine > 4-amine > 1-amine > 2-amine > 5-amine. The ring-opening rate of epoxides containing amine-type curing agents could be enhanced by the presence of phenol compounds so that high thermal conversion was observed in the resin sample containing 2,4,6-tris(dimethylamino-methyl)phenol.

(3) Addition of tertiary amines also effectively improved the thermal properties of the UV-curable epoxide resins. Among the five amine types under study, 2,4,6-tris(dimethylamino-methyl)phenol was found to be the best that the highest T_g (72.3°C) and lowest CTE (70.8 ppm/°C) were achieved in the resin samples. Improvement on thermal properties was attributed to the highest crosslinking density resulted from the fastest thermal polymerization in comparison with other types of amines. The fastest thermal conversion and the highest crosslinking density occurring in the resin containing 2,4,6-tris(dimethylamino-methyl)phenol also implied satisfactory adhesion properties on various types of substrates: glass (> 199 kg/cm²); ITO (> 182 kg/cm²); PET (~ 115 kg/cm²); stainless steel (~ 232 kg/cm²). We note that the data for glass and ITO did not represent the true adhesion strengths of resin on these substrates since the examination of fracture

morphologies revealed that the failures are in fact propagate in the resin matrix rather than along the resin/substrate interfaces. Higher adhesion strengths on glass and ITO substrates are hence expected for the resin containing 2,4,6-tris(dimethylamino-methyl)phenol.

- (4) Adhesion sample preparation was found that sufficient supply of oxygen is required for completing UV curing of epoxide resins containing tertiary amines. The amount of amine addition was limited to 1.0 wt.% since excessive content resulted incomplete curing of resin samples. This was due to the fact that the lone pair of electrons owned by nitrogen atom on tertiary amines might react with $H^+SbF_6^-$ to produce ammonium salts that, in turn, inhibit the UV curing of resins.
- (5) Though addition of 2.0 wt.% BPO in UV-curable epoxide resins accelerated the crosslinking density, it generated the phenol free radicals during UV irradiation by inducing the photolysis of sulfonium salt photoinitiator and consequently deteriorates the etiolation of resins. This work found that etiolation could be substantially improved by adding the imidazole or tertiary amines in the UV-curable epoxide resins. The most effective one was found to be the addition of 2,4,6-tris(dimethylamino-methyl)phenol that the values of ΔE^*_{ab} and ΔYI are respectively equal to 6.48 and 11.27 for the sample contains 1.0 wt.% 2,4,6-tris(dimethylamino-methyl)phenol in contrast to 33.12 and 63.06 for the sample free of amines. 2,4,6-tris(dimethylamino-methyl)phenol also possessed the highest UV reactivity in the resins that the least phenol radicals were produced to react with oxygen. Etiolation improvement was hence attributed to good oxygen scavenging capability of tertiary amines that might effectively inhibit the formation of hydroperoxide in the resins.
- (6) The optimum UV irradiation time and post curing temperature were found to be

10 min and 80°C, respectively, in order to achieve satisfactory etilation properties of the UV-curable epoxide resins.

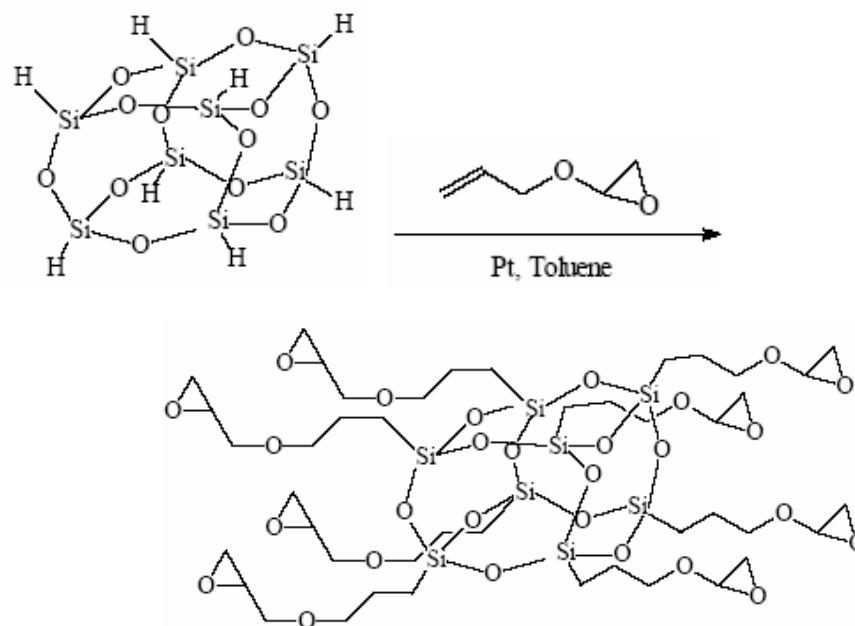
Part (iv): **Epoxide resins containing hBN (hexagonal boron nitride) as inorganic filler for underfill of flip-chip interconnection:**

- (1) Dielectric constant of the hBN-resins decreased with an increase in test frequencies but increased with an increase of filler content. Dielectric constant and tangent loss of the composite resins were correlated with the presence of polar groups in the filler. The interfacial polarization of SiO₂ is larger than that of hBN due to the presence of surface hydroxyl groups on SiO₂. The dielectric properties of SiO₂-resins are hence inferior to those of hBN-resins.
- (2) DSC analysis indicated that addition of hBN filler to epoxide resins increases the conversion of thermal polymerization and values of T_g for the composites. It was suggested that the amine groups on the plane edges of the hBN filler are able to promote the polymerization and, therefore, enhance the crosslinking of the resins on thermal curing.
- (3) The thermal conductivity of composite resin increased with the increase of hBN content. The resin containing 25.7 vol.% hBN exhibited the largest thermal conductivity (1.08 W/m²K).
- (4) Adhesion strengths of the hBN-resins on various substrates were in the order of: Al₂O₃ > Si wafer > eutectic PbSn solder. Increase of filler content decreased the adhesion strength of the hBN-resin on these substrates.

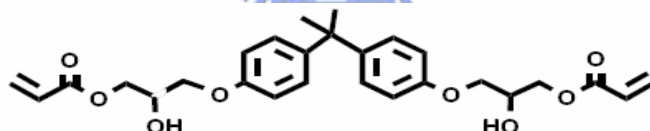
Prospective Researches

This work studied the effects of monomer, organic-functional silanes and tertiary amines on the adhesion and related physical properties of UV-curable epoxide resins. In view of the applications to OLED packaging, resistance to moisture permeation of UV-curable resins must be included in the study in addition to the adhesion property. In our research group, we utilized the concept of nanocomposites and prepared various types of organic-inorganic polymeric resins that might possess satisfactory moisture/oxygen resistance. Another Ph.D. student carried out this part of work and the purpose of research was to enhance the resistance to moisture permeation *in* the resin matrix. This thesis work studied the adhesion and enhancement methods of resin matrix that the suppression of moisture permeation *via* the resin/substrate interface was explored. Though a complete study on the adhesion property of UV-curable epoxide resins has been reported in this work, the enhancement of moisture permeation resistance is still the ultimate purpose of study if the resins were intended to be applied OLED packaging. In the following, several prospective works that might reduce the moisture permeation and further enhance the adhesion of UV-curable resins are proposed:

(1) Addition of Polyhedral Oligomeric Silsesquioxanes (POSS) to Inhibit the Moisture Permeation: The chemical formulation of POSS is $(\text{RSiO}_{1.5})_n$ and the structure of silsesquioxanes is ladder and polyhedron (cage structure and partial cage structure). There are studies reported that mixing the POSS in UV-curable resins may produce octa[dimethylsiloxypropylglycidylether] octasiloxane so as to inhibit the moisture permeation. The UV-curable acrylate-silicate and epoxy-clay resin systems have been thoroughly studied by our research group. The incorporation of POSS with polymeric resin might be another topic to be studied in the future.

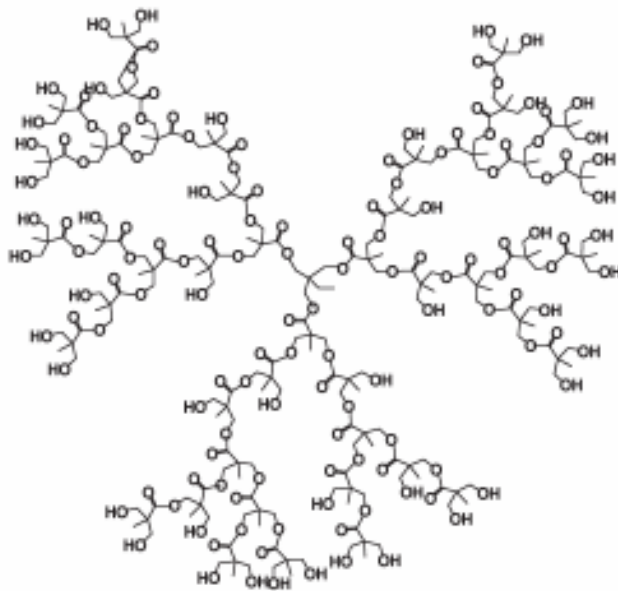


(2) Acrylate Monomer for Improvements of Adhesion and Moisture Permeation: The acrylate monomer has two hydroxyl groups and two acrylate groups. The hydroxyl groups could enhance adhesion strength and the acrylate groups could enhance the moisture resistance.

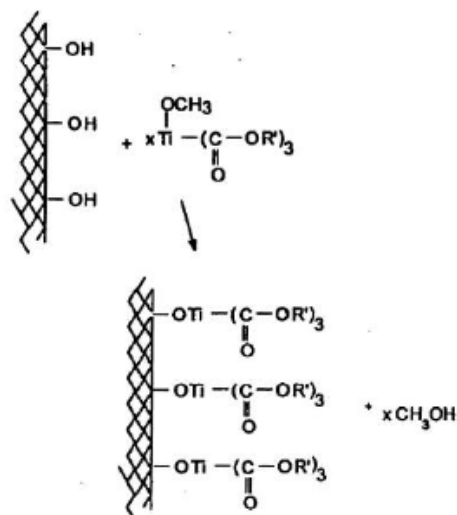


(3) Dendritic Polyester Polyols for Resin Property Refinements: The dendritic polyester polyols present as a new family of aliphatic polyester polyols of high functionality (≥ 6) and relatively low viscosity. Several grades of dendritic polyester polyols are now commercially available. By choosing the combination of polyols, the functionality and nature of the polyols, the properties of resins such as flexibility and chemical resistance can be specifically controlled. The ring opening of the epoxide and/or the oxetane can be accompanied by cross-linking with hydroxyl functional compounds like polyether polyols and Boltorn dendritic polymer polyols. These

polyols act as chain transfer cross-linkers, flexibilizers and adhesion promoter, which can be used up to 30 wt.% of the formulation.

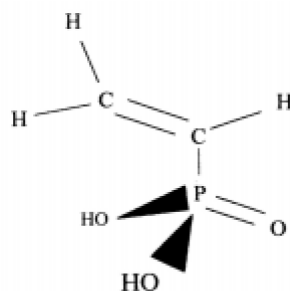


(4) Titanate Coupling Agents for Adhesion Enhancement: In addition to silane coupling agent that may enhance the adhesion strengths, another major classes of coupling agents for similar purpose are the titanates. Titanate coupling agents are more effective than silane coupling agents because they have three pendant organic functional groups compared to one for silanes. The R' groups of titanate coupling agents may contain reactive functional groups such as a vinyl, hydroxyl, mercapto, or amino group which can react with appropriate groups in the resin to produce covalent bonding. The mechanism is schematically illustrated below. The chemically bound titanates on hydroxyl containing surface can interact with the resin to improve adhesion strength.



The mechanism of titanate coupling agent.

(4) Vinylphosphonic Acid for Adhesion Enhancement: Vinylphosphonic acid, $\text{H}_2\text{C}=\text{CH}-\text{P}(\text{O})(\text{OH})_2$, contains vinyl group and $\text{P}(\text{O})(\text{OH})_2$ (see below illustration for molecular structure). Under UV exposure, free radicals will be formed by the photoinitiator to react with vinyl group on $\text{H}_2\text{C}=\text{CH}-\text{P}(\text{O})(\text{OH})_2$. The $\text{P}(\text{O})(\text{OH})_2$ groups of $\text{H}_2\text{C}=\text{CH}-\text{P}(\text{O})(\text{OH})_2$ may react with hydroxyl groups on surface of substrate. Therefore, by varying the organic moiety (such as acrylate or vinyl ether), it is possible to alter surface chemistry and enhance adhesion strength of resins.



Molecular structure of vinylphosphonic acid-VPA

This work also studied the underfill epoxy resin containing hBN filler. We however note that the hBN filler utilized in this work are of irregular shape which, in

turn, severely deteriorates the flow property of underfill resin. Currently there is spherical hBN traded by General Electrics (GE) under the name of PolarTherm* XLR. The replacement of irregular-shaped hBN by such a spherical hBN was suggested for the underfill resins so as to improve the flow property for practical applications.



References

- [1] N.G. Park, M.Y. Kwak, B.O. Kim and O.K. Kwon, "Effects of indium-tin-oxide surface treatment on organic organic light-emitting diodes", *Jpn. J. Appl. Phys.*, **41**(2002), p.1523.
- [2] A.Yoshida, A. Sugimoto, T. Miyadera, S. Miyaguchi, "Organic light emitting devices on polymer substrates", *J. Photopolymer Sci. Technol.* **14**(2001), p. 327.
- [3] M.H. Lu, M.S. Weaver, T.X. Zhou, M. Rothman, R.C. Kwong, M. Hack and J.J. Brown, " High-efficiency top-emitting organic light-emitting devices", *Appl. Phys. Lett.* **81**(2002), p.3921.
- [4] P.E. Burrows, G. Gu, S.R. Forrest, E.P. Vincenzi, T.X. Zhou, "Semitransparent cathodes for organic light emitting devices", *J. Appl. Phys.* **87**(2000), p.3080.
- [5] C. Decker, T.N.T. Viet, D. Decker and E. Weberkoehl, "UV-Radiation Curing of Acrylate/Epoxide Systems", *Polymer*, **42**(2001), p.5531.
- [6] A.K. Fritzsche, H.P. Holladay and M.L. Woodcock, US Patent, 4323454, (1982).
- [7] Y. Chen, W.Y. Chiu and K.F. Lin, "Kinetics study of imidazole-cured epoxy-phenol resins", *J. Polym. Sci. Pol. Chem.* **37**(1999), p.3233.
- [8] S.K. Ooi, W.D. Cook, G.P. Simon and C.H. Such, "DSC studies of the curing mechanisms and kinetics of DGEBA using imidazole curing agents", *Polymer*, **41**(2000), p.3639.
- [9] J.M. Barton, I. Hamerton, B.J. Howlin, J.R. Jones and S. Liu, "Studies of cure schedule and final property relationships of a commercial epoxy resin using modified imidazole curing agents", *Polymer*, **39**(1998), p.1929.
- [10] C.W. Tang and S.A. Van Slyke, "Organic electroluminescent diodes", *Appl. Phys. Lett.* **51**(1987), p. 913.

- [11] A.N. Krasnov, “High-contrast organic light-emitting diodes on flexible substrates”, *Appl. Phys. Lett.* **80**(2002), p. 3853.
- [12] G. Gu, G. Parthasarathy and S.R. Forrest, “A metal-free, full-color stacked organic light-emitting device”, *Appl. Phys. Lett.* **74**(1999), p.305.
- [13] J. Shi and C.W. Tang, “Anthracene derivatives for stable blue-emitting organic electroluminescence devices”, *Appl. Phys. Lett.* **80**(2002), p.3201.
- [14] Y. Leterrier, “Durability of nanosized oxygen-barrier coatings on polymers”, *Prog. in Mater. Sci.* **48**(2003), p. 1.
- [15] K. Yamashita, T. Mori and T. Mizutani, “Encapsulation of organic light-emitting diode using thermal chemical-vapour-deposition polymer film”, *J. Phys. D. Appl. Phys.*, **34**(2001), p. 740.
- [16] Y.-F. Liew, H. Aziz, N.-X. Hu, H. S.-O. Chan, G. Xu. And Z. Popovic, “Investigation of the sites of dark spots in organic light-emitting devices”, *Appl. Phys. Lett.* **77**(2000), p. 2650.
- [17] P.E. Burrows, V. Bulovic, S.R. Forrest, L.S. Sapochak, D.M. McCarty, and M.E. Thompson, “Reliability and degradation of organic light emitting devices”, *Appl. Phys. Lett.* **65**(1994), p.2922.
- [18] H. Kanno, Y. Hamada and H. Takahashi, “Development of OLED with high stability and luminance efficiency by Co-Doping methods for full color displays”, *IEEE J. Sel. Topics Quantum Electron.*, **10**(2004), p. 30.
- [19] T.B. Harvey, S. Q. Sgi, and F. So, US Patent, 5757126 (1998)
- [20] D. Affinito, US Patent, 6268695 (2001)
- [21] P.E. Burrows, G.L. Graff, M.E. Gross, P.M. Martin, M.K. Shi, M. Hall, E. Mast, C. Bonham, W. Bennet and M.B. Sullivan, “Ultra barrier flexible substrates for flat panel displays”, *Displays*, **22**(2001), p.65.
- [22] C. Sanchez, B. Julián, P. Belleville and M. Popall, “Applications of hybrid

- organic-inorganic nanocomposites, *J. Mat. Chem.* **15**(2005), 3559.
- [23] J.V. Crivello, "Photocurable monomers and oligomers for space applications", *High Perf. Polym.* (11)1999, p.141.
- [24] J.V. Crivello, J. Ma and F. Jiang, "Synthesis and photoactivity of novel 5-aryltanthrenium salt cationic photoinitiators", *J. Polym. Sci. A Polym. Chem.* **40**(2002), p.3465.
- [25] K.J. Schafer, J.M. Hales, M. Balu, K.D. Belfield, E.W. Van Stryland and D. J. Hagan, "Two-photo absorption cross-sections of common photoinitiators" *J. Photochem. Photobio. A: Chem.*, **162**(2004), p.497.
- [26] S.M. Ellerstein, S.A. Lee and T.K. Palit, *Radiation Curing in Polymer Science and Technology Volume IV Practical Aspects and Applications*, Edited by J.P. Fouassier and J.F.Rabek, Elsevier applied science, London, (1993), Chapter 4.
- [27] K. Studer, C. Decker, E. Becl and R. Schwalm, "Overcoming oxygen inhibition in UV-curing of acrylate coatings by carbon dioxide inerting: Part II", *Prog. Org. Coat.* **48**(2003), p.101.
- [28] S.A. Walata, C.R. Newman, *Radiation-Curable Coatings*, Research Triangle Park, (1991), Chapter 3.
- [29] V. Strehmel, *Handbook of Photochemistry and Photobiology, Volume 2, Organic Photochemistry*, Edited by H.S. Nalwa, American Scientific Publishers, (2003), Chapter 1.
- [30] R.N. Kumar, C.K. Woo, A. Abusamah, "UV curing of surface coating system consisting of cycloaliphatic diepoxide-ENR-glycidyl methacrylate by cationic photoinitiators-characterization of the cured film by FTIR spectroscopy", *J. Appl. Polym. Sci.* **73**(1999), p. 1569.
- [31] J.V. Crivello and U. Varlemann, "The Synthesis and study of the photoinitiated cationic polymerization of novel cycloaliphatic epoxides", *J. Polym. Sci., A*,

- Polym. Chem.*, **33**(1995), p.2463.
- [32] J.V. Crivello, B. Falk, M.R. Zonca, "Photoinduced cationic ring-opening frontal polymerizations of oxetanes and oxiranes", *J. Polym. Sci., A, Polym. Chem.*, **42**(2004), p.1630.
- [33] S. Kanoh, M. Naka, T. Yokozuka, S. Itoh, T. Nishimura, M. Honda, M. Motoi and N. Matsuura, "Cationic monomer-isomerization polymerization of oxetanes having an ester substituent, to give poly(orthoester) or polyether", *Macrom. Chem. Phys.*, **203**(2002), p. 511.
- [34] J.N. Wood, "Radiation-Curable adhesives", *Radiation Curing: Science and Technology*, edited by S.P. Pappas, Plenum Press, New York (1992), Chapter 9.
- [35] J.V. Crivello and R. Narayan, "Novel Epoxynorbornane Monomers. 2. Cationic Photopolymerization", *Macromolecules*, **29**(1996), p. 439.
- [36] H. Sasaki, J.M. Rudzinski and T. Kakuchi, "Photoinitiated cationic polymerization of oxetane formulated with oxirane", *J. Polym. Sci., A, Polym. Chem.*, **33**(1995), p.1807.
- [37] S. Searles, M. Tamres and E.R. Lippincott, "Hydrogen Bonding Ability and Structure of Ethylene Oxides", *J. Am. Chem. Soc.*, **75**(1953), p. 2775.
- [38] U. Bulut and J.V. Crivello, "Reactivity of oxetane monomers in photoinitiated cationic polymerization", *J. Polym. Sci., A, Polym. Chem.*, **43**(2005), p.3205.
- [39] 謝添壽, "有機發光二極體用封裝材料", *工業材料*, **193**(2003), p.153.
- [40] S.P. Pappas, *Photopolymerisation and Photoimaging Science and Technology*, Edited by S. Allen, Elsevier applied science, London, (1989), Chapter 2.
- [41] J.V. Crivello, J.H.W. Lam and C.N. Volante, "Photoinitiated cationic polymerization using diaryliodonium salts", *J. Radiat. Curing.*, **1**(1977), p. 2.
- [42] J.W. Knapzyck and W.E.J. McEwen, "Reactions of triarylsulfonium salts with bases", *J. Amer. Chem. Soc.* **91**(1969), p.145.

- [43] J.W. Knapzyck and W.E.J. McEwen, "Photolysis of triarylsulfonium salts in alcohol", *J. Org. Chem.*, **35**(1970), p.2539.
- [44] J.V. Crivello, J.H.W. Lam, J.E. Moore and S.H. Schroeter, "Triarylsulfonium salts: a new class of photoinitiators for cationic polymerization", *J. Radiat. Curing.*, **5**(1978), p.2.
- [45] B.Stapp, L.Schön and H.Bayer and M.Hoffmann, "Photo- and thermoinitiated curing of epoxy resins by sulfonium salts", *Angew. Makromo. Chemie*, **209**(1993), p.197.
- [46] L.N. Price, "Free radical and cationic photoinitiators in ultraviolet light curable coatings", *J. Coatings. Technol.*, **67**(1995), p.27.
- [47] Y. Takimoto, *Radiation curing in polymer science and technology-volume III polymerization mechanisms*, Edited by J.P. Fouassier and J.F. Rabek, Elsevier applied science, London, (1993), Chapter 8.
- [48] J.V. Crivello, J.L. Lee and D.A. Conlon, "Aromatic bisvinyl ethers: a new class of highly reactive thermosetting monomers", *J. Radiat. Curing.*, **10**(1983), p.6.
- [49] J.V. Crivello and R.A. Ortiz, "Synthesis of epoxy monomers that undergo synergistic photopolymerization by a radical-induced cationic mechanism", *J. Polym. Sci., A, Polym. Chem.*, **39**(2001), p.3578.
- [50] J.V. Crivello, "UV and electron beam-induced cationic polymerization", *Nucl. Instrum. Methods Phys. Res., B*, **151**(1999), p.8.
- [51] B. Falk, M.R. Zonca, J.V. Crivello, "Photoactivated cationic frontal polymerization", *Macromol. Symp.* **226**(2005), p.97.
- [52] C. Decker, H.L. Xuan and T.N.T. Viet, "Photo-cross-linking of functionalized rubber .III. Polymerization of multifunctional monomers in epoxidized liquid natural rubber", *J. Polym. Sci., A, Polym. Chem.*, **34**(1996), p.1771.
- [53] H. Itoh, A. Kameyama, and T. Nishikubo, "Synthesis of silicon-containing vinyl

- ether monomers and oligomers and their photoinitiated polymerization”, *J. Polym. Sci., A, Polym. Chem.*, **35**(1997), p.3217.
- [54] S. Wu, W.T. Sears and M.D. Soucek. “Siloxane modified cycloaliphatic epoxide UV coatings”, *Prog. Org. Coat.*, **36**(1999), p.89.
- [55] Y. Yagci, and W. Schnabel, “On the mechanism of photoinitiated cationic polymerization in the presence of polyols”, *Die Ange. Makro. Chemie*, **270**(1999), p.38.
- [56] S. Kaur, J.V. Crivello and N. Pascuzzi, “Synthesis and cationic photopolymerization of 1-butenyl and 1-pentenyl ethers”, *J. Polym. Sci., A, Polym. Chem.*, **37**(1999), p.199.
- [57] D.A. Tilbrook, R.L. Clarke, N.E. Howle and M. Braden, “Photocurable epoxy-polyol matrices for use in dental composites I”, *Biomaterials*, **21**(2000), p.1743.
- [58] Y.J. Toba, “Anthracene-Sensitized Polymerization of Vinyl Ethers by Onium Tetrakis(Pentafluorophenyl)Borate Initiators”, *J. Polym. Sci. A Polym. Chem.*, **38**(2000), p.982.
- [59] F.Y.C. Boey, N.K. Chia, S.K. Rath, and M.J.M. Abadie, “Low-energy-electron beam-induced cationic polymerization with onium salts”, *J. Appl. Polym. Sci.*, **82**(2001), p.3099.
- [60] F. Boey, S.K. Rath, K.A. Ng and M.J.M. Abadie, “Cationic UV Cure Kinetics for Multifunctional Epoxies”, *J. Appl. Polym. Sci.*, **86**(2002), p.518.
- [61] C.C. Chappelow, C.S. Pinzino, M.D. Power, A.J. Holder, J.A. Morrill, L. Jeang, and J.D. Eick, “Photoreactivity of Vinyl Ether/Oxirane-based Resin systems”, *J. Appl. Polym. Sci.*, **86**(2002), p.314.
- [62] H. Braun, Y. Yagci and O.Nuyken, “Copolymerization of butyl vinyl ether and methyl methacrylate by combination of radical and radical promoted cationic

- mechanisms”, *Eur. Polym. J.*, **38**(2002), p.151.
- [63] M. Pantiru, D.M. Vuluga, D.S. Vasilescu and M.J.M. Abadie, “Study of the cationic photopolymerization kinetics of cyclic acetals”, *Polymer Bulletin*, **47**(2002), p.485.
- [64] M. Sangermano, G. Malucelli, R. Bongiovanni, A. Priola, U. Annby and N. Rehnberg, “Cationic photoinitiated copolymerization of 1-propenyl-vinyl ether systems”, *Eur. Polym. J.*, **38**(2002), p.655.
- [65] J. Chen and M.D. Soucek, “Photoinitiated cationic polymerization of cycloaliphatic epoxide with siloxane or alkoxy silane functionalized polyol coatings”, *Eur. Polym. J.*, **39**(2003), p.505.
- [66] J. Chen and M.D. Soucek, “Ultraviolet curing kinetics of cycloaliphatic epoxide with real-time fourier transform infrared spectroscopy”, *J. Appl. Polym. Sci.*, **90**(2003), p.2485.
- [67] N. Yonet, Y. Yagci, B. Ochiai and T. Endo, “Photoinitiated cationic ring-opening polymerization of monothiocarbonate”, *Macromolecules*, **36**(2003), p.9257.
- [68] M. Jang, and J.V. Crivello, “Photoinitiated cationic ring-opening polymerization of monothiocarbonate”, *J. Polym. Sci., A, Polym. Chem.*, **41**(2003), p.3056.
- [69] M. Sangermano, G. Malucelli, R. Bongiovanni, and A. Priola, “Photoinduced cationic ring-opening frontal polymerizations of oxetanes and oxiranes”, *Eur. Polym. J.*, **40**(2004), p.353.
- [70] M. Sangermano, R. Bongiovanni, G. Malucelli, A. Priola, J. Olbrych, and A. Harden and N. Rehnberg, “Photopolymerization of oxetane based systems”, *J. Polym. Sci. A Polym. Chem.*, **42**(2004), p.1415.
- [71] M. Sangermano, R. Bongiovanni, G. Malucelli, A. Priola, R.R. Thomas, R.E. Medsger, Y. Kim, and C.M. Kausch, “Synthesis and cationic photopolymerization of new silicon-containing oxetane monomers”, *Polymer*, **45**(2004), p.2133.

- [72] S. Penczek and P. Kubisa, *Proceedings of the IUPAC International Symposium on Macromolecules, Frontiers of Macromolecular Science*. (1988), p.107.
- [73] J.V. Crivello and R.A.Ortiz, “Benzyl alcohols as accelerators in the photoinitiated cationic polymerization of epoxide monomers”, *J. Polym. Sci. A Polym. Chem.*, **40**(2002), p.2298.
- [74] J.V. Crivello and S.S. Liu, “Photoinitiated cationic polymerization of epoxy alcohol monomers”, *J. Polym. Sci. A Polym. Chem.*, **38**(2000), p.389.
- [75] W. Schnabel, “Cationic photopolymerization with the aid of pyridinium-type salts”, *Macromol. Rapid Commun.* **21**(2000), p.628.
- [76] A. Gandini and H. Cheradame, *Encyclopedia of polymer science and engineering vol. 2/Anionic polymerization to cationic polymerization*, edited by H.F. Mark and J.I. Kroschwitz, Wiley, New York, (1985), p.729.
- [77] S.K. Rajaraman, W.A. Mowers and J.V. Crivello, “Interaction of epoxy and vinyl ethers during photoinitiated cationic polymerization”, *J. Polym. Sci. A Polym. Chem.*, **37**(1999), p.4007.
- [78] J.H. He and V.S. Mendoza, “Interaction of epoxy and vinyl ethers during photoinitiated cationic polymerization”, *J. Polym. Sci. A Polym. Chem.*, **34**(1996), p.2809.
- [79] P. Dufour, *Radiation curing in polymer science and technology, I. Fundamentals and methods*, edited by J.P. Fouassier and J.F. Rabek, Elsevier applied science, London, (1993), p.1.
- [80] E.P. Plueddemann, *Silanes and Other Coupling Agents*, edited by K.L. Mittal, VSP, Utrecht, (1992), p.3.
- [81] L.J. Mathias and J.A. McGowen, “Cationic cure of epoxy resins via benzlsulfonium salts covalently bound to glass surfaces”, *Polym. Composites*,

18(1997), p.332.

- [82] P.G. Pape and E.P. Plueddemann, “Methods for improving the performance of silane coupling agents”, *J. Adhesion Sci. Technol.*, 5(1991), p.831.
- [83] P.H. Harding and J.G. Berg, “The adhesion promotion mechanism of organofunctional silanes”, *J. Appl. Polym. Sci.*, 67(1998), p.1025.
- [84] X.H. Gu, G. Xue and B.C. Jiang, “Effect of deposition conditions for γ -aminopropyltriethoxy silane on adhesion between copper and epoxy resins”, *Appl. Surface. Sci.*, 115(1997), p.66.
- [85] Y.J. Chen, E.T.Kang and K.G. Neoh, “Electroless metallization of glass surfaces functionalized by silanization and graft polymerization of aniline”, *Langmuir*, 17(2001), p.7425.
- [86] S.K. Medda, D. Kundu and G. De, “Inorganic-organic hybrid coatings on polycarbonate. Spectroscopic studies on the simultaneous polymerizations of methacrylate and silica networks”, *J. Non-Cryst. Solids.*, 318(2003), p.149.
- [87] N.M., Mohsen, R.G. Craig and F.E. Filisko, “The effects of different additives on the dielectric relaxation and the dynamic mechanical properties of urethane dimethacrylate”, *J. Oral Rehabil.*, 27(2000), p.250.
- [88] S. Zhao, J. Zhang, S. Zhao, W. Li and H. Li, “Effect of inorganic–organic interface adhesion on mechanical properties of Al_2O_3 /polymer laminate composites”, *Composites Sci. Technol.*, 63(2003), p.1009.
- [89] V. Viengkhou, L.T. Ng and L. Garnett, “Role of additives on UV curable coatings on wood”, *J. Appl. Polym. Sci.*, 61(1996), p.2361.
- [90] N.B. Madsen, *Modification and Characterization of the Interface in Polymer/Inorganic Composites*, Risø National Laboratory, Roskilde, Denmark, (1999), Chapter 1.

- [91] C. Decker, K. Moussa and T. Bendaikha, "Photodegradation of UV-cured coatings II. Polyurethane-acrylate networks, *J. Polym. Sci. A Polym. Chem.*, **29**(1991), p.739.
- [92] A. Hult, Y.Y. Yuan and B. Ranby, "Photo-stability of photo-cured organic coatings: part iii - photo-degradation of organic coatings photo-cured with alkoxyacetophenone and hydroxy alkylacetophenone photo-initiators", *Polym. Deg. Stab.* **8**(1984), p.241.
- [93] N. Filipescu and F.L. Minn, "Photoreduction of benzophenone in isopropyl alcohol", *J. Am. Chem. Soc.* **90**(1968), p.1544.
- [94] C. Decker and K. Zahouily, "Light-stabilization of polymeric materials by grafted UV-cured coatings", *J. Polym. Sci. Pol. Chem.* **36**(1998), p.2571.
- [95] J.D. Cho, H. K. Kim, Y. S. Kim and J. W. Hong, "Dual curing of cationic UV-curable clear and pigmented coating systems photosensitized by thioxanthone and anthracene", *Polym. Test.* **22**(2003), p.633.
- [96] N.S. Allen, D. Lo and S. Salim, "Aspects of the inhibition of post-cure photo-yellowing of novel amine diacrylate terminated ultraviolet- and electron-beam cured TMPTA-based coatings", *Polym. Degrad. Stab.* **45**(1994), p.277.
- [97] C.K. Noren, "Cationic UV-curable formulations containing hydroxyl functional fluoropolymer resins", *J. Coat. Technol.* **72**(2000), p.53.
- [98] N.J. White, N.S. Allen and P.J. Robinson, *Photopolymerisation and Photoimaging Science and Technology*, edited by N.S. Allen, Elsevier applied science, London, England, (1989), Chapter 8.
- [99] K.R. Millington and L.J. Kischenbaum, "Detection of hydroxyl radicals in photoirradiated wool, cotton, nylon and polyester fabrics using a fluorescent probe", *Color. Technol.* **118**(2002), p.6.

- [100] Y. Qi, X. Meng, J. Yang, Z. Zeng and Y. Chen, “ Synthesis and properties of ultraviolet/moisture dual curable polysioxane acrylates”, *J. Appl. Polym. Sci.* **96**(2005), p.846.
- [101] R.S. Davidson, *Radiation Curing in Polymer Science and Technology-Volume III Polymerisation Mechanisms*, edited by J.P. Fourassier and J.F. Rabek, Elsevier applied science, London, England, (1993), p.153.
- [102] N. Arsu, S. Davidson and R. Holman, “Factors affecting the photoyellowing which occurs during the photoinitiated polymerization of acrylates”, *J. Photochem. Photobiol. A-Chem.*, **87**(1995), p.169.
- [103] A.V. Pocius, *Adhesion and adhesives technology an introduction*, Habser, London, (1997), Chapter 5.
- [104] S. Wu, *Polymer Interface and Adhesion*, Marcel Dekker, New York, (1982), Chapter 11.
- [105] A.V. Pocius, *Adhesion and adhesives technology an introduction*, Habser, London, (1997), Chapter 3.
- [106] A. Ahagon and A. N. Gent, “Effect of interfacial bonding on the strength of adhesion”, *J. Polym. Sci. Pol. Phys.*, **13**(1975), p. 1285.
- [107] E.M. Davis, W.E. Harding, R.S. Shwartz and J.J. Corning, “Solid logic technology: versatile high performance microelectronics,” *IBM J. Res. Develop.*, (1964), p.102.
- [108] C.P. Wong, M.B. Vincent, and S. Shi, “Fast-flow underfill encapsulant: flow rate and coefficient of thermal expansion”, *IEEE Trans. Compon., Packaging, Manuf. Technol., Part A.* **21**(1998), p.360.
- [109] D.C. Tancred, A.J. Carr and B.A. O. McCormack, “The sintering and mechanical behavior of hydroxyapatite with bioglass additions”, *J. Mater. Sci.*,

Mater. Med. **12**(2001), p.81.

- [110] X.S. Dai, M.V. Brillhart, M. Roesch, and P.S. Ho, "Adhesion and toughening mechanisms at underfill interfaces for flip-chip-on-organic-substrate packaging", *IEEE Trans. Compon. Packaging Technol.* **23**(2000), p.117.
- [111] A.A. Solomo, J. Fourcade, S.G. Lee, S.K. Kuchibhotla, S. Revankar, R. Latta, P.L. Holman, and J.K. McCoy, *Proceedings of the 2004 international Meeting on LWR Fuel Performance*, Orlando, Florida, (2004), p.1028.
- [112] M. Hussain, Y. Oku, A. Nakahira, and K. Niihara, "Effects of wet ball-milling on particle dispersion and mechanical properties of particulate epoxy composites", *Mater. Lett.* **26**(1996), p.177.
- [113] P. Bujard, G. Kühlein, S. Ino, and T. Shiobara, "Thermal conductivity of molding compounds for plastic packaging", *IEEE Trans. Compon., Packaging, Manuf. Technol., Part A.* **17**(1994), p.527.
- [114] L. Haiying, K.I. Jacob and C.P. Wong, "An improvement of thermal conductivity of underfill materials for flip-chip packages", *IEEE Trans. Comp., Packag., Manufact., Technol. Advanced Packaging*, **26**(2003), p.25.
- [115] W. Kim, J.W. Bae, I.D. Choi, and Y.S. Kim, "Thermally conductive EMC (epoxy molding compound) for microelectronic encapsulation", *Polym. Eng. Sci.* **39**(1999), p.756.
- [116] J.W. Bae, W. Kim, S.W. Park, C.S. Ha, and J.K. Lee, "Advanced underfill for high thermal reliability", *J. Appl. Polym. Sci.* **83**(2002), p.2617.
- [117] M.T. Huang, and H. Ishida, "Investigation of the boron nitride/polybenzoxazine interphase", *J. Polym. Sci., B, Polym. Phys.* **37**(1999), p.2360.
- [118] H. Janssen, J.M. Seifert, and H.C. Karner, "Interfacial phenomena in composite high voltage insulation", *IEEE Trans. Dielect. Electr. Insul.* **6**(1999), p.651.
- [119] A.F. Júnior and D.J. Shanafield, "Thermal conductivity of polycrystalline

- aluminum nitride (AlN) ceramics”, *Ceramics* **50**(2004), p.247.
- [120] Y.C. Chen, H.C. Lin and Y.D. Lee, “The Effects of Filler Content and Size on the Properties of PTFE/SiO₂ Composites”, *J. Polym. Res.*, **10**(2003), p.247.
- [121] J. Park, J.S. Lee, and C.C. Lee, *Electronic Components and Technology Conference*, 2003, Proceedings, 53rd, (2003), p.1800.
- [122] M.L. Sham, and J.K. Kim, “Adhesion characteristics of underfill resins with flip chip package components”, *J. Adhes. Sci. Technol.* **17**(2003), p.1923.
- [123] Y. Xu, X. Luo, and D.D.L. Chung, “Sodium silicate based thermal interface material for high thermal contact conductance”, *J. Electron. Packag.* **122**(2000), p.128.
- [124] Y. Xu, and D.D.L. Chung, “Increasing the thermal conductivity of boron nitride and aluminum nitride particle epoxy-matrix composites by particle surface treatments”, *Compos. Interfaces.* **7**(2000), p.243.
- [125] M.J. Hodgins, and R.H. Estes, *Proceedings of the Technical Programs, NEPCON WEST Conference*, (1999), p.359.
- [126] W.S. Lee and J. Yu, “Comparative study of thermally conductive fillers in underfill for the electronic components”, *Diam. Relat. Mat.* **14**(2005), p.1647
- [127] C.A. Latham and M.F. McGuigan, US Patent, 5011872 (1991).
- [128] C.P. Wong, and R.S. Bollampally, “Comparative study of thermally conductive fillers for use in liquid encapsulants for electronic packaging”, *IEEE Trans. Adv. Packag.* **22**(1999), p.54.
- [129] Y. Liu, Y.F. Wang, T.G. Gerasimov, K.H. Heffner, and J.P. Harmon, “Thermal analysis of novel underfill materials with optimum processing characteristics”, *J. Appl. Polym. Sci.* **98**(2005), p.1300.
- [130] T. Serikawa and F. Omata, “High-mobility poly-Si TFT’s fabricated on flexible stainless-steel substrates”, *IEEE Electron Device Lett.*, **20**(1999), p.574.

- [131] CIE-Colourimetry. *Official Recommendations of the International Commission on Illumination*. Publication CIE (supplement No 21), Paris, France: Bureau Central de la CIE, (1978), p.15.
- [132] P. Blum, *PP Handbook*, (1997), Chapter 7.
- [133] DIN EN 27491. *Dentistry: Dental Materials: Determination of Colour Stability of Dental Polymeric Materials*. Beuth, Belgium: International Standardization Organization—ISO 7491, (1985).
- [134] ASTM D 1925 Test method for yellowness index of plastics, (1962).
- [135] N.M. Mohsen, R.G. Craig, and F.E. Filisko, “Cytotoxicity of urethane dimethacrylate composites before and after aging and leaching”, *J. Biomed. Mater. Res.* **39**(1998), p.252.
- [136] H.C. Chien, M.H. Tseng, W.W. Ke, C.Y. Wang, and Y.S. Chen, US Patent 6663278 B1 (2003).
- [137] Y.J. Hua, F.M. Jiang and J.V. Crivello, “Photosensitized onium-salt-induced cationic polymerization with hydroxymethylated polynuclear aromatic-hydrocarbons”, *Chem. Mater.*, **14**(2002), p.2369.
- [138] C. Decker and K. Moussa, “Kinetic study of the cationic photopolymerization of epoxy monomers”, *J. Poly. Sci. A Polym. Chem.*, **28**(1990), p.3429.
- [139] R. Vabrik, I. Czajlik, G. Tury, I. Rusznak, A. Ille and A. Vig, “A Study of epoxy resin-acrylated polyurethane semiinterpenetrating polymer networks”, *J. Appl. Polym. Sci.*, **68**(1998), p.111.
- [140] I. Yarovsky and E. Evans, “Computer simulation of structure and properties of crosslinked polymers: application to epoxy resins”, *Polymer*, **43**(2002), p.963.
- [141] M. Braithwaite, R.S. Davidson, R. Holman, C. Lowe, P.K.T. Oldring, M.S. Salim and C. Wall, *Chemistry & technology of UV&EB formulation for coatings, inks & paints, IV. Formulation*, edited by P.K.T. Oldring, United Kingdom,

London, (1991), p.37.

- [142] P. Bernhard, M. Hofmann and M. Hunziker, *Radiation curing in polymer science and technology, IV, Practical aspects and applications*, edited by J.P. Fouassier and J.F. Rabek, Elsevierapplied science, London, (1993), p.196.
- [143] T.H. Chiang, T.-E. Hsieh, “The effect of organofunctional silanes on the adhesion of epoxide resins to ITO glass”, *J. Adhes. Sci. Technol.* **19**(2005), p.1.
- [144] C. Dursun, M. Degirmenci, Y. Yagci, S. Jockusch and N.J. Turro, “Free radical promoted cationic polymerization by using bisacrylphosphine oxide potoinitiators: substituent effect on the reactivity of phosphinoyl radicals”, *Polymer*, **44**(2003), p.7389.
- [145] Y. Yađic, J. Borbely and W. Schnabel, “On the mechanism of acrylphosphine oxide promoted cationic polymerization”, *Eur. Polym. J.* **25**(1989), p.129.
- [146] T. Kobayashi, S. Takahashi and N. Fujii, “Silane coupling agent having dithiocarbamate group for photografting of sodium styrene sulfonate on glass surface”, *J. Appl. Polym. Sci.*, **49**(1993), p.417.
- [147] T. Maruno and N. Murata, “Properties of a UV-curable, durable precision adhesive”, *J. Adhesion Sci. Technol.*, **9**(1995), p.1343.
- [148] A. Fang, H.T. Ng, X. Su, and S.F.Y. Li, “Soft-lithography-mediated submicrometer patterning of self-assembled monolayer of hemoglobin on ITO surfaces”, *Langmuir*, **16**(2000), p.5221.
- [149] C.O. Kim, S.Y. Hong, M. Kim, S.M. Park and J.W. Park, “Modification of indium-tin oxide (ITO) glass with aziridine provides a surface of high amine density”, *J. Colloid Interface Sci.*, **277**(2004), p.499.
- [150] E.L. Bruner, A.R. Span, S.L. Bernasek and J. Schwartz, “Reaction between tetrakis(diethylamino)tin and indium tin oxide”, *Langmuir*, **17**(2001), p.5696.
- [151] C. Priola, A. Alonso, F. Catalina and W. Schnabel, “Using linear and branched

- polysilanes for the photoinitiated polymerization of a commercial silicone – acrylate resin. A real time FTIR study”, *J. Photochem. Photobiol., A Chem.*, **141**(2001), p.85.
- [152] W.C. Wake, *Adhesion and the Formulation of Adhesives*, Applied Science Publishers Limited, London, (1976), p.269.
- [153] J. McMurry, *Fundamentals of Organic Chemistry*, Plenum Press, New York, (1986), p.144.
- [154] N.S. Allen and M. Edge, “UV and electron-beam curing”, *J. Oil Colour Chem. Assoc.*, **73**(1990), p.438.
- [155] D.R. Randell, *Radiation Curing of Polymers*, Plenum Press, London, (1987), p.116.
- [156] P. Chiniwalla, Y.Q. Bai, E. Elce, R. Shick, W.C. McDougall, S.A.B. Allen and P.A. Kohl, “Crosslinking and decomposition reactions of epoxide functionalized polynorbornene. Part I. FTIR and thermogravimetric analysis”, *J. Appl. Polym. Sci.*, **89**(2003), p.568.
- [157] D.H. Choi, S.J. Oh, H.B. Cha and J.Y. Lee, “Photochemically bifunctional epoxy compound containing a chalcone moiety”, *Eur. Polym. J.*, **37**(2001), p.1951.
- [158] N. Nishiyama, K. Komatsu, K. Fukai and K. Nemoto, “Influence of adsorption characteristics of silane on the hydrolytic stability of silane at silica-matrix interface”, *Composites*, **26**(1995), p.309.
- [159] G.M. Loudon, *Organic Chemistry*, Third ed., Plenum Press, New York, (1995), Chapter 23.
- [160] D. Zhu and W. van Ooij, “Corrosion protection of metals by water-based silane mixtures of bis-[trimethoxysilylpropyl] amine and vinyltriacetoxysilane”, *Prog. Organic Coatings*, **49**(2004), p.42.

- [161] V. Palanivel, D. Zhu and W.J. van Ooij, "Nonoparticle-filled silane films as chromate replacements for aluminum alloys", *Prog. Organic Coatings*, **47**(2003), p.384.
- [162] L.C. Gupta and A. Dhuldhoya, US Patent Application, 20030004265 (2003).
- [162] E.P. Plueddemann, *Silane Coupling Agents*, 2nd ed., Plenum Press, New York, (1991), p.158.
- [164] J. Matysik, Alia, B. Bhalu and P. Mohanty, "Molecular mechanisms of quenching of reactive oxygen species by praline under stress in plants", *Curr. Sci.* **82**(2002), p.525.
- [165] S.J. Park, F.L. Jin, J.R. Lee and J.S. Shin, "Cationic polymerization and physicochemical properties of a biobased epoxy resin initiated by thermally latent catalysts", *Eur. Polym. J.* **41**(2005), p.231.
- [166] S.J. Park and H.C. Kim, "Thermal stability and toughening of epoxy resin with polysulfone resin", *J. Polym. Sci. Pt. B-Polym. Phys.* **39**(2001), p.121.
- [167] J.D. Holbrey, M.B. Turner, W.M. Reichert and R.D. Rogers, "New ionic liquids containing an appended hydroxyl functionality from the atom-efficient, one-pot reaction of 1-methylimidazole and acid with propylene oxide", *Green Chem.* **5**(2003), p.731.
- [168] J.J. Lin, G.P. Speranza and H.G. Waddill, "Synthesis and reactivity of Mannich-derived polyoxyethylene amines as epoxy curing agents", *J. Appl. Polym. Sci.* **66**(1997), p.2339.
- [169] H. Suzuki, A. Matsui and T. Inoue, US Patent, 3950451 (1973).
- [170] J.L. Lin, S.F. Lin, T.T. Kuo, F.C. Chang and F.P. Tseng, "Synthesis and epoxy curing of mannich bases derived from bisphenol A and poly(oxyalkylene)diamine", *J. Appl. Polym. Sci.* **78**(2000), p.615.
- [171] S.D. Theiss and S. Wagner, "Amorphous silicon thin-film transistors on steel

- foil substrates”, *IEEE Electron Device Lett.* **17**(1996), p.578.
- [172] R.S. Howell and S.V. Karnik, “Poly-Si thin-film transistors on steel substrates”, *IEEE Electron Device Lett.*, **21**(2000), p.70.
- [173] C.C. Wu, S.D. Theiss, G. Gu, M.H. Lu, J.C. Sturm, S. Wagner and S.D. Forrest, “Integration of organic LEDs and amorphous Si TFTs onto flexible and lightweight metal foil substrates”, *IEEE Electron Device Lett.* **18**(1997), p.609.
- [174] L. Angiolini, D. Caretti, C. Carlini and N. Lelli, “Polymeric photoinitiators based on side-chain benzoin methyl ether and tertiary amine moieties for fast UV curable coatings”, *Polym. Adv. Technol.* **4**(1993), p.375.
- [175] T.H. Chiang, T.-E. Hsieh, “A study of UV-curable epoxide resins containing tertiary amines”, *Polymer*, (2006), submit in processing.
- [176] C.E. Hoyle and K.J. Kim, “The effect of aromatic amines on the photopolymerization of 1,6- hexanediol diacrylate”, *J. Appl. Polym. Sci.* **33**(1987), p.2985.
- [177] D. Lu, D. Wong, and C.P. Wong, “Properties of conductive adhesives based on different curing agents”, *J. Electron. Manuf.* **9**(1999), p.241.
- [178] J.E. Frommer, R.R. Chance, and AR. Corporation, in *Electrical and Electronic Properties of Polymers: A State-of-the-Art Compendium*, Edited by J.I. Kroschwitz, Plenum Press, New York, (1988), p.101.
- [179] S.H. Mansour and S.L. ABD-EL-Messieh, “Electrical and mechanical properties of some polymeric composites”, *J. Appl. Polym. Sci.* **83**(2002), p.1167.
- [180] S. George, K.T. Varughese, and S. Thomas, “Dielectric properties of isotactic polypropylene/nitrile rubber blends: Effects of blend ratio, filler addition, and dynamic vulcanization”, *J. Appl. Polym. Sci.* **73**(1999), p.255.
- [181] R.L. Jr. Smith, S.B., Lee, H. Komori, and K. Arai, “Relative permittivity and

- dielectric relaxation in aqueous alcohol solutions”, *Fluid Phase Equilib.* **144**(1998), p.315.
- [182] J.B. Birks, and J.H. Schulman, *Progress in Dielectrics*, Vol. I, John Wiley & Sons, New York, (1959), p.256.
- [183] H.P. Higginbottom, US Patent, 4501864 (1985).
- [184] H.P. Higginbottom, and M.F. Drumm, US Patent, 4557979 (1985).
- [185] J. Qu, and C.P. Wong, ”Effective elastic modulus of underfill material for flip-chip applications”, *IEEE Trans. Compon. Packaging Technol.* **25**(2002), p.53.
- [186] G. Wang, J.H. Zhao, M. Ding and P.S. Ho, *Inter Society Conference on Thermal Phenomena*, (2002), p.869.
- [187] M. Bonneau, and J. Stewart, *Proceedings of the International Symposium and Exhibition on Advanced Packaging Materials Processes, Properties and Interfaces*, (1997), p.57.
- [188] D.J. Siegel, L.G. Hector, and J.B. Adams, “*Ab initio* study of Al-ceramic interfacial adhesion”, *Phys. Rev. B* **67**(2003), p.092105-1.
- [189] V.K. Pujari, W.T. Collins, and J.J. Kutsch, US Patent, 6645612B2 (2003).

Curriculum Vitae

Tzu-Hsuan Chiang (江姿萱)

PERSONAL DATA

Born: October 24, 1972, Miao-Li, Taiwan.

Nationality: Taiwan, the Republic of Chian.

Office Address: Department of Materials Science and Engineering, National Chiao-Tung University, 1001, Ta-Hsueh Rd., Hsinchu 30050, Taiwan, ROC.

Tel: 886-3-5712121 ext. 55338.

E-mail: cjjiang@ms.chinmin.edu.tw

EDUCARION

Ph.D. candidate, Department of Materials Science and Engineering, National Chiao-Tung University, Hsinchu, Taiwan, present.

Master of Science, Department of Chemical and Materials Engineering, Chang Gung University, Tao-Yuan, Taiwan, July (2002).

Bachelor of Science, Department of Chemical Engineering, National Taiwan University of Science and Technology, Taipei, July (1996).

PUBLICATIONS

Journal Articles:

1. **Tzu Hsuan Chiang** and T.-E. Hsieh, (2005), "The Effect of Organofunctional Silanes on the Adhesion of Epoxide Resins to ITO Glass", *Journal of Adhesion and Science Technology*, **19**(1), p.1-18.

2. **Tzu Hsuan Chiang** and T.-E. Hsieh, (2006), “A Study of Monomer’s Effect on Adhesion Strength of UV-curable Resins”, *International Journal of Adhesion & Adhesive*, **26**(7), p.520-531.
3. **Tzu Hsuan Chiang** and T.-E. Hsieh, (2006), “A Study of Encapsulation Resin Containing Hexagonal Boron Nitride (hBN) as Inorganic Filler. *Journal of Inorganic & Organometallic Polymers & Materials*, in press.
4. **Tzu Hsuan Chiang** and T.-E. Hsieh, (2006), “A Study of UV-curable Epoxide Resins Containing Tertiary Amines”, submitted to *Polymer*.
5. **Tzu Hsuan Chiang** and T.-E. Hsieh, (2006), “The Effect of Tertiary Amines on Etiolation of UV-curable Epoxide Resins”, submitted to *Journal of Physical Chemistry B*.

Conference Papers:

1. **Tzu Hsuan Chiang** and T. E. Hsieh (2004), The Effect of Silane Coupling Agents on Adhesion Strength of UV-curable Resin on ITO Glass of OLEDs, *Taiwan Display Conference (TDC)*, 04-019.
2. **Tzu Hsuan Chiang** and T. E. Hsieh (2004), The Effect of Polyol Monomers on the Adhesive Strength of Photo-Curable Epoxy Resins on Glass Substrate, *MACRO2004-40th IUPAC World Polymer Congress*, Paris, 4.3.5.
3. **Tzu Hsuan Chiang** and T. E. Hsieh (2005), A Study of Dielectric Properties of Underfill Containing Hexagonal Boron Nitride (hBN) Inorganic Filler, *European Polymer Congress*, Moscow, p5.4-11.